Aalto-yliopisto
Aalto-universitetet
Aalto University

Master's Programme in Mechanical Engineering

Design and routing of detector services on a particle tracker

Mikko Barinoff

Master's Thesis
2021

Aalto-yliopisto
Aalto-universitetet
Aalto University

Aalto-yliopisto
Aalto-universitetet
Aalto University

Author Mikko Barinoff

Title of thesis Design and routing of detector services on a particle tracker

Programme Mechanical Engineering

Thesis supervisor Prof. Kari Tammi

Thesis advisor MSc. Antti Onnela

Collaborative partner CERN

Date 05.04.2021 **Number of pages** 67 **Language** English

Abstract

The goal of this thesis was to do both the conceptual and the detailed design of the TB2S ladder services, and to validate the feasibility of the design with a mock-up -prototype. Concurrently to support the design process, the aim was to investigate and pilot the usage of novel design tools and to utilize the best practices obtained from the latest research done in the field.

The design process started by investigating the solutions used in the structures of the previous detector and establishing the different constrains and driving factors for the new design. After that the routing concept was laid down, and the detail design was done. Solutions for all the pigtails and octopus/naked-fanout routings were detailly modelled, and accessory parts were designed. Usage of an advanced CATIA add-on specialized for cabling design was piloted during the design process with perspective of expanding the usage in the organization. Finally, a mock-up -prototype demonstrating functionality of all the service features was constructed, and several studies related to space envelopes and ease of assembly were performed.

The project goals were met successfully, as the service design was finalized, and its feasibility was validated with positive results. Several issues initially obstructing the routing were overcome without generating additional problems to the affiliated constructions. Valuable benchmarking was done, and information of the design methods and tools was investigated and reported in the literature review for similar design projects in the future. Novel design tools were successfully utilized during the process, and great amount of potential in escalating the usage in the organization level was recognized.

Keywords CERN, CMS, Particle tracker, Cable harness design, DFMA, Flexible cable modelling, Mock-up

Aalto-yliopisto
Aalto-universitetet
Aalto University

Tekijä Mikko Barinoff

Työn nimi Detektorin johdotusten reititys ja suunnittelu hiukkasilmaisimessa

Koulutusohjelma Konetekniikka

Vastuuopettaja/valvoja Prof. Kari Tammi

Työn ohjaaja DI Antti Onnela

Yhteistyötaho CERN

Päivämäärä 05.04.2021 **Sivumäärä** 67 **Kieli** englanti

Tiivistelmä

Tämän diplomityöprojektin tavoitteena oli suunnitella TB2S ladder -rakenteeseen liittyvien sähkökaapeleiden, optisten kuitujen ja jäähdytysputkien reititys, sekä niiden tarvitsemat tukirakenteet, ja validoida suunnittelutyö prototyypin avulla. Suunnittelutyön tukena oli tarkoitus tutkia ja pilotoida nykyaikaisia suunnittelutyökaluja, ja hyödyntää parhaita menetelmiä ja käytäntöjä alalla tehdystä viimeisimmästä tutkimuksesta.

Suunnittelutyö alkoi tutkimalla edellisessä detektorissa käytetyt vastaavat ratkaisut, ja tunnistamalla kohdetta koskevat rajoitteet sekä tärkeimmät vaatimustekijät. Tämän jälkeen todettiin paras reitityskonsepti, jonka pohjalta kokonaisvaltainen suunnittelutyö tehtiin. Reititysratkaisut sekä saparoille että johtosarjoille mallinnettiin, ja reititystä tukevat komponentit suunniteltiin. Edistyksellistä kaapelointisuunnitteluun erikoistunutta CATIA-lisäosaa hyödynnettiin suunnittelutyössä, ja sen laajempia käyttömahdollisuuksia organisaatiossa pohdittiin. Lopuksi rakennettiin reititysten funktionalisuutta demonstroiva prototyyppi, ja useita tilarajoitteisiin ja kokoonpantavuuteen liittyviä tutkimuksia suoritettiin sen avulla.

Diplomityöprojektin tavoitteet saavutettiin onnistuneesti, kun suunnittelutyö saatiin päätökseen ja sen soveltuvuus todistettiin kelvollisin tuloksin. Useita alkutilanteessa olleita ongelmia saatiin ratkaistua monimutkaistamatta muuta rakennetta tai aiheuttamatta uusia ongelmia muilla kannoilla. Hyödyllistä vertailua ja selvitystyötä suunnittelutyötapoihin ja työkaluihin liittyen tehtiin, ja tulokset raportoitiin kattavasti kirjallisuuskatsauksessa tulevia samanlaisia suunnitteluongelmia varten. Edistyksellisiä suunnittelutyökaluja hyödynnettiin suunnittelutyön aikana, ja potentiaalia niiden laajempaan käyttöön organisaatiossa tunnistettiin.

Avainsanat CERN, CMS, Hiukkasilmaisin, Johtosarjasuunnittelu, DFMA, Joustavan kaapelin mallinnus, Prototyyppi

Contents

Preface

Firstly, I would like to express my sincere gratitude to my thesis advisor Antti Onnela both for sharing his endless professional knowledge on tracker mechanics, and for personally helping me on integrating into the local society on a difficult pandemic situation. Thanks to all of my colleagues involved in the ladder collaboration for productive co-operation throughout the whole project. Thanks to Professor Tammi for his constructive feedback and advices on academic writing.

Finally, I want to thank my family and friends back in Finland for countless FaceTime-calls and messages easing the occasional homesickness.

Meyrin, Switzerland

05 April 2021

Mikko Barinoff

Symbols and abbreviations

Symbols

A	Cross-section of the cable
E	Young's modulus of the cable material
E_{pot}	Total potential energy of the spring systems
F^e	Sum of external forces affecting the system
G	Shear modulus of the cable material
g	Cost of movement to the node from the start
h	Estimated cost of movement to the end from the node
I	Second moment of inertia of the cross-section
I_p	Polar moment of inertia of the cross-section
l	Distance between adjacent mass points
l_o	Nominal length of the cable link
l_i	Initial length of the cable link
L_w	Length of the wire measured in feet
n	Node in question
N_w	Number of wires or cables
N_{wc}	Number of wire-contact -pairs in the connector
N_{wp}	Number of wire-pin -pairs in the connection to be soldered
p_T	Transverse momentum
T_a	Time required for laying the wires or cables
T_c	Time required for cutting in seconds
T_p	Time required for connector-wire coupling in seconds
T_s	Time required for soldering process in seconds
x	Matrix containing the position coordinates of the point
β	Angle between adjacent cable links
θ	Material twisting angle per a single cable link
φ	Geometric torsion angle between adjacent cable links

Abbreviations

2S	Two-strip
ALICE	A large ion collider experiment
AR	Augmented reality
ATLAS	A toroidal LHC apparatus
AWG	American wire gauge
BMC	Bulk moulding compound
BTL	Barrel timing layer
CAD	Computer aided design
CBS	CMS binary chip
CCA	Copper cladded aluminium

CEO	Chief executive officer
CERN	Conseil européen pour la recherche nucléaire
CMS	Compact muon solenoid
CTE	Coefficient of thermal expansion
DFA	Design for assembly
DFMA	Design for assembly and manufacturing
FCC	Future circular collider
FEH	Front-end hybrid circuit board
FEM	Finite element method
HL-LHC	High-luminosity large hadron collider
HMD	Head-mounted-display
IP	Interaction point
IPHC	Institut pluridisciplinaire Hubert Curien
IT	Inner tracker
KBE	Knowledge-based engineering
LHC	Large hadron collider
LHCb	Large hadron collider beauty
LHCf	Large hadron collider forward
LINAC2	Linear collider 2
LS3	Long shutdown 3
MoEDAL	Monopole and exotics detector at the LHC
MPO	Multi-fibre push on
MT	Mechanically transferable
NCP	National centre for physics
OT	Outer tracker
PCB	Printed circuit board
PP0	Patch panel 0
PS	Pixel-strip
PS	Proton synchrotron
PSB	PS Booster
SEH	Service hybrid circuit board
SMC	Sheet moulding compound
SPS	Super proton synchrotron
TB2S	Tracker barrel with 2S-modules
TBPS	Tracker barrel with PS-modules
TEDD	Tracker endcap double-discs
TOB	Tracker outer barrel
TOTEM	Total elastic and diffractive cross section measurement
VR	Virtual reality
VTRx+	Versatile Transceiver

1 Introduction

1.1 CERN

CERN (*Conseil Européen pour la Recherche Nucléaire*) is the largest and the most advanced particle physics research facility in the world. Locating on the Switzerland-France -border just outside the city of Geneva, CERN hosts its state-of-the-art research equipment which are utilized by scientists striving to provide answers to the most fundamental questions of the universe. (CERN 2019.) Probably the most famous finding done at CERN, was the discovery of the so-called Higgs-particle in 2012, which was observed by CERN's ATLAS and CMS experiments. On the following year, Peter Higgs and François Englert were awarded with the Nobel prize in physics for their successful theory behind this finding. (Stjernlöf 2013.)

CERN is a remarkable example of successful international co-operation. Since its foundation in 1954, CERN has steadily grown to its current constitution of 23 member states and other international contributors. In 2019, total of 17 600 individuals from different universities, institutes and partner companies were involved in the CERN activities. CERN's annual budget in 2019 was 1.26 billion Swiss francs, and it is financed with membership fees collected from the member states and other collaborators. (CERN 2019.)

The crown jewellery of CERN's research equipment is the Large hadron collider (LHC), as it stands as the most powerful particle accelerator in the world. The LHC is 27 km long by its circumference, and it is constructed in a tunnel dug over 100 m under the ground. The design of LHC started already in 1980's when the initial physics requirements and technical specifications were outlined by CERN's physicists and engineers. The LHC project was approved by the CERN council in 1994, and one of the most complex machinery ever designed by human started to come together. International co-operation acted a crucial part, when in addition to the member states observer states like the USA, Japan and India contributed financially to the hugely expensive project totally costing over 4.3 billion Swiss Francs (CERN 2020). LHC started operating in 2008, when the initial tests and commissioning of the equipment started. (CERN 2017.)

A particle accelerator alone does not provide much insight to physicists. The actual scientific measurements are made at so-called “experiments” located along the accelerator. The seven experiments built along the LHC are: A Large Ion Collider Experiment (ALICE), A Toroidal LHC ApparatuS (ATLAS), Compact Muon Solenoid (CMS), Large Hadron Collider beauty (LHCb), Large Hadron Collider forward (LHCf), TOTal Elastic and diffractive cross section Measurement (TOTEM), and the Monopole and Exotics Detector at the LHC (MoEDAL). ATLAS and CMS are general-purpose experiments, whereas the rest focus each on more specific areas of physics. The mission of the experiments is to observe and characterize the secondary particles that emerge from the particle beam collision events. For example, measuring the trajectory of a particle in a controlled magnetic field gives information on the electric charge and quantity of motion of the measured particle. (CERN 2017.)

1.2 CERN’s particle accelerator complex

The backbone of CERN’s research infrastructure is its particle accelerator complex. Several accelerator units built in series accelerate particles to successively increasing energies and steer them to collide at the experiments. Protons or charged ions are currently used in the main accelerator chain at CERN. The generation of the proton beams starts from a small bottle of hydrogen gas. Protons are extracted from the gas by forcing out the single electrons of hydrogen from each nucleus. The extracted protons are then injected to the PS Booster (PSB) using the Linear collider 2 (LINAC2) with energy of 50 MeV. In PSB the protons are accelerated to the energy of 1.4 GeV, and the beam is passed on to the Proton Synchrotron (PS) which accelerates the protons to 25 GeV. The next in line is the Super Proton Synchrotron (SPS), where the protons are further accelerated to 450 GeV. The final step of the acceleration sequence is when the proton bunches are injected from SPS to both clockwise and anti-clockwise trajectories in to the LHC. The protons are accelerated in the LHC until they reach an energy of 6.5 TeV and are travelling by 99.9999991% of the speed of light. (CERN 2017.) A schematic of the current CERN accelerator infrastructure is shown in Figure 1.

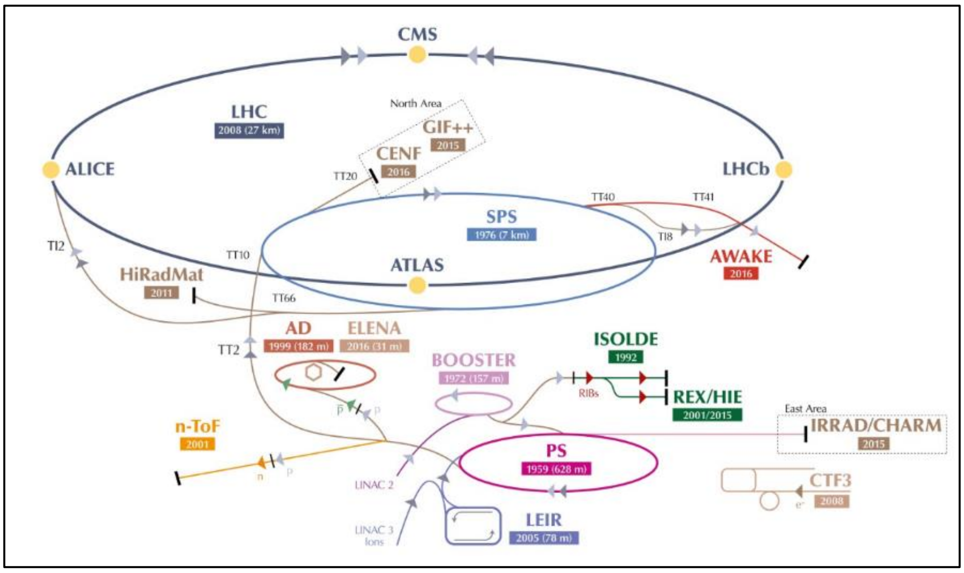

Figure 1: CERN accelerator complex (Mobs 2016).

Even after the discovery of the Higgs-particle that completed the standard model of particle physics, there are still several fundamental aspects of the universe that remain as mysteries. Astronomers have observed that the motion of celestial bodies and whole galaxies is alternating in such ways, that it is not possible to be explained by the gravity interaction of surrounding apparent matter. Therefore, it has been inferred that there has to be some kind of an unknown element, that causes a notable gravitational effect, but no – or so minimal electromagnetic charge that it is impossible to observe or interfere even with the most advanced instruments existing. The constitution of this so called of dark matter and the reason behind matter-antimatter asymmetry of the universe are questions to which current physics theory cannot provide answers. Scientists are now franticly trying to figure out, is the dark matter made of some kind of new fundamental particles, and does it have any other interactions with apparent matter other than gravity. (Randall 2018.) To support this mission, there are already plans to construct even larger and higher energy accelerators such as CERN's Future circular collider (FCC) -project. The FCC would be 100 km long and be capable of proton-proton collision energies of 100 TeV. The whole lifespan of the FCC project including design, construction and different operations is estimated to be 70 years. (FCC 2019.)

1.3 CMS

CMS (Compact Muon Solenoid) is a general-purpose experiment designed to be used in research of broad scale of particle physics phenomena induced by the LHC accelerator. The concept of CMS experiment was presented first time in 1990, and the detailed technical proposal was published in 1994. The principal concept driving the design of CMS was to generate a strong magnetic field allowing to accurately measure the momentum of muons in a "compact" space. Thus, the core element of CMS's structure is a superconducting solenoid magnet which is 13 meters long, six meters in diameter, and capable of producing a magnetic field of 4 T that provides enough bending force to achieve satisfactory momentum measurement resolution. (CMS 1994.) A sectioned schematic view of the CMS structure is shown in Figure 2.

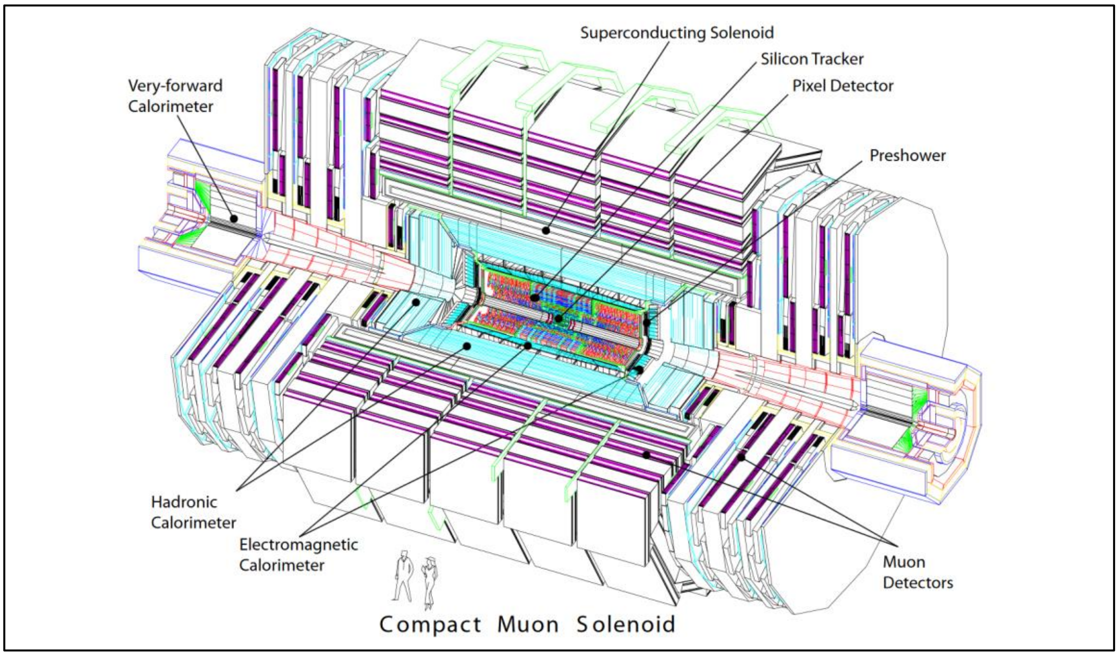

Figure 2: A sectioned view of the CMS structure (CMS 2006).

The outermost layers of CMS are muon detector stations. As the name suggest, muon stations record the trajectory of muons, which – unlike most of the other particles – are capable of penetrating through CMS's inner layers all the way up to the outer layers. Each muon station has several layers of aluminium drift tubes on the barrel section, and cathode strip chambers on the endcap section. The drift tube units have charged anode wire inside small gas chambers filled with $ArCO_2$. As a particle travels through the chamber, it causes ionization in the gas and the free electrons transfer to the surface of the positively charged anode which after amplification induces an electrical signal that is read. The cathode strip chambers on the endcap disks have a similar principle, but instead of single wire they have an array of anode-cathode conductors inside the gas chambers for more precise 3D-trajectory recording. (CMS 1997a.)

Radially inwards from the solenoid magnet, are the hadron and electromagnetic calorimeters. The function of the calorimeters is to capture particles and thus measure their momentum energy. The hadron calorimeter (HCAL) structure is made from a barrel section, which is closed from both ends with end-cap sections. The HCAL is a so-called sampling calorimeter, as it consists of interleaving layers of dense absorbers and scintillator detectors. The copper absorber layers decrease the particle momentum resulting it to scatter, from which photons are then detected as light signals in the plastic scintillator elements. (CMS 1997b.) The electromagnetic calorimeter (ECAL) sits inside the HCAL and has a similar barrel-endcap structure. On the ECAL the scintillator elements are made from heavy lead-tungsten crystals, to achieve high energy measurement accuracy in a compact space required by the ECAL. (CMS 1997c.)

The innermost sub-detector of CMS is the silicon tracker (Figure 3). Consisting of inner pixel tracker, and outer silicon-strip tracker, the function of the whole system is to record particle trajectories with high spatial resolution while having minimal influence on the tracks and momentums of the particles. This means that the amount of material inside the tracking volume must be kept minimal, while still achieving hermetic tracking coverage. The basic unit of the tracker are its over 15 000 silicon detector modules, providing over 200 m2 of active silicon sensor area. Each module consists of the silicon sensor and its electronics, which are supported on a carbon fibre frame. When a charged particle travels through the silicon sensor, it creates electron-hole pairs, which are attracted to opposite electrodes. This creates a current which is amplified by the module electronics and passed on as a signal. (CMS 1998.) Figure 3 shows the silicon-strip tracker being installed in CMS in December 2007 after an intense construction phase of seven years.

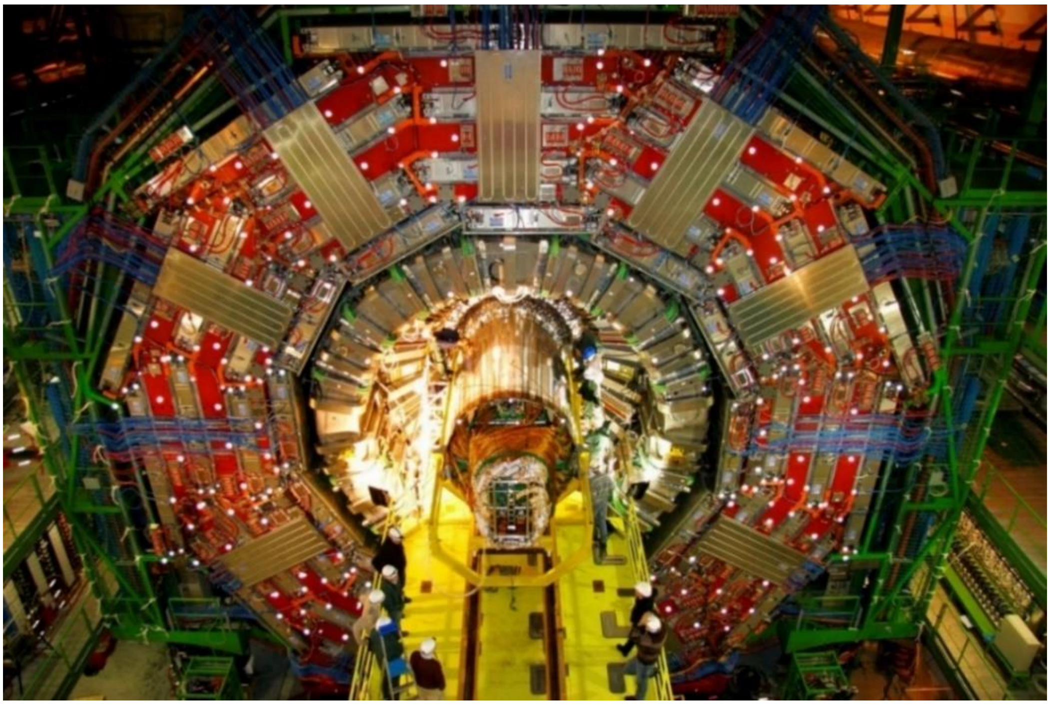

Figure 3: The silicon-strip tracker (on top of the yellow platform) being installed to CMS (Hoch 2008).

1.4 Background

The CMS Phase-2 Upgrade -project will bring significant changes to the CMS detector hardware. Higher radiation levels and increased particle density resulting from the High-Luminosity upgrade of the LHC accelerator (HL-LHC) will set requirements to the detector hardware for better radiation durability, increased detector granularity and higher bandwidth to cope with increased amount of data. The HL-LHC project was approved in 2016 by the CERN council, and the corresponding detector upgrades are due to be installed in CMS during LHC Long shutdown 3 (LS3) in 2025-2027. (CMS 2017.)

The tracking system of CMS will be completely replaced with re-designed and more performant detector modules, support structures and auxiliary systems. The new tracker will consist of the Inner Tracker (IT) with silicon pixel modules, and of the Outer Tracker (OT) with silicon pixel and silicon strip modules. All modules of the OT will consist of a sandwich of two super-positioned sensor planes. These innovative p_T-modules will be individually capable of discarding signals caused by particles that are below designated transverse momentum (p_T) threshold. The module types used in the OT are called Two-Strip (2S) and Pixel-Strip (PS), and they are displayed in Figure 4, respectively. In Figure 5 the 2S-modules are coloured in red and the PS-modules in blue. The total number of modules in the OT will be 13 305. (CMS 2017.)

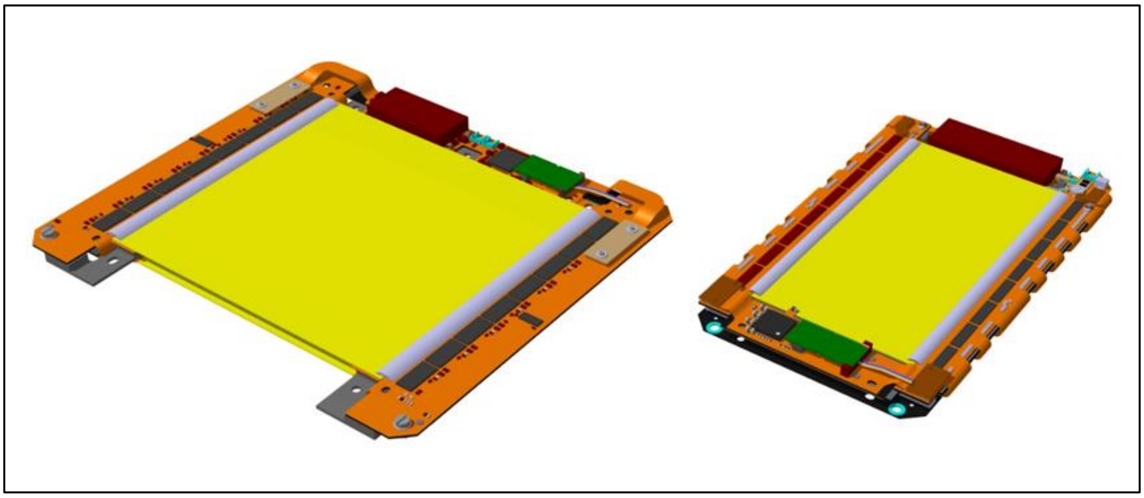

Figure 4: The 5-pad variant of the 2S-module, and the PS-module 3D-models, respectively. The silicon sensors located in the middle of both modules are coloured in yellow and surrounding electronic hybrid circuit boards in orange.

The OT will consist of three subdetector systems called Tracker barrel with 2S-modules (TB2S), Tracker barrel with PS-modules (TBPS) and Tracker endcap double-discs (TEDD). TB2S and TBPS form a six-layer barrel construction, in which the modules in TBPS are placed in tilted orientations when moving outwards from the beam interaction point (IP) on the tracker Z-axis. The barrel construction is closed at its both ends by five-layer TEDD-subdetectors. The exact location and orientation of each module is specified in the tracker layout (Figure 5) to achieve satisfactory tracker hermeticity. This means that any particle emerging from the IP is guaranteed to pass through a minimum of six module layers in the Outer Tracker. (CMS 2017.)

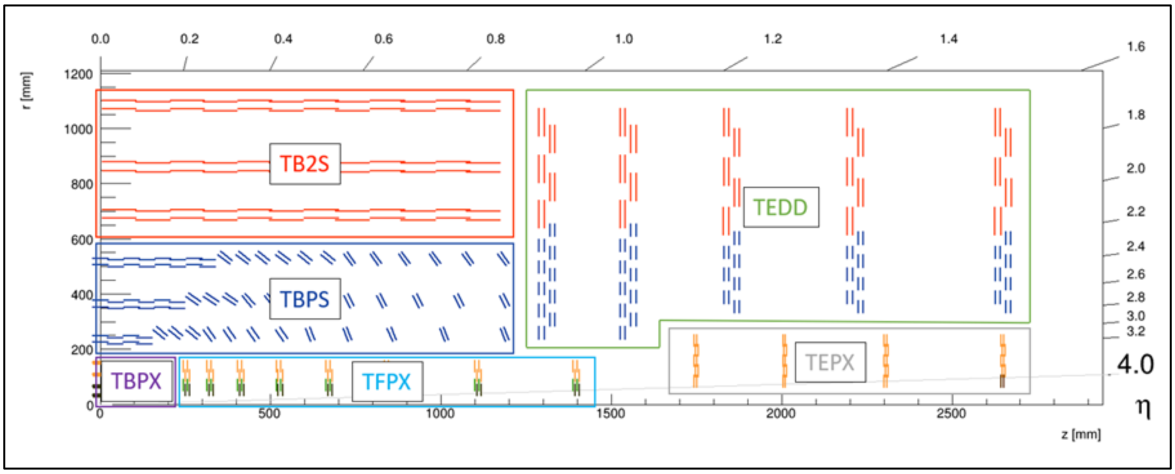

Figure 5: A schematic of a quarter section of the upgraded tracker layout. Z-axis is parallel with the beam line of the accelerator and r-axis is the radial direction. Different subdetectors are labelled in the schematic.

1.5 Research problem

The TB2S-subdetector will use somewhat similar concept on its module support structures as its predecessor TOB (Tracker outer barrel) that is currently in use in CMS. The wheel structure consists of four circular carbon fibre disks, that support the ladder frames on which the 2S-modules are fixed. The major difference between the new TB2S-ladder and the existing TOB-rods is the totally new module design, and that propagates as significant design changes to the ladder support structure and the module services.

Module services consist of electrical wirings for module powering, optical fibres for data transfer and a CO2 cooling circuit to cool down the 2S-modules to their ideal operating temperature. The design of these services is an extensive multi-domain problem and must take in to account a lot of elements such as the physical routing, aspects in ease of assembly and performance of the cooling system.

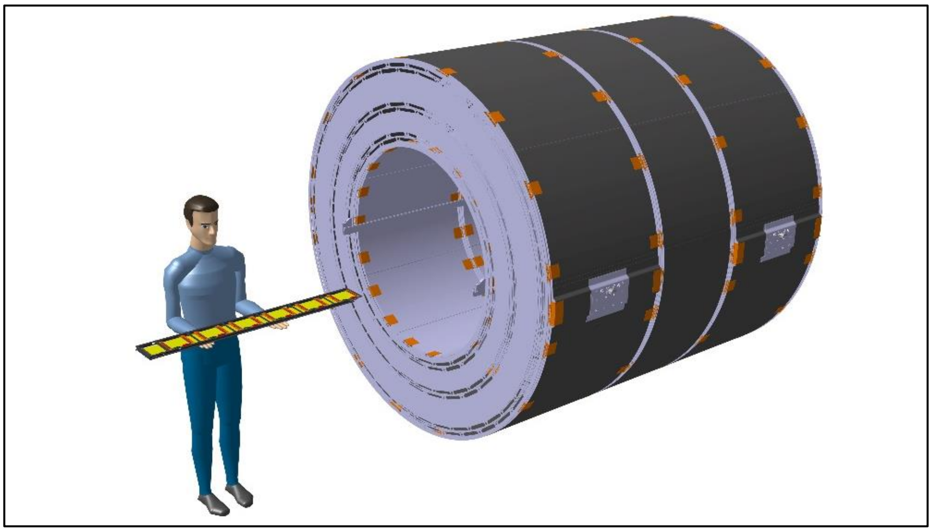

Figure 6: An assembler holding the TB2S ladder in front of the wheel.

1.6 Objectives

The goal of this thesis is to make the conceptual and detailed design of the TB2S ladder services and test their feasibility with prototypes. The aim is to have a validated design, ready to be used in the final production phase of the TB2S ladders which is due to start in the second half of 2021. During the design process novel design tools and methods are tested, and if proven efficient, potential of their broader utilization in the organization is reviewed.

The conceptual design shall combine the best practices from the previous detector designs and from the latest research made in the field. The detail design must include the physical routing of the services, placement of connectors and accessories and all the modifications that must be made to the ladder structure to adjust. These are such as the service through holes, modifications on module support inserts, and the design of the front interface panel where the services exit from the ladder and connect to the services of the whole OT. Lastly the feasibility of the service design has to be validated with a physical mock-up prototype, where the service routing, connections, module assembly, and the need for auxiliary tools and fixtures can be fully studied and demonstrated.

1.7 Scope

The scope of this thesis is confined to the TB2S ladder (Figure 6) mechanical service design. Effects that the services design may have on the electrical, thermal, or other performance of the system are taken into account, but they are not in the main scope in the thesis. The interface area between the ladder and the wheel requires some crossover work with the wheel service design, and the ladder is subordinate to any constraints set by the wheel environment.

1.8 Methods

The thesis consists of a literature review and of a case study. The literature review presents the latest research knowledge from the field of digital cable design tools and the related product development theory to support the execution of the case study.

On the case study the actual design work is performed by 3D-modeling with CATIA which is a modern and versatile CAD-system. Some advanced and specific add-ons like CATIA's Electrical harness discipline -workbenches are utilized to analyse the behaviour of module cables and fibres during different assembly phases. The feasibility of the virtual design is proven with a real-sized physical mock-up, which is built with combined manufacturing methods such as machining, 3D-printing and waterjet cutting.

The work included in the thesis is carried out in close co-operation with TB2S project collaborators NCP (*National Centre for Physics*) from Islamabad and IPHC (*Institut pluridisciplinaire Hubert Curien*) from Strasbourg. NCP is responsible for the serial production of the TB2S ladder frames, and IPHC will perform the module and service installation to the ladders. CERN CAD Service is also partnering on providing the mentioned CATIA add-ons and evaluating if they should be utilized on a broader level at CERN.

2 Literature review

2.1 Design and manufacturing of cable harnesses

Cable harnesses are a crucial element of almost any electromechanical system. They distribute electrical power and control signals to the electrical components scattered around the product layout. A cable harness often consists of a main trunk in which the wires and cables are bundled together with spiral wrap or another fixing element. Smaller sections of cables which leave the main trunk in breakout points are called branches, and they propagate separately towards a smaller subset of components. (Aguirre & Raucent 1994.) Even though the importance of cable harnesses is well recognized, often their design is seen as a secondary objective and carried out only in the very end of the product development cycle. This can lead to last minute product-level design changes and cause major delays on finalizing the design. (Ng 2000.) A real-world industry example of this happened on the case of Airbus A380 development. A fundamental design flaw with the plane's cable harnesses noticed in the pre-production phase delayed its delivery schedule by over a year, led to cancellation of orders and soon after to resignment of the company's CEO. (Hellemans 2007.) Also, malfunctions caused by insufficient cable harness design are one of the most common warranty reclamations obtained by car manufacturers (Ng 2000).

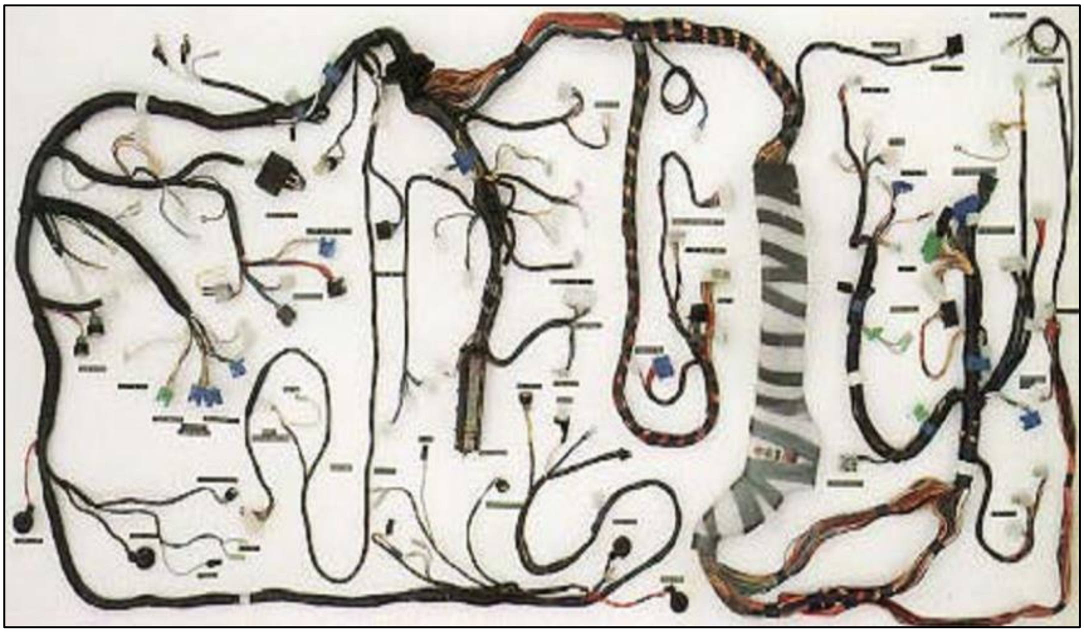

Figure 7: An assembled cable harness (Ng 2000).

According to Park et al. (1994) the electrical harness design process starts by examining the electrical specification and identifying environmental constraints of the product. Electrical specification should include a schematic diagram of the electric system where pin-pin connections between systems are specified. Depending on the case, other electrical aspects may be addressed such as impedance, signal noises, voltage drops and thermal effects (Scully 2020). The environmental specification contains the necessary information of the product geometry and points out the zones that are off limits for the harness routing for thermal or other functional reasons. (Park 1994.)

Once the specifications and constraints are clear, the basic configuration of the harness is defined. The partitions are specified, meaning how many trunks and branches there will be on each section of the harness. The form of the harness starts to build up, as the harness configuration and the electrical schematic define the wire number on each branch and trunk. The number of wires and the specification of possible wire cross-sections and insulations is used to determine the physical properties and constraints for the harness itself such as weight, cost per unit of length and minimum bending radiuses in different sections. (Park 1994.)

After the basic configuration is defined, the detailed physical routing path of the harness is designed. The first step is to roughly approximate the harness geometry based on the configuration and see how well it fits on top of the component layout. If this attempt seems feasible, it can be iterated to a more detailed geometry. If major issues are instantly evident, the configuration or even the component layout must be rearranged. As the harness geometry iterates towards its detailed form, several environmental constraints such as physical obstacles and minimum bending radiuses must be assessed. (Park 1994.)

After the routing is determined, the final stage is specification of the standard parts. This includes the wires, insulators and other protectors, connectors, ferrules, and fixing elements. The selection criteria includes factors like component mass, price and availability, and the weight of each varies case by case. The final specification of components can have influence on for example routing design, so naturally the whole design process is iterative and will go in cycles. (Park 1994.)

Cable harnesses are often assembled manually by arranging the wires on to a jig which is specifically made for the harness in question. The jig is usually a planar board, to which a full-size schematic of the harness is printed, and the wire paths are constrained with physical objects like pegs or nails. Connectors are fixed on their definite positions and wire ends that remain yet without terminations are temporarily fixed to the jig with a spring clamp. After all wires and cables are fixed and routed properly, the harness sections are tied together using spiral wrap, laces, tubing, or electrical tape. The whole assembly procedure can be carried out by single assembler, or through multiple assembly stations if necessary. For example, in large scale series production the wire preparation is separated to its individual station, and even the harness assembly can be made in several stages. After the wire harness is assembled, it may be connected to a test bench, where an automated system checks that the wiring and connections are made properly, and signals are transmitting to correct destinations. (Boothroyd 2010.)

The level of automation especially in more complex cable harness assembly processes is relatively low even in today's industry. Automation can be utilized mostly in the wire preparation stages, where the wires can be trimmed to desired lengths and the ends can be stripped and crimped to connectors. Almost all the handling and cable routing must be done as labour work carried by human operator. This is because flexible and variable-shaped objects as wires are a challenging use-case for industrial robots, which execute pre-programmed recurrent actions and motion paths. A human worker can adapt by using his/her superior human senses, and effortlessly carry out the task even if the conditions change little every time. (Boothroyd 2010.)

2.2 DFMA on cable harness design

Traditionally it has been thought that broad knowledge of different manufacturing methods is an obvious competence for a skilled designer to be able to design cost effective products. While this is still true, increased complexity of the designed products and grown amount of advanced manufacturing methods available makes conquering both fronts increasingly hard. Boothroyd (1996) has created Design for Manufacturing and Assembly (DFMA) which is a systematic set of methods to increase manufacturing cost efficiency in modern product development processes. In DFMA, different design concepts are quantitatively analysed and ranked against each other in early product development phases. (Boothroyd 1996.)

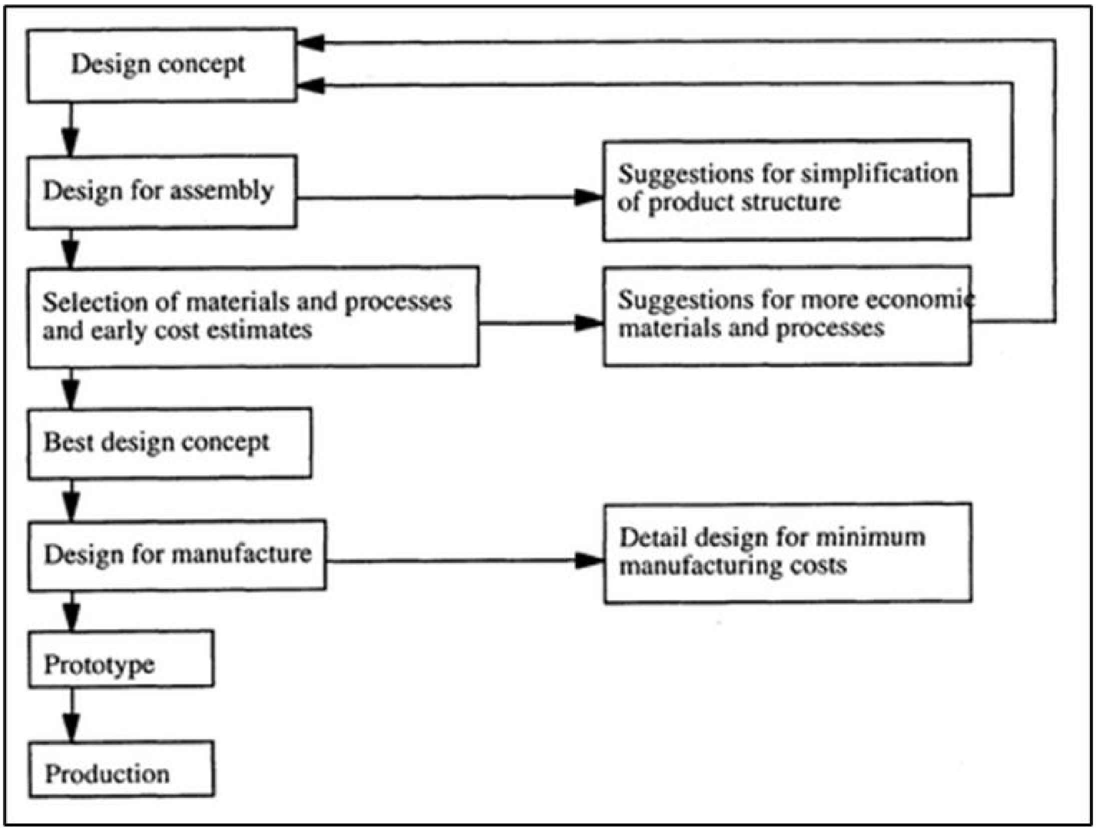

Figure 8: DFMA process flowchart in simultaneous engineering work (Boothroyd 1996).

On the DFMA process, Design for assembly (DFA) analysis is performed first for the design concept under study. DFA focuses largely on simplification of the product structure by minimizing the number of individual components. Each component is evaluated under following three criteria to judge whether their existence is justifiable as individual instances:

1. Does the component have to move relative to the rest of the assembly to make the product functional?
2. Does the component have to be made from different material than the rest of the assembly because of a fundamental functional reason?
3. Does the component have to be individual from the rest of the assembly to make other components possible to be assembled or disassembled?

If the answer is unconditionally positive to one of these questions, then it can be considered reasonable to keep the component as an individual instance. If all three answers are negative, then the individual instance should be kept only for a very good reason. (Boothroyd 1996.)

After the product structure is reviewed, the following step is to evaluate the assembly time required for the design concept and estimate its efficiency by means of complexity of the assembly procedures. Each component in the design is evaluated by two conditions: how the component is handled during the assembly, and how it is inserted and fixed to the assembly. The assembly difficulty factor is determined from specific criteria, and standard assembly times can be read from a table in which they are empirically defined by Boothroyd. Summing all the individual components together the theoretical assembly time of the product can be defined. When this is multiplied by hourly operating costs, an estimate of the assembly cost is found out. In this way the result is a numerical figure which can be easily compared against other design concepts. (Boothroyd 1996.)

After the DFA aspects are analysed and hence emerged modifications are made to the product structure, next phase is the Design for manufacturing (DFM) -analysis. DFM focuses on providing tools to estimate the manufacturing costs of individual components, and again to rank different design concepts against each other. A lot of empirical research has been made with different manufacturing methods, and DFM provides the data to a designer in a numerical form, which supports decision-making in the early component design phases. Knowing the products economical basis such as expected production volumes, one can quickly compare with DFM should a specific component be made by for example machining, casting, or sheet metal forming. (Boothroyd 1996.)

Traditional DFMA analysis is fairly straight forward when it is applied for purely mechanical products that are manually assembled. However, when electrical components and their required wiring and connections are added to the mix, a more adequate approach is required. As described on the previous chapter, the work related to cable harnesses is very much laborious and far exceeds the assembly times required in cases where there are only mechanical parts and their fasteners to handle. Improving cost efficiency of a cable harness design starts similarly from streamlining the structure of the product by examining different component alternatives and manufacturing process options available. (Boothroyd 2010.) Product architecture is a key thing when starting to think about minimizing the number of components. Ideally the electrically linked systems should be placed side-to-side relative to each other in the product layout or even merged together completely. This would mean getting rid of the need for cable harnesses in between the systems, and hence removing of all the related assembly and material costs. If connecting wires must be used, they should primarily have direct pin-pin connections between the systems, instead of routing them through separate terminals or connectors which all add up to total component amount which have to be separately procured, logistically handled and installed. The fixing elements of the harness should be integrated in the product chassis whenever feasible. For example, to add simple fixing elements to an injection moulded casing it is not often a drastic cost increase, if hence on the harness assembly some individual cable ties, taping and other auxiliary elements can be removed. (Ong & Boothroyd 1991.)

The analysis of the wire harness product structure is natural to start from the wires and cables themselves. Wire is usually referred as a construct which contains a single bare or insulated conductor, whereas cable is constructed of multiple conductors inside a common insulation. The wires can have a solid or stranded core, and cables can be configured for example as multi-wire, twisted-pair, ribbon-cable, or as coaxial cables. While the electrical performance and most essentially the current transferring capability are the driving properties for the conductor selection, nevertheless also many other factors must be considered in the selection process such as mechanical strength, insulation type and price. Solid core wires perform well in high-frequency current transfer, but do not offer the same mechanical elasticity as stranded core wires. Thus, they should be only used in applications where the wire ends are sturdily connected and not exposed to vibration to avoid mechanical failures of the wire. Widely used standard in the industry for conductors is the American Wire Gauge (AWG), which defines the cross-section parameters of the conductor. In a twisted pair -cable, two wrapped stranded core wires are twisted together in helix form. Hence, the wires cancel each-others magnetic fields, and the signal noise is reduced to minimal. Another low-noise cable construction is the coaxial-cable, which is used widely in radio- and TV-signal cables. There the core conductor is wrapped first in insulation, and radially on top of that is a conductive braided shield before the outmost insulation layer. Flat ribbon cable is a multi-wire -cable where the wires are fixed side-to-side inside a common rectangularly cross-sectioned insulation. The advantage of the ribbon cable is that it is very cost efficient because multiple wires can be prepared and terminated in one operation with often automated processes. Ribbon cables also perform well in transferring rapid digital signals, and the relative electrical properties of the single conductors to each other such as capacitance are well controlled. (Boothroyd 2010.)

When selecting the wire and cable specifications for the design, the effect they have to preparation stages in the cable harness assembly process must be analysed. Ong and Boothroyd (1991) present generalized methods to estimate assembly times in different assembly phases of cable harness products. They state based on their experimental research, that wire cutting time in typical mechanized processes where the machine feeds the wire from a spool and cuts it to a designated length is directly proportional to the length of the cut wire, in form of an equation:

$$T_c = 0.1 + 2.8 * L_w \qquad (1)$$

where T_c is the time required for cutting in seconds
L_w is the length of the cut wire measured in feet

After the wire or cable is cut to desired length, usually the insulation must be stripped off from the ends for further connections. The time for the stripping operation can be assumed to be manually 7 seconds, and 3 seconds with mechanized process. (Ong & Boothroyd 1991.)

After the preparation, normally the individual conductors must be terminated to a connector or a terminal pin. These connections can be classified in three categories based on the connection technique used in each case, namely soldered connections, low-pressure connections, and high-pressure connections. The aspects to consider when choosing the connection type are the electrical requirements of the systems they are connected to, the conductor types used, the number of contacts needed, and the cost of both materials and operations. (Boothroyd 2010.)

Soldered connection is the most all-around and solid solution in joining conductors to connector or terminal pins. When properly made, soldered connection provides a strong mechanical joint, and a well performing electrical coupling. The downside of soldered connections is that they are by far the most time-consuming, and thus the most expensive type of connection available. The procedure may include several unproductive preparation steps, such as pre-fixing the conductors to the counterpart or separate soldering lugs. The technician performing the job must be highly qualified, and yet the risk remains for faulty connections where the electrical performance does not meet the requirements. (Boothroyd 2010.) When determining the process time for soldering a regular connector to set of wires, the defined process starts from inserting the connector to a fixture and filling its solder cups with solder. The operator handles the wire-set in one hand and inserts them one-by-one into the corresponding connector pins while simultaneously applying heat to the solder cups remelting the material. The wire ends are held in their position until the solder solidifies before moving to the next coupling. The elapsed time for the whole process can be estimated from the following equation:

$$T_s = 7 + 11.4 * N_{wp} \quad (2)$$

where T_s is the time required for soldering process in seconds
N_{wp} is the number of wire-pin -pairs in the connection to be soldered

(Ong & Boothroyd 1991.)

A low-pressure connection is any connection that can be connected and disconnected by hand without separate tooling. Most of the regular electrical connectors fall under this category, and they offer a compromise between decent electrical performance and ease of assembly. Low-pressure connectors can be further classified in sub-groups of rectangular and circular connectors. An example of rectangular connectors are card-edge connectors, that can be plugged straight on the edge of a PCB (printed circuit-board), to which the circuit conductors are terminated on PCB's side. A card-edge connector is often single sided, but rectangular connectors can also be two-sided with both male- and female contacts in separate halves. Shielded DIN, coaxial and other circular cross-sectioned connectors with receptacle and plug parts can be categorized as circular connectors. Proper coupling between the connector halves is important especially in environment where the product is exposed to vibrations or other kinetic impacts. Several coupling solutions are offered in industrial solutions, such as snap-fit, latch, friction, or bayonet couplings (Figure 9). The major advantage of using connectors is the fact that they can be easily assembled and disassembled. The risk for mistakes on the assembly and especially on maintenance is decreased, when the wires remain on proper configuration when the connector halves are separated. (Boothroyd 2010.)

Bare wire ends are often connected to the connector contacts by crimping. In manual crimping, the wire end and its contact terminal are placed to a crimping tool. The jaws of the tool are pressed together with a high force such, that the cylindrical partition of the contact terminal is plasticly deformed squeezing the bare wire forming an electrical coupling and a permanent mechanical joint. Crimped wire-contact -pairs are then installed to the connector body by hand or with a separate installation tool depending on the connector design. In the harness assembly process this can be carried out already in the wire preparation stage, or when the harness is assembled on the jig depending on the harness configuration. The total time required for assembling a connector is:

$$T_p = 2.6 + 17.3 * N_{wc} \quad (3)$$

where T_p is the time required for connector-wire coupling in seconds
N_{wc} is the number of wire-contact -pairs in the connector

(Ong & Boothroyd 1991.)

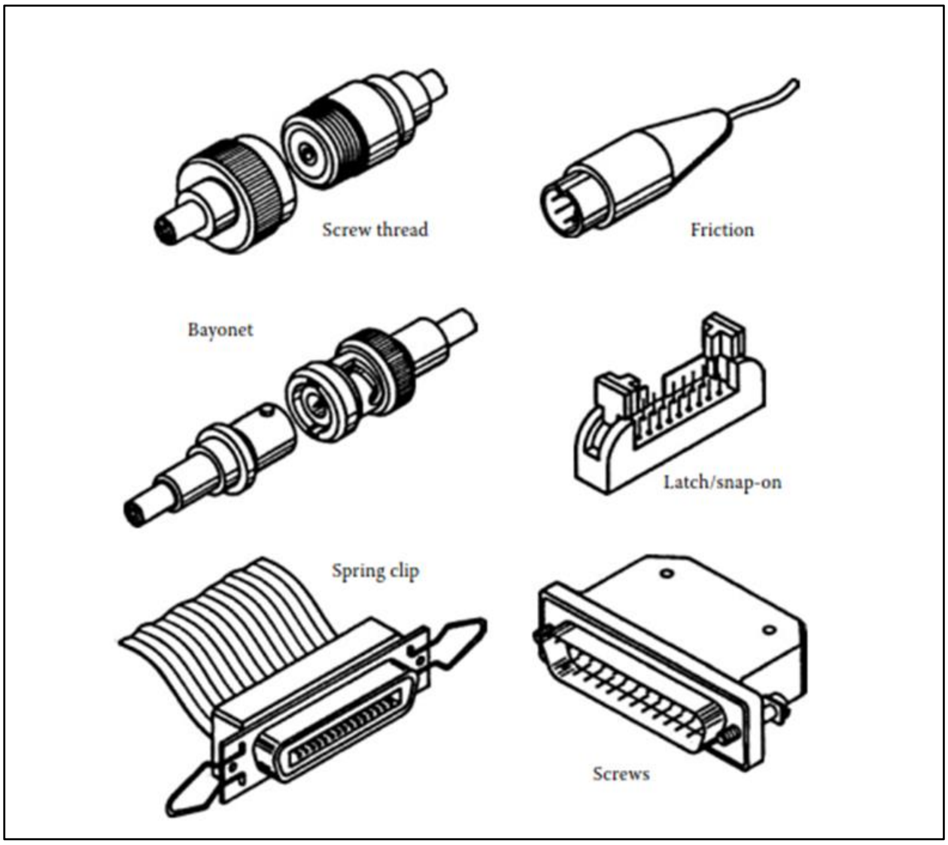

Figure 9: Different connector and coupling types (Boothroyd 2010).

For semi-automatic crimping processes, using 3 seconds for the crimping and 6 seconds for manually inserting the crimped wires to the connector contacts is recommended in the initial analysis. More advanced machines can perform the stripping of the wire and crimping it to the contact terminal successively on a single wire insertion. In this case the total time elapsed can be assumed to be 3.6 seconds. Ultimately in highly automated wire preparation processes the machine can perform feeding, cutting, stripping, and crimping of the wires automatically. In such well optimized process, a process time of 1.8 seconds per wire end per ten feet of wire length can be assumed. (Ong & Boothroyd 1991.)

Crimping is an example of a high-pressure connection, which is such connection where a tool or a separate process is needed to generate the metal-metal contact by plastic deformation or pressure. Other examples of this class are screw-locking and wire-wrapping. In wire-wrapping, the bare conductor end is wrapped tightly in a spiral form around the pin of the connecting end. This results in a reliable mechanical connection with large contact area and thus good electrical performance. A well-made wire wrap is airtight, and with time the materials of the conductor and pin will diffuse, and the connection becomes stronger and weld-like. A screw connection is a configuration that is for example used for most traditional car batteries. A bare conductor end or a lug is clamped down to the counterpart with a screw or a nut. This is a simple and robust connection used in improvised field conditions, but it has its own drawbacks. For example, the screw connection becomes easily exposed for corrosion, and the electrical performance is not exclusively great either. (Boothroyd 2010.)

After the wire and cable preparation including cutting, stripping, and terminating the wires is completed, the following step in the cable harness assembly process is to lay the wires and cables to the harness assembly jig. A single wire or cable is fixed to the jig from the other end with a temporal spring-fastener or the connector in which the wire is terminated to is placed into a fixing element on the jig. The wires and cables are then manually routed through their designated path defined in the electrical schematic. Lastly the other end of the wire or cable is fixed to the jig from the other end as well. If a group of wires or cables have exactly the same starting and ending points as well as routing, they should be inserted to the jig in a single action. The required time for laying wires and cables (without connectors attached) to the harness assembly jig can be derived from an equation:

$$T_a = 6.4 + 3.8 * N_w + (0.5 + 0.4 * N_w)L_w \qquad (4)$$

where T_a is the time required for laying the wires or cables
N_w is the number of wires or cables
L_w is the length of the wires measured in feet

After all the wires and cables have been laid to the assembly jig, partitions of the harness having common routing are wrapped together, thus forming the trunks and the branches of the harness. This can be done by cable ties, taping or tubing. For cable tie insertion including acquiring, looping, tightening, and trimming the end a time of 14.4 seconds is given for the whole procedure per a single cable tie. Similarly inserting a one layer of tape locally around a bundle can be assumed to take 13.8 seconds. The time required in installing a pre-trimmed wrap or sleeve around the bundle varies a lot depending on the configuration, like the diameter difference between the bundle and tube. However, values of 7.4 second for the first inch of the bundle, and 2.4 seconds per inch when proceeding after the start can be used in the initial analysis. The final stage of the cable harness assembly process is to connect the rest of the loose wire ends to connectors or wire terminals. (Ong & Boothroyd 1991.)

2.3 Flexible cable modelling

Conventionally the cable routing design and the assembly feasibility have been validated with physical mock-up -prototypes of the product. It is not unusual that feasibility issues and even design flaws are noticed only at this stage, and they can lead to significant changes in the product architecture. This kind of validation process is repetitive and creates notable costs both through labour and materials. The development on the field of computer-aided design (CAD) has digitalized the product development processes even further in the aim of overall cost reduction and better design quality. (Lv 2020.)

The basic fundament that makes the virtual cable modelling difficult is the same than in the previous chapter concerning the actual physical assembly. Compared to solid parts, cables are flexible, and their shape and behaviour vary a lot depending on the external conditions. Traditionally in CAD-systems cables have been modelled in similar way like solid parts, usually by a given cross-section that follows a specified set of continuous geometrical lines and splines. This method is purely based on mathematical approximation and does not necessary well represent the real behaviour of the cables and might lead to prominent uncertainties in the length definition for the cables. For this reason, a lot of commercial CAD-software developers provide add-ons integrated into their systems that are specialized for cable routing and cabling assembly design, to best fulfil the special requirements set by the tasks. With these tools, the designer can simulate the cable behaviour more completely considering the effects of gravity, stretching, shearing, and bending of the cable. The physics model in the CAD-tool has to provide a realistic representation of the cable behaviour and at the same time be efficient enough to provide the results in real-time without significant processing times. (Lv 2020.)

The simplest physics models assume the cables to be rigid cross-sectioned, one dimensional elastic bodies. The most common models of this type are mass-spring, multi-body, elastic rod, dynamic spline, and finite element method. When advancing beyond those and adding more factors in to the mix, the models can take into account the inhomogeneous and branched internal constitutions of the cable, plastic deformation occurring in the bends and deformation of the cable cross-section. Factors like temperature variation, and dynamic strain imposed to the cable structure during its lifetime are still often disregarded, nevertheless they might have significant effect on the cable's geometry. (Lv 2020.)

The mass-spring model is used broadly in commercial applications, due to its simplicity and thus excellent real-time simulation performance. Lv et al. (2017) present an advanced mass-spring model developed for flexible cable simulations, where they have combined the effects of stretching, bending, and twisting of the cable, and added collision detection to simulate the effects of surrounding constraints to cable routing. The model is based on singular mass points, which are interconnected with different types of springs, which together define the shape of the cable. When a fixed control point is manipulated by the user, the remaining unconstrained points move towards their equilibrium state, meaning their acceleration and momentum caused by the spring forces approaches minimum. (Lv 2017.)

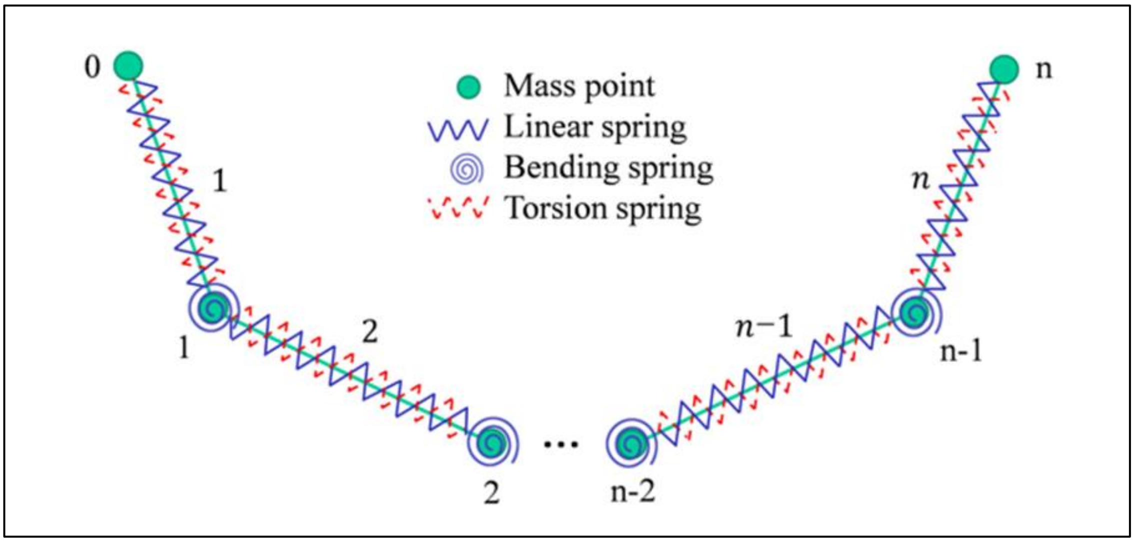

Figure 10: A mass-spring representation of a flexible body (Lv 2017).

The total force affecting a designated mass point can be derived from Newton's second law of motion by taking a partial derivative from the potential energy of the mass point in respect to its position, and adding the external forces like gravity and normal forces to it:

$$F_{tot} = -\frac{\partial E_{pot}}{\partial x} + F^e \qquad (5)$$

where	E_{pot}	is the total potential energy of the spring systems
	F^e	is the sum of external forces affecting the system
	x	is the matrix containing the position coordinates of the point

The potential energies used above in equation 5 are each extracted from following equations. The potential energy stored in a linear spring causing the axial elongation and compression effect of the cable can be calculated from:

$$E_l = \frac{1}{2}\frac{EA}{l_0}(l - l_0)^2 \qquad (6)$$

where	E	is the Young's modulus of the cable material
	A	is the cross-section of the cable
	l	is the distance between adjacent mass points
	l_o	is the nominal length of the cable link

The potential energy stored in a bending spring causing the bending effect of the cable can be calculated from:

$$E_b = \frac{3EI}{2l_i}\beta^2 \quad (7)$$

where	E	is the Young's modulus of the cable material
	I	is the second moment of inertia of the cross-section
	l_i	is the initial length of the cable link
	β	is the angle between adjacent cable links

The potential energy stored in a torsion spring causing the twisting effect of the cable can be calculated from:

$$E_t = \frac{GI_p}{2l_i}(\varphi + \theta)^2 \qquad (8)$$

where	G	is the shear modulus of the cable material
	I_p	is the polar moment of inertia of the cross-section
	l_i	is the initial length of the cable link
	φ	is the geometric torsion angle between adjacent cable links
	θ	is the material twisting angle per a single cable link

(Lv 2017.)

When all three spring mode calculations have been iterated over the mass points such that the system reaches equilibrium state, a geometrical curve is fitted over the points to obtain a smooth graphical result. For example, piecewise Bézier-method can be used for fitting the curve. Figure 11 shows that the shape and behaviour of a cable modelled with mass-spring method seems to correspond relatively well to a real one. (Lv 2017.)

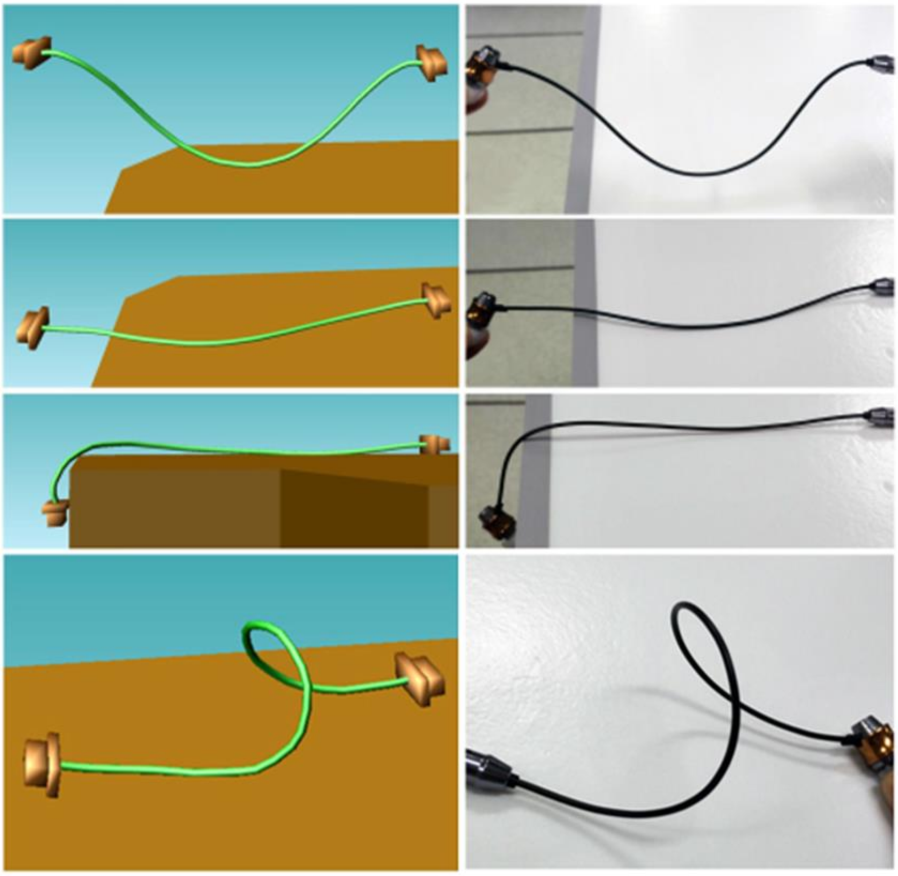

Figure 11: Cables modelled with mass-spring method (left) vs. real cables (right) (Lv 2017).

2.4 Cable harness design in virtual environments

After simulating the cable behaviour with a suitable physical model, natural continuation to improve the representation is to put the model into a virtual environment to fully investigate the ease-of-assembly -aspects by utilization of virtual reality (VR) and augmented reality (AR). Ritchie et al. claims that a traditional CAD-software user-interface is creating notable interruptions for the user especially when performing assembly process design. A more intuitive way of working, like recording the assembly sequence through user's actual motions would be more efficient rather than describing it definitely. (Ritchie 2007.) In a prior study it was discovered, that in specific cable routing tasks the designers completed the task 2-4 times faster in the VR integrated design tool than by utilizing traditional CAD-systems they were familiar with (Holt 2004). Integrating the design process to VR and AR environments allows the designer to simulate the cable assembly process already in very early design phase, when the product level changes are still easy to perform. These novel tools can greatly reduce the total amount of time spent on product development process and improve the quality of the design. (Yang 2019.)

Virtual reality is a broad and somewhat indefinite cluster of technologies. When addressing engineering design related VR-applications, most commonly head-mounted-displays (HMD) based VR systems come into question. HMD-device or more commonly VR-headset consist of a graphics interface directly set up on user's field of sight, and some additional sensors and equipment to track motions and generate sounds and other feedback to the user. VR-based design environments can re-define the means how product development engineers and designers create the concepts, do the design, and plan the manufacturing procedures. (Ritchie 2007.) In engineering, virtual prototyping combined with VR is hastily overcoming traditional physical prototypes in product development processes. CAD-VR integration for plain illustrating purposes has been around for quite some time already, but recently a lot of research and development has been allocated to build a complete and intuitive CAD-VR -user-interfaces that would provide efficient working environment for the designer. Assembly and maintenance simulations have turned out to be especially challenging subjects, since they require a lot of user interaction with the model and a lot of demanding real-time simulations. However successfully simulating these domains would be particularly beneficial, as there are significant cost reduction possibilities included. (Sá & Zachmann 1999.)

Figure 12: User performing design in COSTAR-tool through an HMD and interactive gloves (COSTAR 2004).

Ritchie et al. (2007) developed a VR-based cabling design tool called COSTAR, which had an HMD as the graphical interface and gloves coupled with a magnetic tracking system for user interaction interface with the system (Figure 12). COSTAR was made for completely VR-immersed design process using intuitive human gestures to perform actions in the environment, to avoid interruptions during the creative process. The user was able to route a cable harness by inserting points to desired locations using his/her fingertips, and the cable geometry was generated in real time. Modifying the routing happened by pushing or pulling cable sections, bundling them together or inserting fasteners and connectors to desired locations using the integrated menus. (Ritchie 2007.)

In augmented reality, computer-generated graphics are augmented to real world environments, and the result is projected to the user's vision. The projection can be made either with an HMD, handheld devices, or projectors, and typically the applications include separate user tracking systems and devices for user interaction and haptic feedback. AR has been utilized in the industry for example by car manufacturers, who have had different digital interior design options visualized in AR while the user is sitting in a real car body mock-up. Still, the technology has been used mostly only for similar visualization purposes, and real-time modifications and full CAD integrations are still awaiting themselves. (Nee 2012.)

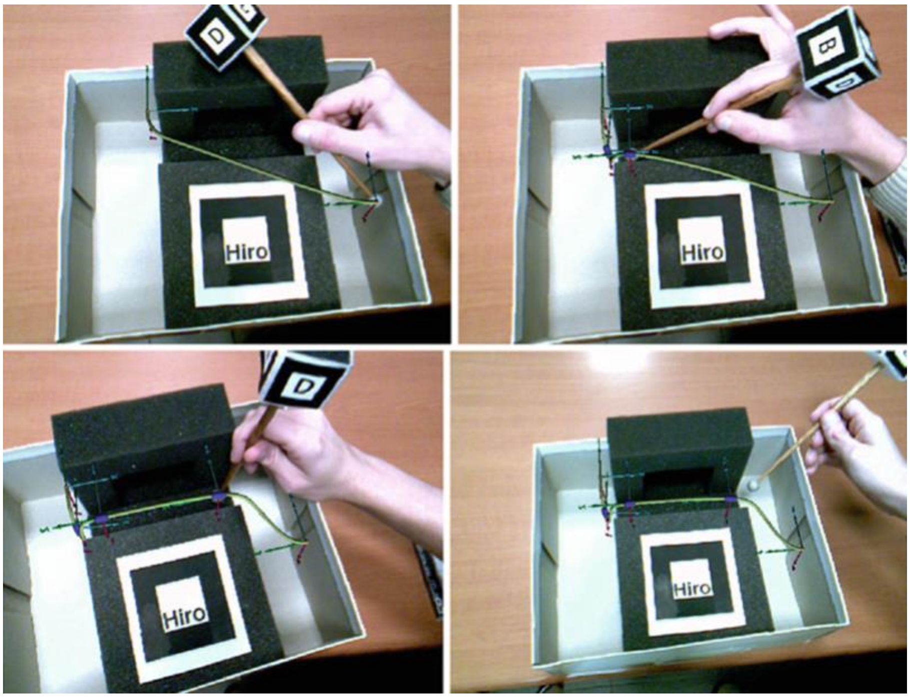

Figure 13: User manipulating cable routing in AR-environment using a pointer (Valentini 2011).

There is a lot of potential use cases for AR in engineering, where for example designers could try to fit still digital and incomplete design to real existing surroundings. In the domain of cable harness design this can be found useful, and there is particular potential in training and testing assembly and maintenance sequences before the actual execution. Also, AR has some benefits in the technical perspective, such that the interaction with the environment is easier and more intuitive for the user, when user's hands are not digitally generated. On Valentini's (2011) AR-integrated cable harness design tool, the virtual cable routing is interactively sketched to its real-world surroundings using a pointer (Figure 13). User is equipped with an HMD, and the surroundings and motions are captured with a normal camera mounted to the front of it. The design process starts by inserting the start and end points of the cable on their desired positions. An initial routing between these points is generated, and a first visual representation of the cable harness is augmented to the users' vision. User can then start intuitively manipulating the routing and placing fixing elements to constrain the harness to a desired shape. The geometry of the cable harness is generated in real-time using elastic-spline -computation method, in which mathematical splines are combined to mechanical elasticity. (Valentini 2011.)

2.5 Automated cable harness routing

To overcome the tedious process of repetitive cable routing design, and to minimize the re-courses spent on the product development process on this stage, there is a lot of effort put on developing completely automated cable harness routing systems. Ideally the system should be such, that it would generate the complete routing as the output, when the designer would feed the connection scheme, mechanical requirements, and environmental constraints as the input. (Yang 2019.)

Zhu et al. (2011) state, that large-scale cable harness routing problems are ideal objectives to be solved with knowledge-based engineering (KBE) -methods. KBE tools are definitely scoped systems, that gather and maintain design information related to the product and help to take the benefits of the former work. In practice this includes automating trivial and unproductive design tasks and transferring knowledge between design domains on understandable format depending on the designers' background. (La Rocca 2012.) On the context of automated cable harness routing, there are a lot of multi-domain design inputs that must be taken into account, to generate correct manufacturing information outputs. All these relevant inputs from mechanical, electrical, and manufacturing aspects are collected into the knowledge base, which also contains the information on relationships between the design inputs. (Zhu 2011.)

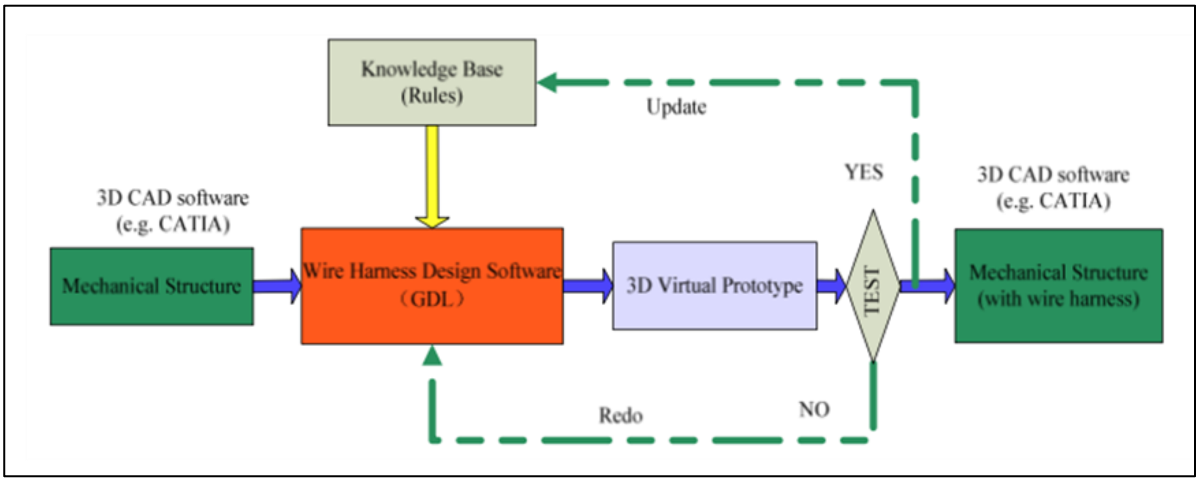

Figure 14: A Schematic of the KBE-based automated cable harness routing system (Zhu 2011).

In the core of the system is the actual harness routing block, to which the design rules and the surrounding environment are inputted (Figure 14). For the harness routing Zhu et. al have developed a so-called W*-algorithm, which is modified from the famous A*-algorithm widely used in pathfinding problems. A*-algorithm is based on dividing the environment to equal nodes, and iterating a simple function for each node:

$$f(n) = g(n) + h(n) \quad (9)$$

where	n	is the given node
	g	is the cost of movement to the node from the start
	h	is the estimated cost of movement to the end from the node

The route in then selected by progressing through the nodes choosing a lowest function value from available nodes each time until the end is reached. (Zhu 2011.)

Since the cable harness routing in practice usually follows some surfaces of the surrounding structures to which the harness is fastened, Zhu et al. developed their W*-algorithm (wall attraction A*-algorithm), to utilize the prior strategy efficiently in 3D-space. They meshed the 3D-model of the environment into tiny cubes, which are classified to belong to wall structure or empty space. The start and end points of the harness are defined, and the W* algorithm starts to look for the optimal routing along the cube faces that are classified as walls structure. The routing geometry can be exported as general CAD file formats like STEP and IGES, for further manual adjustments in CAD. Figure 15 shows a cable harness routing generated with W*-algorithm inside an aircraft wing structure. (Zhu 2011.)

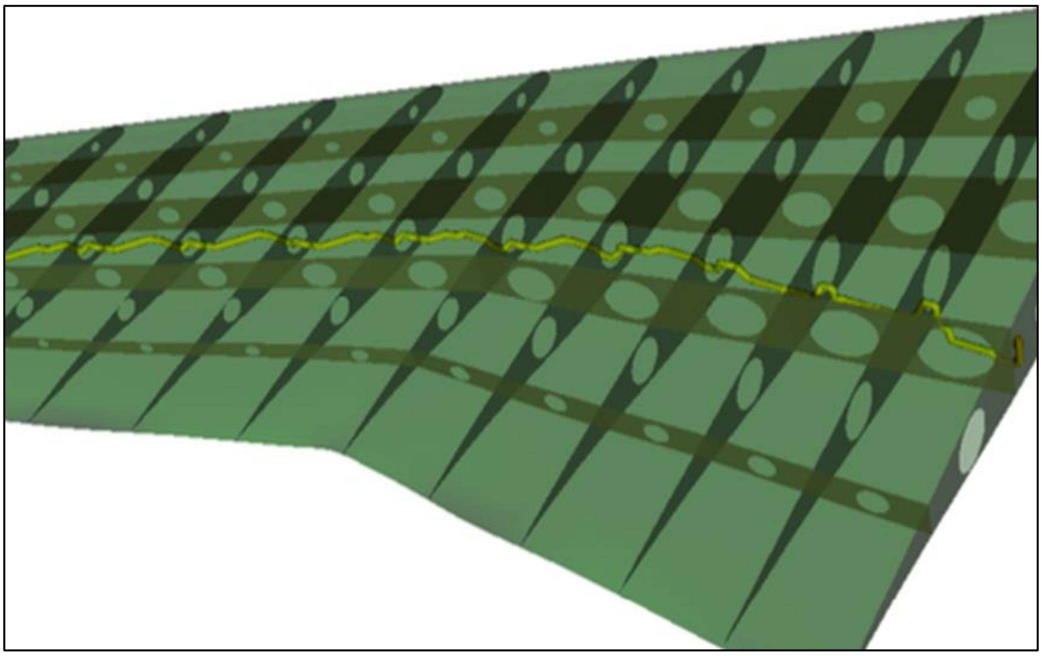

Figure 15: A cable harness (light green) generated with W*-algorithm routed through a wing structure (Zhu 2011).

Combining the physics simulation of a flexible cable to an automatic routing algorithm is a giant leap in terms of model complexity and therefore needs more computational resources. Hermansson et al. (2016) have approached this problem by creating a two-phase grid-search algorithm combined with simulation of the physical behaviour of the cable based on Cosserat rod theory. The first stage of the sequence is called nominal routing, where the spatial grid is comprehensively pre-processed to rule out unusable zones and a heuristic cost field is formed. A so-called $\mathbb{R}^3$-sweep is performed first over the spatial grid, to provide an initial understanding of possible collision free routes and estimate their cost fields. Dijkstra's algorithm is launched from the start node to generate a network of optimal routes to accessible nodes. When the full routing roadmap and the cost field have been derived with $\mathbb{R}^3$-sweep, roadmap zones that do not likely include the optimal route are excluded. This is done by setting up an exclusion factor μ that defines a sub-set of nodes, for which the cost for ideal route connecting through is at maximum μ times bigger than the cost. A path searching algorithm based on A* is then iterated for the sub-set gradually increasing μ until a satisfactory routing is established. (Hermansson 2016.)

After the nominal routing phase, the local refinement phase is executed. The nominal routing created formerly does not take into account the physical internal stresses imposed to the harness by it or gravity effecting it depending on the orientation. When the flexible cable simulation model is established, it might be that the initial routing does not meet the design rules, or it might collide with the surroundings. The simulation model that Hermansson et al. uses is Cosserat rod theory, which is based in shearing, stretching, bending and torsion of one-dimensional slender rods. One dimensional in this context means, that one of the three dimensions of the body is substantially larger than the two others, which is the length in the cable's context. The potential energy density of the rod is derived based on shearing/stretching and bending/torsion strain components stored in the initial routing configuration resulting from nominal routing phase. Gravity and contact forces with the environment are added to the mix, and then the local refiner -algorithm starts to iterate the cable configuration towards mechanical equilibrium state that fulfils the design rules and is locally optimized for the routing cost. (Hermansson 2016.)

Hermansson et al. demonstrated their approach on a routing task of aluminium gas pipe in a confined engine compartment of a vehicle. On Figure 16 left side they illustrate three different routings with varying weights on given optimization criteria. The red route is optimized for length, green is optimized for clearance in respect to the surroundings, and blue is optimized for number of turns. On the right side is the result of the aluminium gas pipe routing task optimized for length. The computation time for that specific task was 7.4 seconds, performed with a regular desktop PC. (Hermansson 2016.)

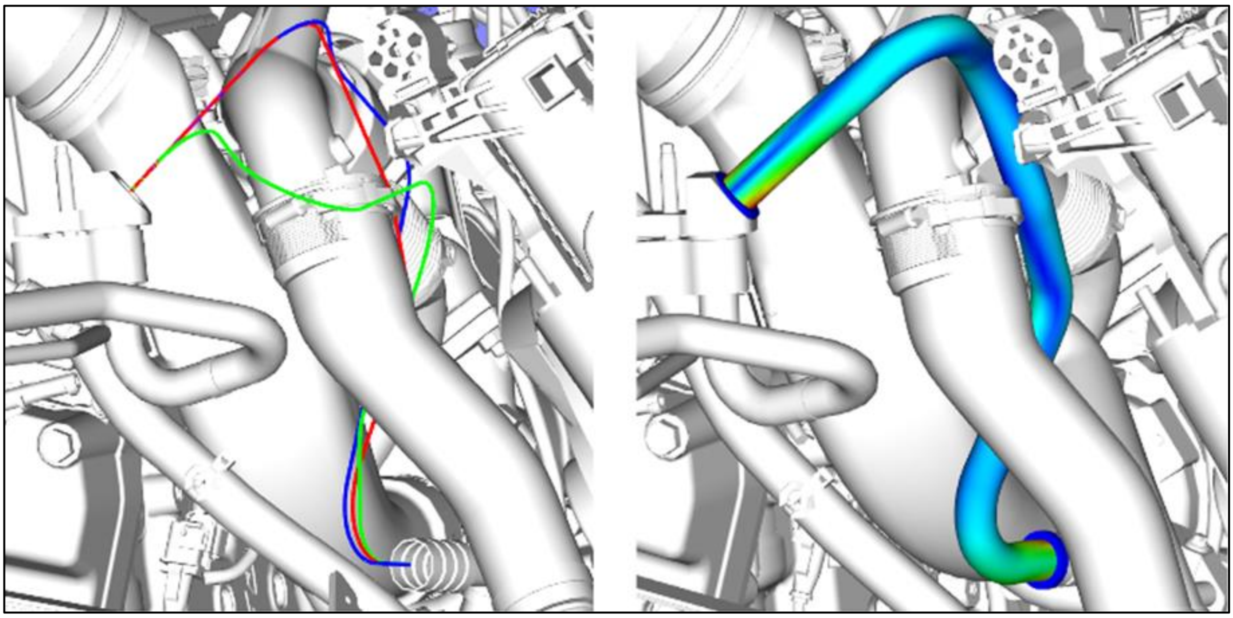

Figure 16: An aluminium gas pipe routing in an engine compartment of a vehicle (right side). Routing options with different weighing are displayed on the left. (Hermansson 2016.)

3 The design of TB2S ladder services

3.1 Starting point of the design

The ladder will be the primary support structure for the 2S-modules in the TB2S sub-detector, and it is structurally based on to the same concept as its predecessor TOB-rod. The main frame made from carbon fibre constructs of two longitudinal C-profiles which are joined together by transversal crossbars. Aluminium inserts are glued to the C-profiles in a high-precision jig, and they ensure the rigid support, accurate positioning, and the cooling heat-transfer for the 2S-modules. Each ladder holds 12 modules, which are arranged in two r-planes along the z-axis of the tracker according to the tracker layout (Figure 5). The modules are named such, that module #1 locates on IP's end, and module #12 locates at the outer end. A stainless-steel cooling pipe routes through the mid plane of the ladder connecting to every insert successively and makes a loop in the inner end to route back towards the front end of the ladder. A total of 368 ladders are assembled to the TB2S wheel by sliding them in from the wheel ends, and precision aluminium spheres mate with opposite slot-inserts fixed to the wheel which ensure the accurate positioning of the ladders. There are two variants of the ladder, which are assembled from the opposite ends of the tracker, namely Z-minus- and Z-plus -ladders. The difference between the two is the slight variance on the 2S-module Z-positions, due to the asymmetric tracker layout driven by the magnetic field directions on the CMS detector.

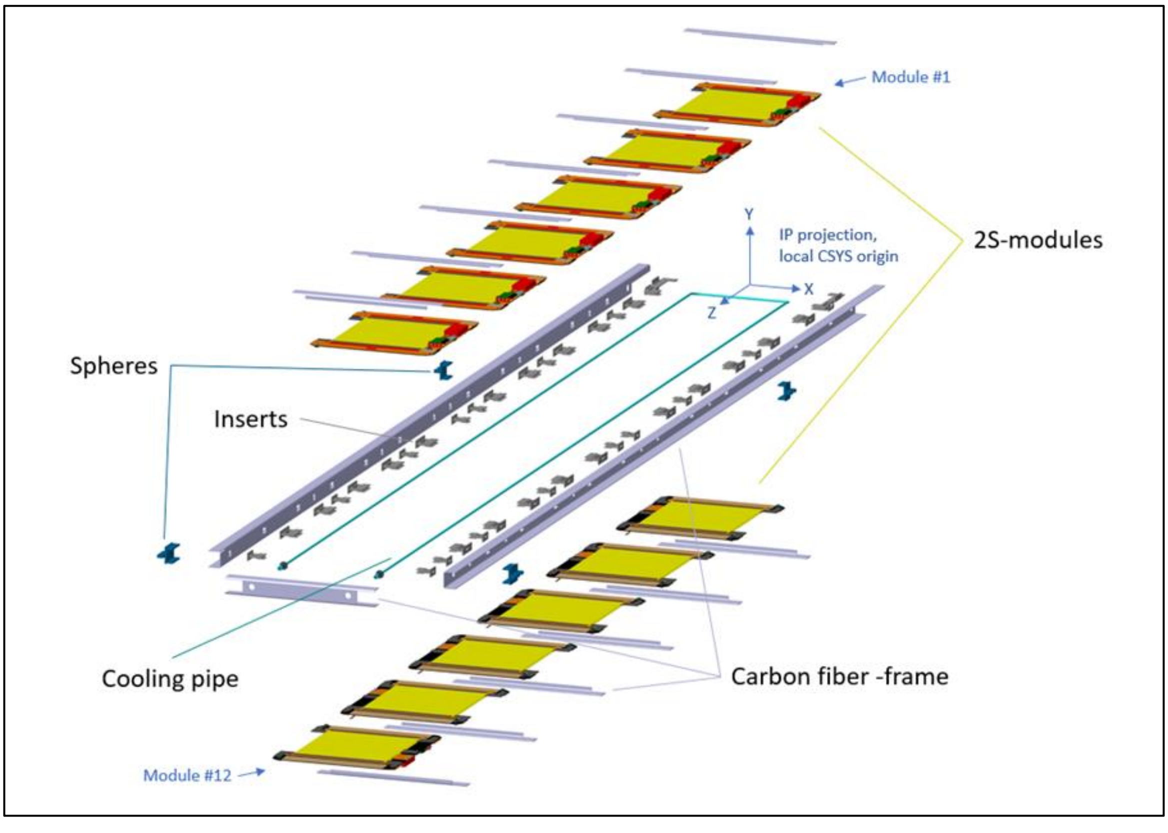

Figure 17: An exploded view of the initial ladder design.

The 2S-module constructs of two strip-sensors on top of each other, their supporting electronics on the three hybrid circuit boards, and from three or four aluminium-carbon fibre - bridges that are the main structural element between the components. The two front-end - hybrid circuit boards (FEH) which are perpendicularly to the strips are connected to the sensors and host the CBC's (CMS binary chip) which collect the analogue signals coming from the silicon strip sensor, amplify them and convert to a binary format. The service hybrid (SEH) which is parallel to the sensor strips holds the rest of the auxiliary electronics and provides connectors for electrical power inputs and for optical control and data links. The module is positioned and fixed to the external support structures from the pads located on the main and stump bridges, and the bridges transfer the heat energy generated on the module to the external cooling loop as well.

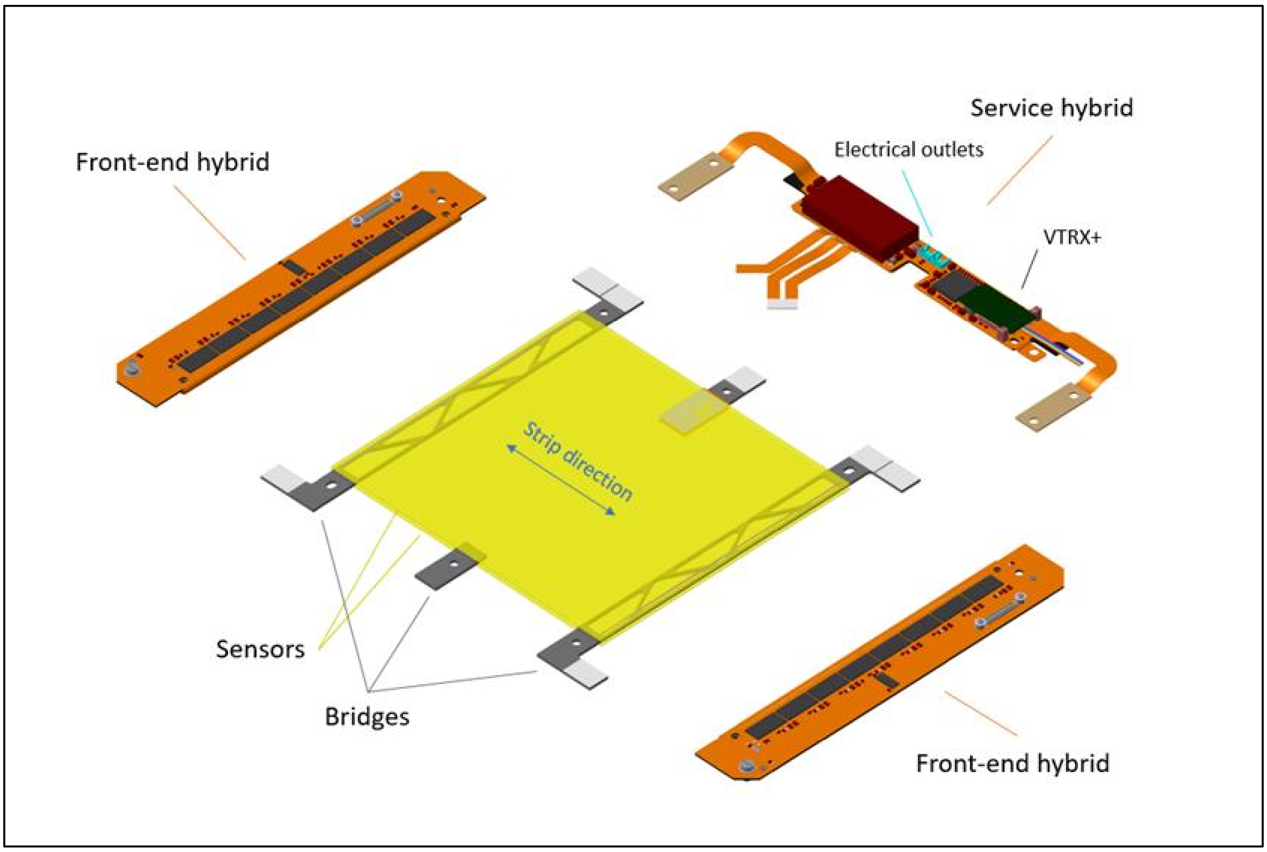

Figure 18: An exploded view of the 6-pad 2S-module design.

The module requires electricity for its powering, optical connection to transfer its data, and cooling to keep the sensor inside its safe operating limits. These module services need to be integrated to the ladder structure to fit in among the internal structures and inside the external space envelopes while having the connectivity interfaces easily accessible during different assembly stages. On the same time the design must fulfil the specifications of the service materials themselves and be feasible to be manufactured and assembled in the serial production. On the start of the thesis project, an initial 3D-design of the ladder existed (Figure 17) with the carbon fibre structures, aluminium inserts and the cooling pipe in place. However the routing, connector positioning and exit interfaces of the electrical and optical

services were not yet considered, and the cooling circuit had some important aspects missing, like the pre-heater location and its wiring.
As the design processes between different domains are advancing simultaneously at CERN, the first phase of the design process was to obtain the latest specifications and schematics of the electrical and optical designs from the respective teams in the organization. Information about the pin-pin connections, conductor, fibre and pipe mechanical properties and the connector types were gathered and studied thoroughly.

The module electric power is carried along three lines, which are namely high voltage (HV), low voltage (LV+) and ground (LV-). The lines are routed from the individual module in the ladder to the PP0 -patch panel which locates on the outer rim of the wheel. The lines are split in to two segments: pigtails and octopuses. The pigtail is a shorter segment which connects to the module SEH and terminates into a connector, which is coupled to corresponding connector in the octopus. The octopus is a wrapped harness, which has branches with connectors connecting to the pigtail connectors. Using such architecture ideally allows to use topologically uniform module design with equal length pigtails installed already in the module assembly centres, instead of having 12 module variants each having slightly different wire lengths depending on their Z-location on the ladder. In the octopus all the wires coming from the module pigtails are terminated to two terminal connectors other one gathering all the LV+'s and LV-'s, and the other one all the HV's. These two terminals are then connected in the PP0-patch panel to cables about 50 meters long that join the modules to the power supplies located in the CMS service cavern.

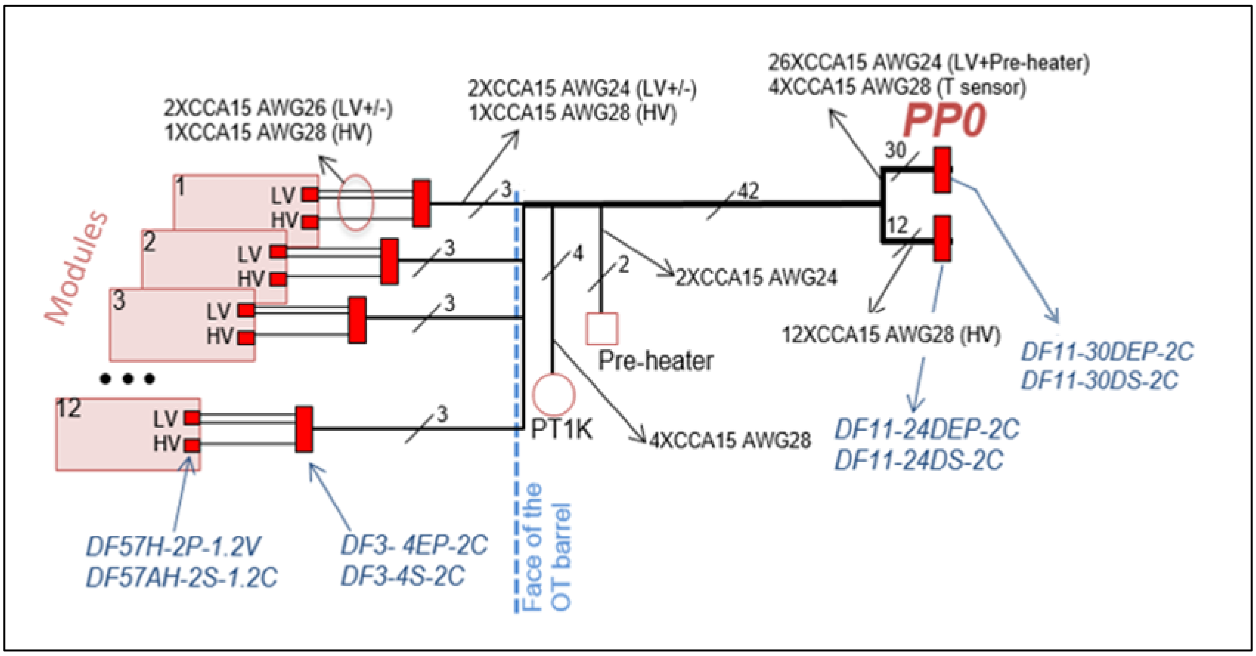

Figure 19: The PP0-Ladder -electrical schematic (Bacchetta 2018).

Copper cladded aluminium (CCA) -wires are used throughout the system up to the PP0 to minimize the mass in the tracking volume. On the module pigtail an AWG26 twisted pair is used for both LV's, and a single AWG28 conductor for the HV. The same type of AWG28 continues on the octopus-partition of the line for the HV's, and the LV's continue as an AWG24 twisted pair. The twisted pairs are used to neutralize the magnetic field induced by the conductors, thus reducing the signal noise in the system. The 2-pin connectors connecting the pigtails to the modules are Hirose's DF57-series, the 4-pin connectors between the pigtails and octopus branches are from their DF3-series, and the 24- and 30-pin connectors connecting the octopus to the PP0 are from their DF11-series. All the used connectors are snap-on -type, in which the conductors are mechanically crimped on.

On the optical domain the architecture is similarly divided to pigtails and a common bundle, which is called the naked-fanout. The pigtail has two active fibres inside a common tubing, and it is connected to the VTRx+ -chip located on the module SEH. On the VTRx+ -chip the optical signals are generated by its laser diode driver and sent out along the pigtail fibres (Troska 2017). The free end of the pigtail terminates into an MT-ferrule, which is a connector casing used to align the optical fibres for a connection. The designated naked-fanout branch for each module has a similar MT-ferrule, the two are joined together along alignment pins put through the MT-ferrules, and a spring clip secures the connection together. The naked-fanout branches are gathered inside a common wrapping, and eventually all 24 fibres terminate into a common MT-ferrule. This MT-ferrule is plugged into an MT/MPO -adapter, to which a patch cord with an MPO-connector is plugged to propagate the signals out from the detector.

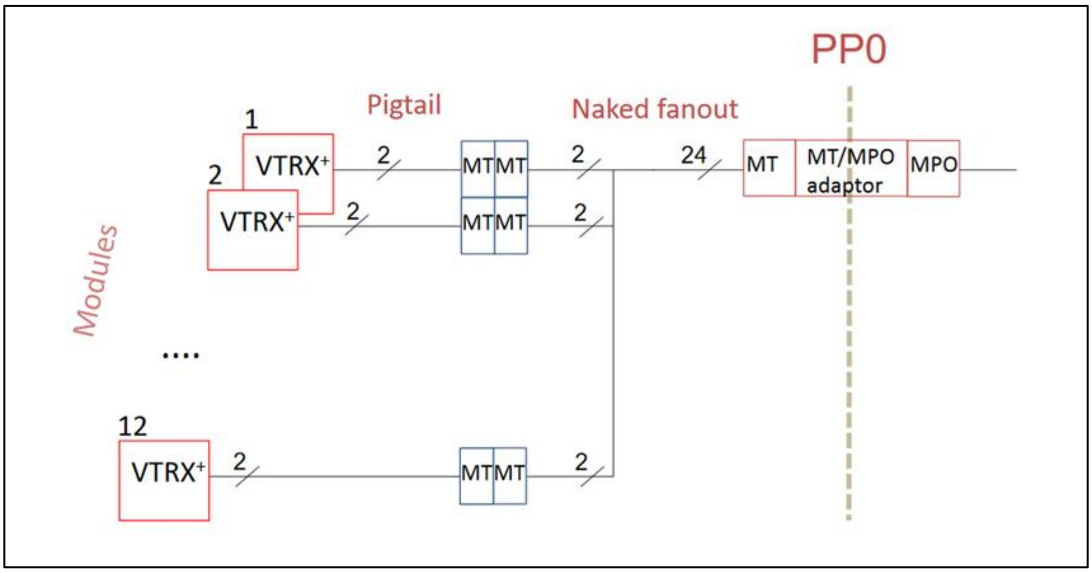

Figure 20: Optical schematic of TB2S (Vasey 2020).

On the optical domain, the crucial parameter that has to be taken into account in the routing, is the minimum allowed bending radius of the fibres. This is because the optical signal propagation in the fibres is based total internal reflection, and sharp bends on the route cause attenuation and in the worst-case the fibre can crack and become inoperative. The MT/MPO -adapter should be placed somewhere towards the outer end of the ladder, so that the MPO-connector is easily pluggable to it after the ladder has been installed into the wheel.

The temperature of the module sensors needs to be maintained sufficiently low to avoid the so-called thermal runaway. Thermal runaway is a critical phenomenon, where the sensor temperature starts to rise exponentially due to a reflexive loop between the leakage current and the sensor temperature. On layer 1 of the detector where the radiation luminosity is the highest, the nominal operation voltage of the silicon sensors needs to be correspondingly high. Increasing the voltage causes larger amounts of leakage current between the sensor layers, and thus heats up the sensor material. As a result, the thermal conductivity of the sensor material decreases attenuating the cooling effect, further escalating the loop and eventually irreversible damage is caused for the sensor. The overall heat dissipation in the OT is about 100 kW, and that is overcome by a two-phase CO_2 cooling system. Using CO_2 as the coolant enables to use small cross-sectioned pipes in the detector, due to its large evaporation pressure and low viscosity. This is beneficial, since minimizing the mass inside the tracking volume is the driving philosophy of the whole tracker design. Before entering the tracker, the liquid CO_2 flows through small cross-sectioned capillary pipe and enters a larger inlet pipe just before the tracker, which causes a significant pressure drop in the CO_2. Fixed on to the inlet pipe there is a pre-heater resistor, which heats up the CO_2 triggering the partial evaporation. After the inlet pipe the CO_2 enters the ladder cooling pipe and ideally flows through the circuit only partially evaporated, thus ensuring maximally efficient heat transfer from the pipe surfaces to the CO_2 itself. The electrical services needed for the pre-heater and its temperature sensor are taken from the octopuses of the ladders in the specific cooling loop.

The heat generated by the module is normally conducted along the module bridges to the ladder inserts that are cooled by the cooling pipe which is directly attached to a slot in the insert edge. Over the IP where the two ladders overlap, the case of module #1s is more difficult. The normal inserts are attached to the ladder mid-plane, and the insert thickness is driven by the deviation of the r-planes of the tracker layout. On module #1 the inserts connecting to the further module pads cannot exceed the ladder mid-plane, because the Z-minus and Z-plus -ladders would then clash each other on the overlap region. Thus on the module #1 region, the last inserts are fully attached to the ladder from the stump bridge contact area only, and the special insert then reaches on along thinner cross-section above the midplane to the further module contact pads. The C-profiles are similarly cut to make the cross-over setup possible. Using such special geometry on the final inserts means, that the conduction length from the further module pads to the cooling pipe is substantially longer than in the configuration of the other modules. Based on FEM-simulations that were done earlier with the preliminary ladder design it was evident that some changes were needed to be done to the geometry of the special insert to increase the thermal performance of module #1.

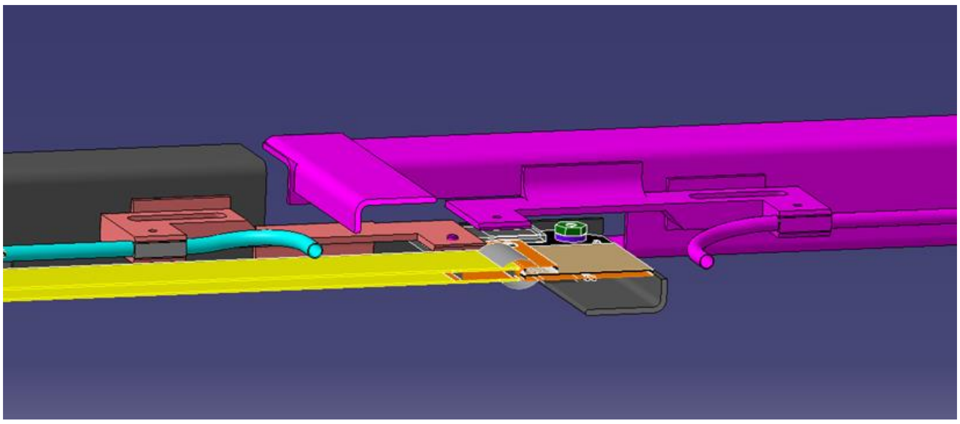

Figure 21: YZ-section view of the special inserts in the ladders' overlap area. The Z-plus ladder is coloured in magenta, and its module #1 is hidden for clarity.

To make the tracker hermetic and light on the other hand, the tracker structure is very packed and the service exit envelopes from the TB2S is very compactly defined. All the TB2S services exit the ladders from the ends of the wheel, and they need to be neatly arranged and routed forward within the envelopes while keeping the assembly procedures simple. As can be seen from the Figure 22, there is only 73mm of space in Z between the TB2S-ladder front, and the TEDD inner end. Both the TB2S and TBPS services must be arranged in this gap before they are routed forward in between the BTL and TEDD to exit the tracker.

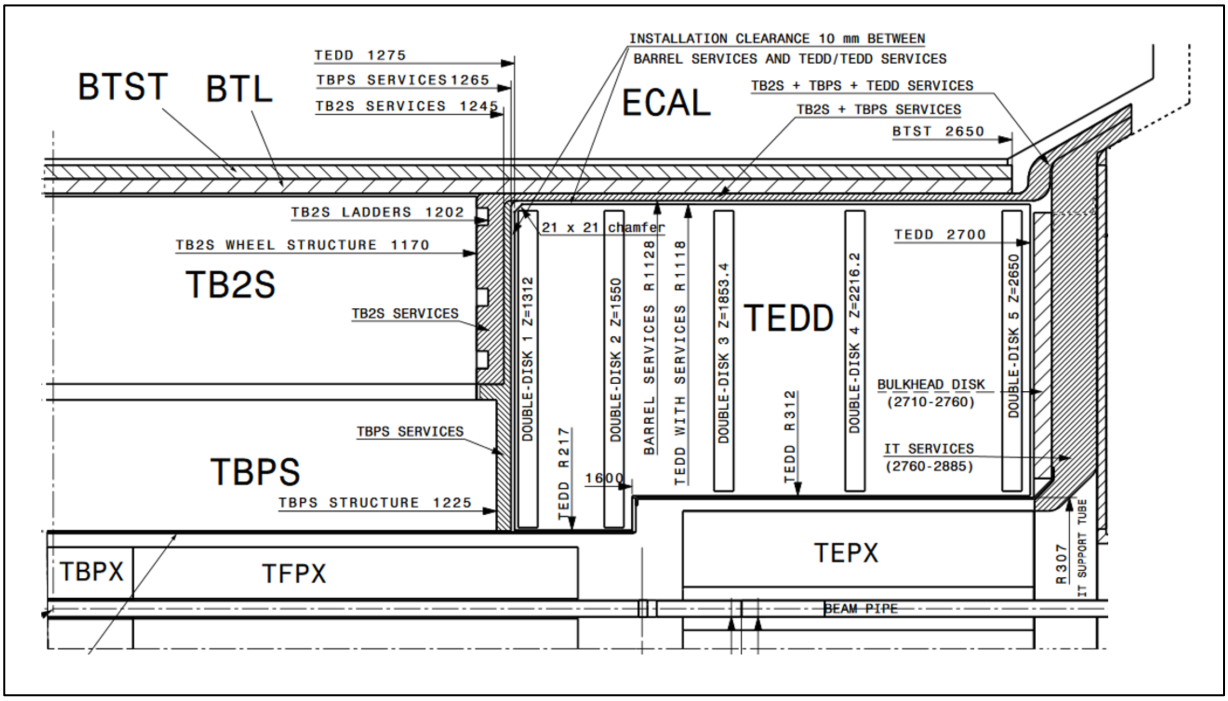

Figure 22: The service space envelopes of the OT. All the annotations are in millimetres in respect to IP (Lenoir 2021).

The worst case for the TB2S is with the layer 3 ladders, where the electrical PP0s are attached just to the front of the ladders. This case is illustrated in Figure 23, where a single layer 3 - ladder is positioned to the TB2S wheel and a PP0 (magenta) is placed on front. There it can be seen that the clearance between the two is less than 25mm, which is really minimal to manage the service exit from the ladder. For example, the optical patch cord which will be attached to the naked-fanout of the ladder with an MPO-connector (Figure 20) requires minimum bending radius of 60mm, so it is clear that this specific area must be studied carefully while designing the service exit interface in the ladder's context.

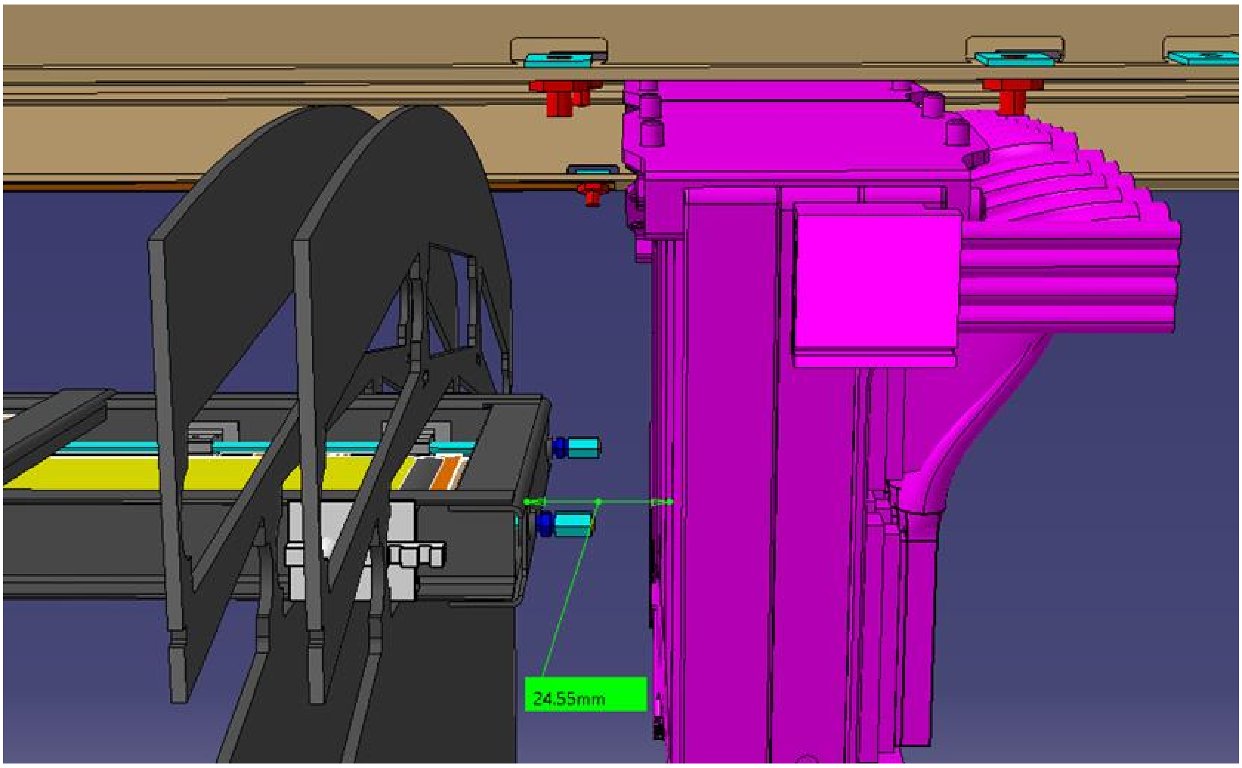

Figure 23: 3rd layer ladder installed inside the TB2S wheel. The PP0- casing on front of it is coloured in magenta.

3.2 Conceptual service design

Modules and especially their sensors are very delicate and sensitive components, and therefore great caution must be conformed while the modules are handled and assembled to the ladder. On the service design all the assembly stages must be carefully thought through, so that all operations can be performed safely when handling loose wire and bundle ends manually and with different tools.

When thinking of the concept for optical and electrical service routing from an individual module towards the outer end and eventually to exit the ladder, it quickly becomes evident that it would be convenient to utilize the longitudinal C-profiles of the ladder as cable channels. This would allow neatly to pack the wires, fibres, and connectors inside the C-profile envelope, dedicating the space in the middle section of the ladder fully for the modules, as any loose wires routed and handled there might potentially cause damage to the sensors. Also, as the SEH's of the modules conveniently locate on the edge next to the C-profiles, the pigtails can be directly guided into the C-profiles. The modules on the two r-planes would be ideally oriented such, that half of the module pigtails would route to the other C-profile, and the other half into the opposite C-profile. The sensor in the module is centred relative to the mounting holes on the bridges, so rotating the module 180° around the Y-axis is possible in any location in the ladder if desired. Opening gates would be cut to the C-profiles to designated locations, such that the pigtails are convenient to string through. The pigtail-octopus/naked-fanout -connection would be made inside the C-profile, and the mating connectors would be attached to the C-profile flange. The octopus/naked-fanout wires and fibres would continue then towards the front of the ladder along the C-profile channel.

In principle the octopuses/naked-fanout trunks could continue all the way to the front-end along the C-profile and exit to the space in front of the wheel. This would however be in many ways a problematic solution, as the trunks of the octopus/naked-fanouts would have to be then united in the front of the ladder, and for example the optical MT-MPO -adapter where the trunks are terminated to, would require a separate support bracket to be attached to the wheel. Doing this especially on the layer 3 (Figure 23) is not feasible simply due to the lack of space available. Also, the octopus/naked-fanout trunks would have to pass through the outer sphere support bracket located on the end of the C-profile and leave enough space for the ladder installation fork which takes support from these same brackets.

Much more attractive solution for the octopus/naked-fanout routing would be re-entering the middle section of the ladder on the backside of module #12, uniting the trunks there, and then exiting through the front panel of the ladder. The front panel could be used as a sort of a patch panel itself, as the cooling pipe connectors, optical MT-MPO -adapter and the electrical octopus could be supported to it directly. With this strategy the services would remain neatly inside the ladder frame envelope, the connection interfaces would be conveniently exposed, and the ladders could be equipped fully with their services before assembling them to the wheel. The routing concept is illustrated as a schematic in Figure 24.

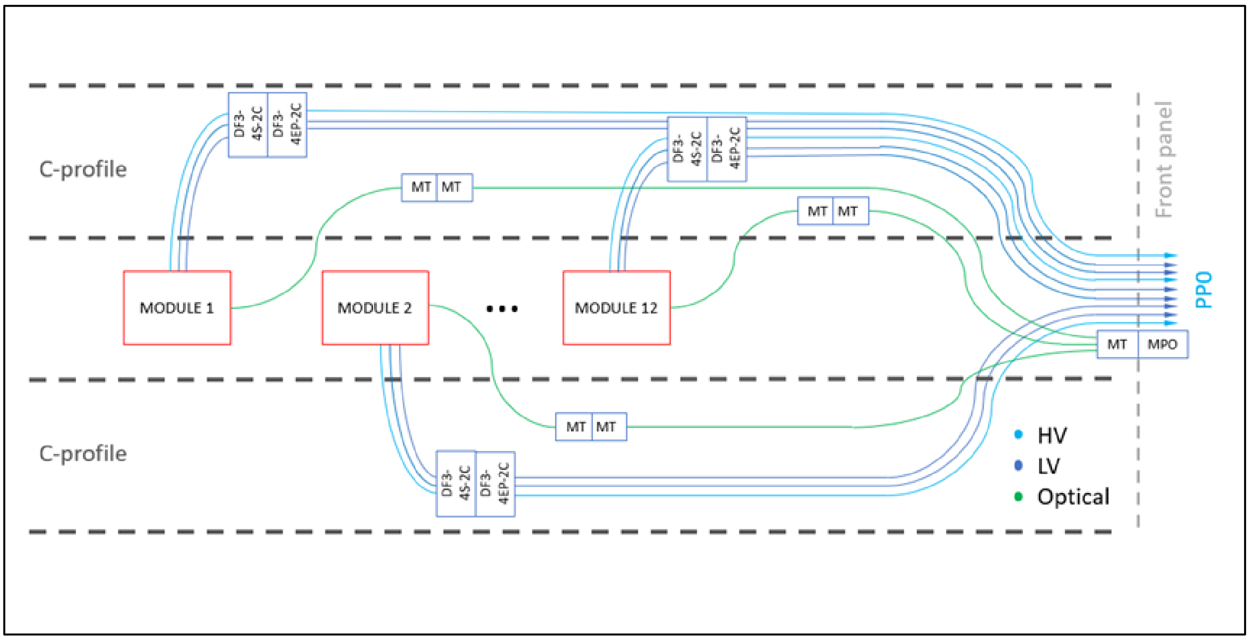

Figure 24: The routing concept for electrical and optical services

The C-profile has an inside envelope cross-section of ~15 x 11 mm. Based on the electrical wire specs it was estimated that the wrapped octopus trunk going in to one C-profile would have a maximum diameter of 5.5 mm, and the size would decrease steadily as more branches break out to connect to module pigtails. The bare optical fibres used in the naked-fanout have such a minimal diameter, that it has practically no effect to the naked-fanout trunk size, but rather the nominal wrapping diameter used in it determines the size. Therefore, a wrapping with nominal diameter of 3mm was selected for the naked-fanout for the whole length, as it is a compact but still easily handleable wrapping size. It is very important that all optical and electrical services remain inside the ladder frame envelope throughout the routing. This is because the ladder is installed to the wheel through a small-clearance gate, and anything sticking out from the frame envelope might be in risk of tangling to the wheel structure, and cause damage during the installation. Looking at the trunk diameters above and the connector sizes from specs, it seems that they would all fit comfortably inside the C-profile envelope (Figure 25).

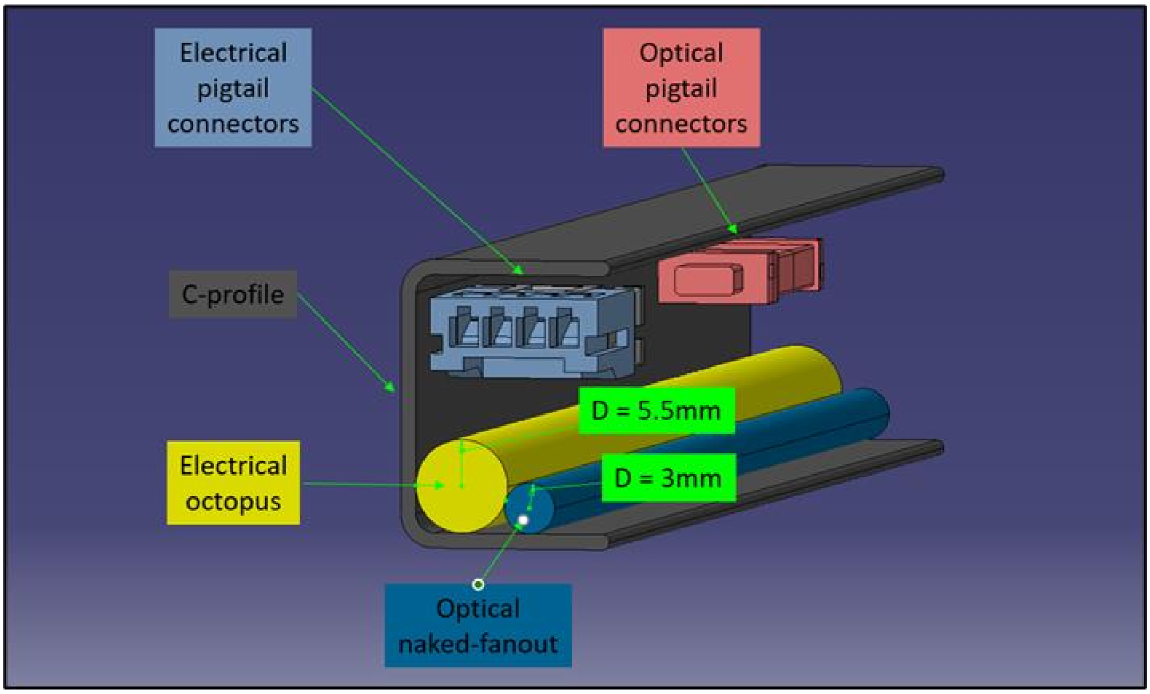

Figure 25: Layout of the service elements inside the C-profile.

When the octopus/naked-fanout trunks re-enter to the middle section of the ladder on the backside of module #12, the module has to be covered with a protective plate that on the same time would support the services on top. The plate would be glued to the aluminium inserts that support the module. The electrical octopus trunk wrapping must be dismantled on top of the plate so that the wires in the trunk can be spread a bit to make sure they will not exceed the frame envelope, which is the top plane of the crossbars. The wires are then united and re-wrapped into a single trunk, that exits through the front panel to continue towards PP0.

The optical naked-fanout has the single MT-ferrule in its end, to which all the 24 fibres are terminated. This MT-ferrule is plugged into the MT-MPO -adapter, which would be ideally mounted to the front panel. Unfortunately, the MT-MPO -adapter is rather bulky and it becomes quickly apparent that using the same standard C-profile size as in rest of the frame (Figure 17) is not possible due to lack of space in between the module #12 backside and the front panel C-profile upper flange. Also due to lack of space in front of the ladder on layer 3 (Figure 23) it is clear that a standard ~60 mm long MPO-connector let alone the patch cord coming out with its minimum allowed bending radius are not possible to fit behind the PP0s. To overcome this problem, it was clear that the MPO-connector and therefore the MT-MPO -adapter would have to be fixed on an angled orientation to the front panel, so that the whole configuration would be possible to fit. It was discovered that the vendor of the optical connectors offers a special angled variant of the MPO-connector, which would be partially solving the problem. However due to the large minimum bending radius specified for the optical patch cord, it was decided that the angled MPO-connector would be coupled with fixing the MT-MPO -adapter on a designated angle such, that the patch cord would result initiating perpendicularly compared to the front panel face normal. Therefore, the specified 60 mm bending radius could be easily achieved, as there is plenty the radial space between the TB2S and TEDD. The downside of all this is that the geometry of the front panel becomes rather complicated and the manufacturing of it must be separately thought, but this was considered to be essential to realise the configuration in the given space envelopes. Figure 26 illustrates a comparison of using the regular and angled MPO-connectors fixed to the front panel. The Z-coordinate extremity of the described angled connector strategy is only 16 mm from the front panel, whereas the regular connector mounted straight would require 119 mm of clearance on the front of the ladder.

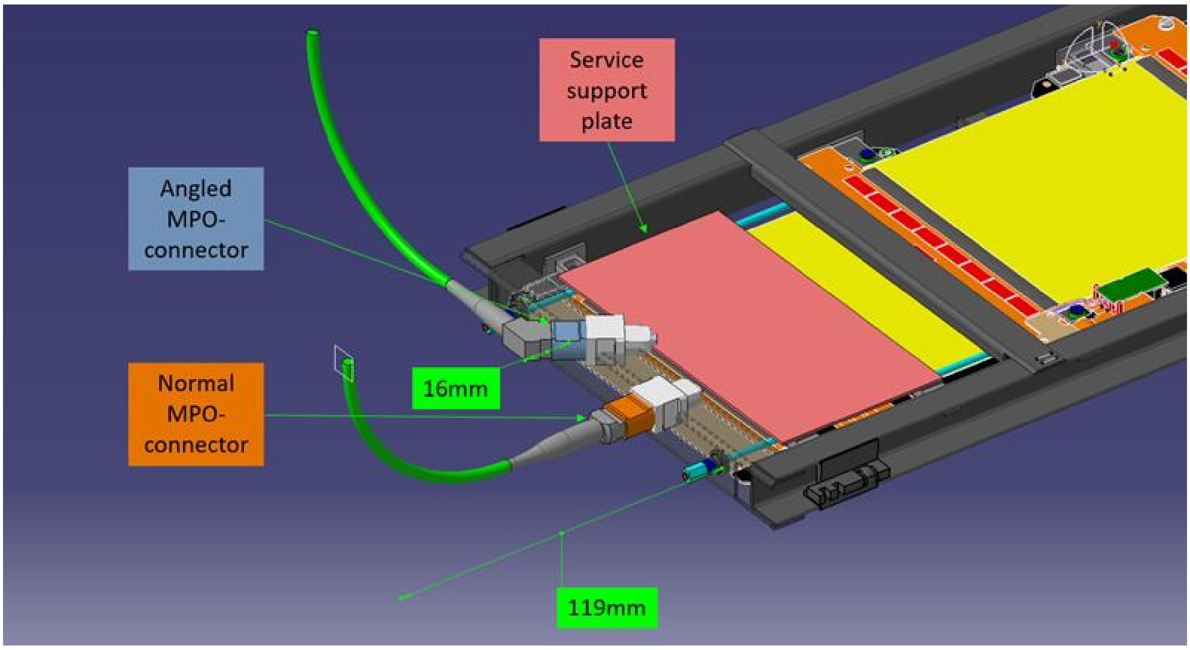

Figure 26: Comparison of the clearance requirements for straight boot MPO-connector (orange), and an angled boot MPO-connector in an angled fixation (blue).

3.3 Detail service design

The detail design is convenient to start from considering the exact assembly procedure of the modules and identifying what are the constrains and fundaments set by the process. In the module assembly stage, the ladder comes already assembled, meaning the frame and inserts are glued together, and it has passed the mechanical quality control. The 2S-modules come assembled and tested as well, and both the optical and electrical pigtails are already attached to them. In the assembly procedure the module is brought to the close proximity of its position in the ladder, the pigtail connectors are strung through their gates on the C-profile (Figure 27). The module is lowered on top of the inserts while the pigtail wires are guided steadily through the gates. When the module is in its position, the fastening screws are tightened, and the pigtails are connected to the octopus and to the naked-fanout. This procedure was rehearsed with very early mock-up pieces, and it was found out that ~100 mm pigtails are ideal for the purpose. The pigtails need to be long enough to allow the assembler to put his/her hand between the module and the ladder frame to string the pigtail connectors through the gates while keeping the module close to its final position. On the same time, the pigtails need to be short enough to keep the routing neat and compact especially for the modules locating close to the outer end of the ladder.

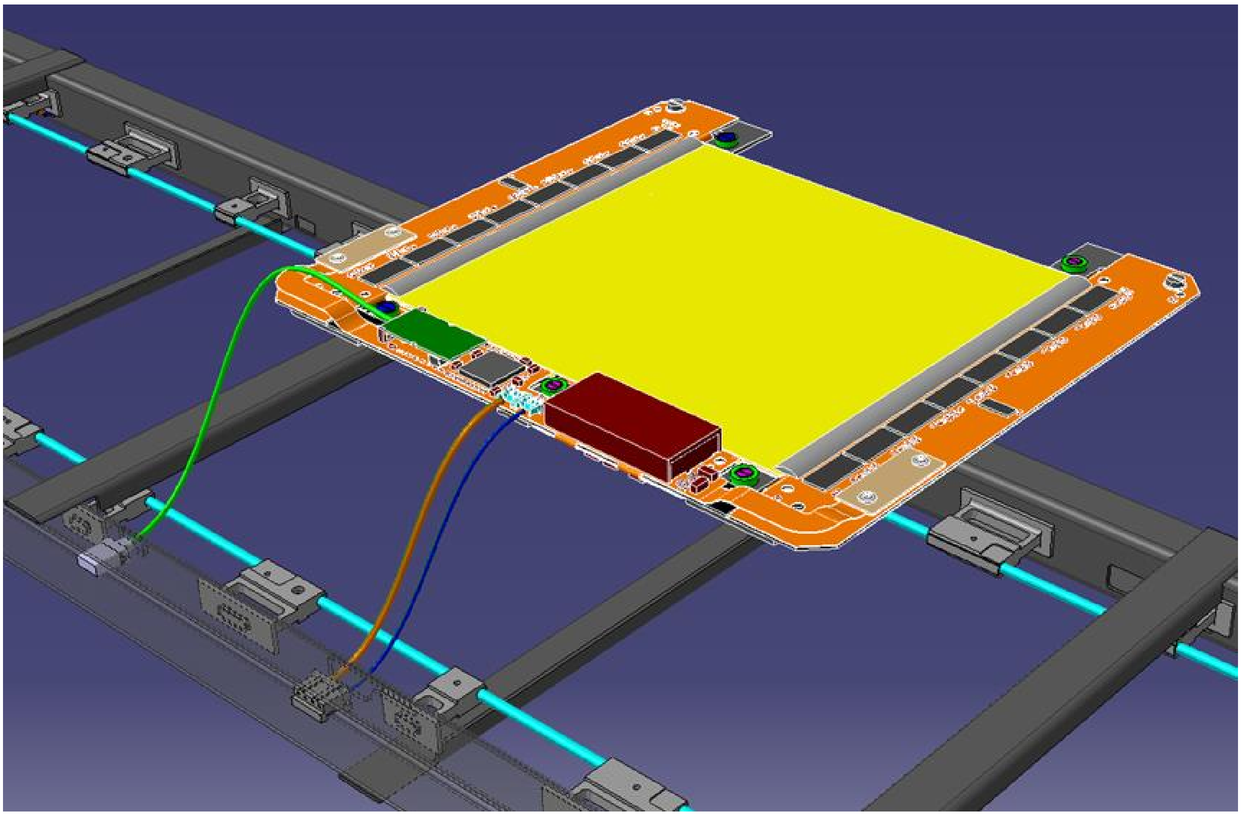

Figure 27: The module is held on close proximity to its final position, and the pigtail connectors are strung through the gates in the C-profiles.

On the module SEH, the electrical pigtail connectors locate just on top of the stump bridge mounting point. The corresponding support point of the ladder is the small insert, and its gluing flange reserves a big footprint of the C-profile surface. That is why the gate for the electrical pigtail to pass through inside the C-profile must have such geometry, that the gate has a bigger slot next to the small inserts flange, and a narrower portion which extends on top of the insert gluing flange (Figure 28). When the pigtail is strung through, the connector is passed through the bigger slot, and when the module is brought eventually to its position, the wires are slipped to the narrow slot to make them align with the SEH connectors.

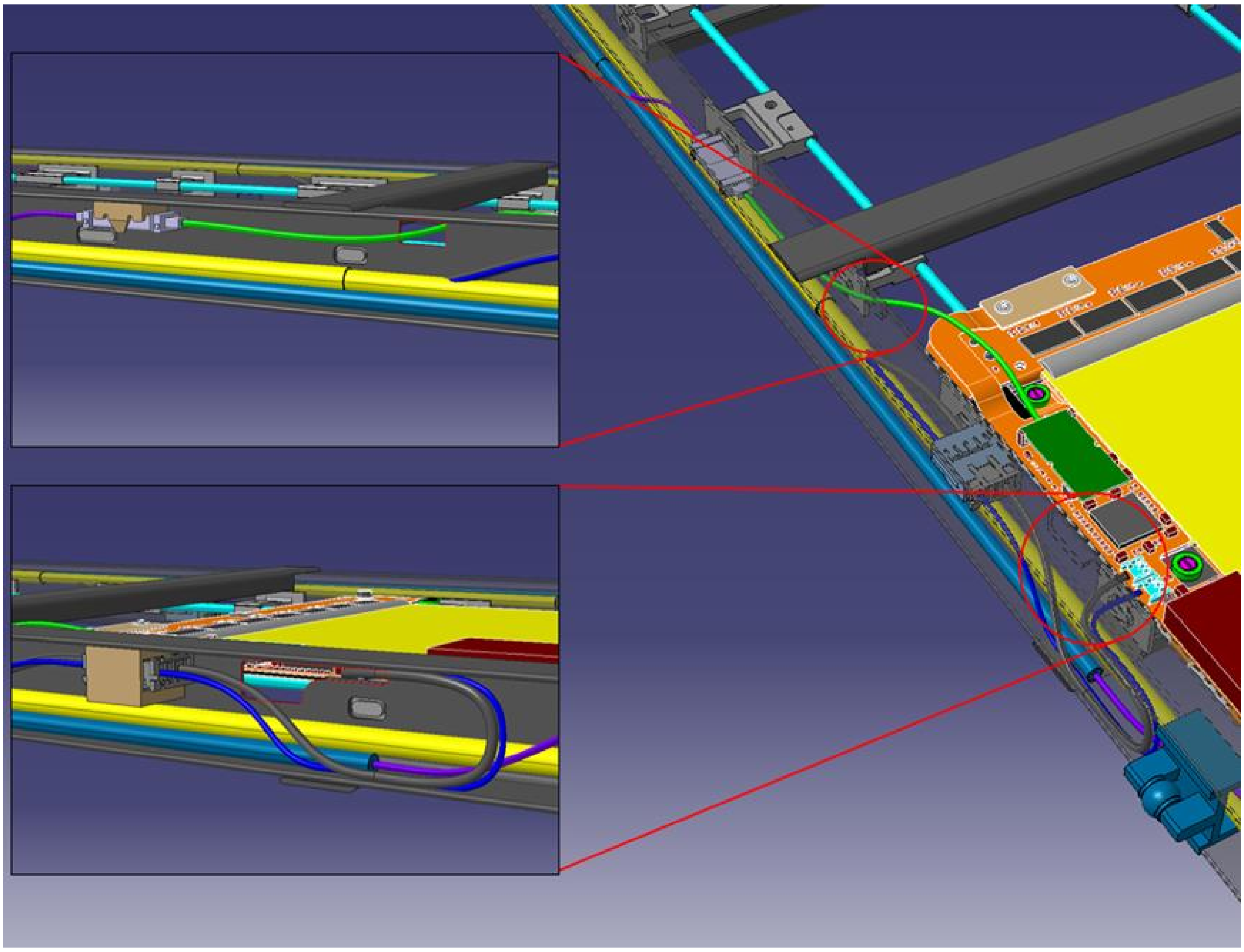

Figure 28: The module pigtail routings, The C-profile in the main view is transparent for clarity. The gates on the C-profile are highlighted with red outlines on the detail views.

The optical pigtails initiate from the VTRx+ -chip more conveniently parallel to the C-profile so the gate position can be more freely chosen. The gates are positioned to the C-profiles around the middle point of the pigtail, so that a gentle S-curve can be formed after passing the pigtail through to inside of the C-profile (Figure 28). For the electrical pigtail, a small loop is made, and the connector is plugged in to the connector of the octopus branch is already fixed into a snap-fit element which is glued to the C-profile flange. The optical pigtail and its corresponding naked-fanout -branch are slightly pulled out from the C-profile, as manipulating the small alignment pins and fixing spring requires some space. When the MT-ferrule pair is connected, they are fixed into their own snap-fit element fastened to the C-profile flange.

This strategy described above can be used in all modules other than #1, #11 and #12. As these modules locate on the extreme ends of the ladder, they require some adjustments to the routing. If module #12 would be oriented in the same way as the other modules on its r-plane, the optical pigtail would initiate towards the outer end of the C-profile, and thus it would be very difficult to route it backwards towards the naked-fanout it would have to connect. Therefore, the module #12's orientation is rotated 180°, such that the optical pigtail initiates "backwards" towards negative Z. The pigtail is then looped along the adjacent cross-bar, where it meets its designated naked-fanout MT-ferrule, and the pair is attached to the crossbar (Figure 29). The electrical pigtail initiates through the C-profile wall already outwards from the main entry gate, where the octopus re-enters the ladder middle section on top of the service support plate. The pigtail is guided individually through the main entry gate, and the connection to the octopus is made on top of the service support plate, and the connectors are attached to the plate with tape (Figure 30).

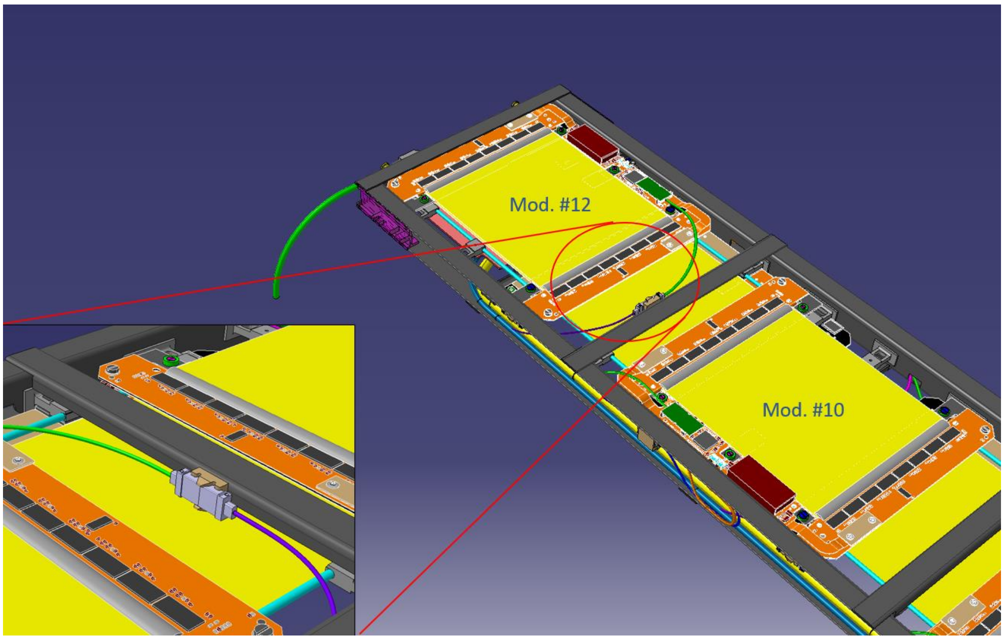

Figure 29: Module #12 optical pigtail routing.

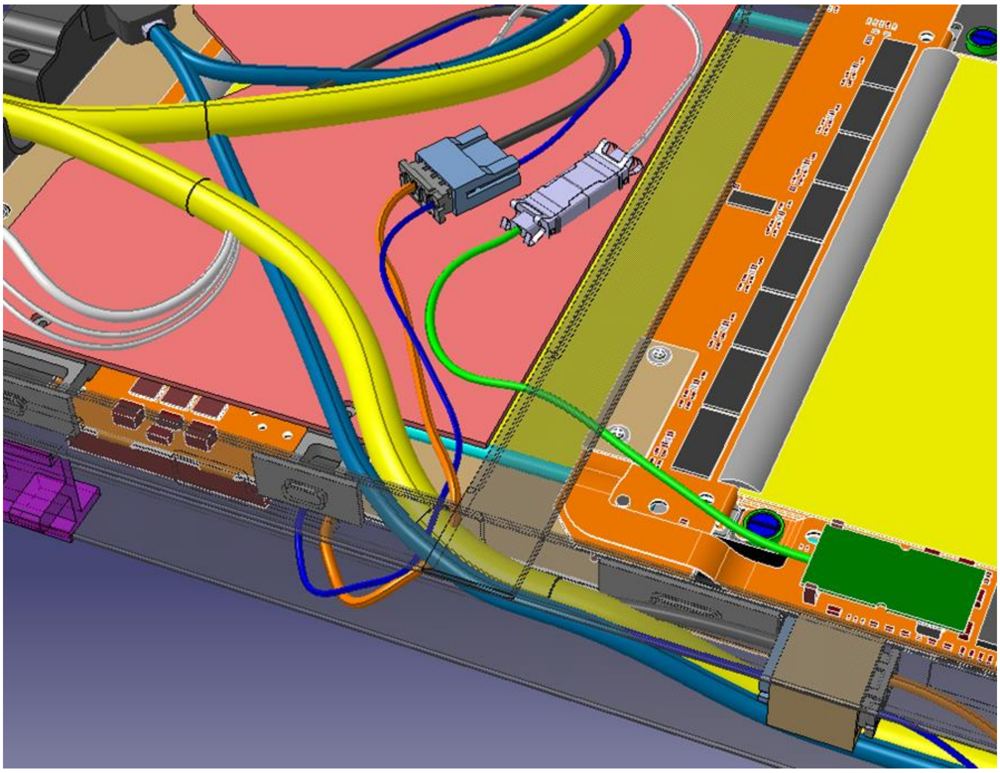

Figure 30: Module #12 electrical-, and module #11 optical pigtail routing.

The module #11's optical pigtail initiates so close to the main entry gate, that it is not feasible to route it through the C-profile. Instead, it is routed straight to the top of the service support plate from under the adjacent crossbar where the flange is cut off on that location. The MT-ferrule pair is secured to the service support plate by taping similarly as the module #12's electrical pigtail connectors (Figure 30).

The module #1's orientation had to be rotated 180° compared to the initial design (Figure 17), such that the optical pigtail's initiation direction became routing-wise impractical, as it initiates towards negative Z. This had to be done, because the DC-DC -converter in the module SEH is a major heat source on the hybrid, and rotating the module brings it above the cooling pipe. There the heat conduction route from the pipe to the insert pads is still normal, compared to the pads that are attached to the further special insert fixing points. Due to the strict minimum bending radius specifications set to the optical pigtail, it became evident that the pigtail is only possible to route to the opposite C-profile along the last crossbar. As the space between the module #1's FEH and the last crossbar is very minimal, it was not possible to place the MT-MT -connection there as was done with the module #11's case. Instead, the pigtail length needed to be increased such, that the pigtail makes the whole loop along the edge of the module and reaches the opposite C-profile where the connection to the naked-fanout is made. This is unfortunate, because doing this meant creating an additional topological variant of the module, but it was inevitable due to thermal and physical constraints.

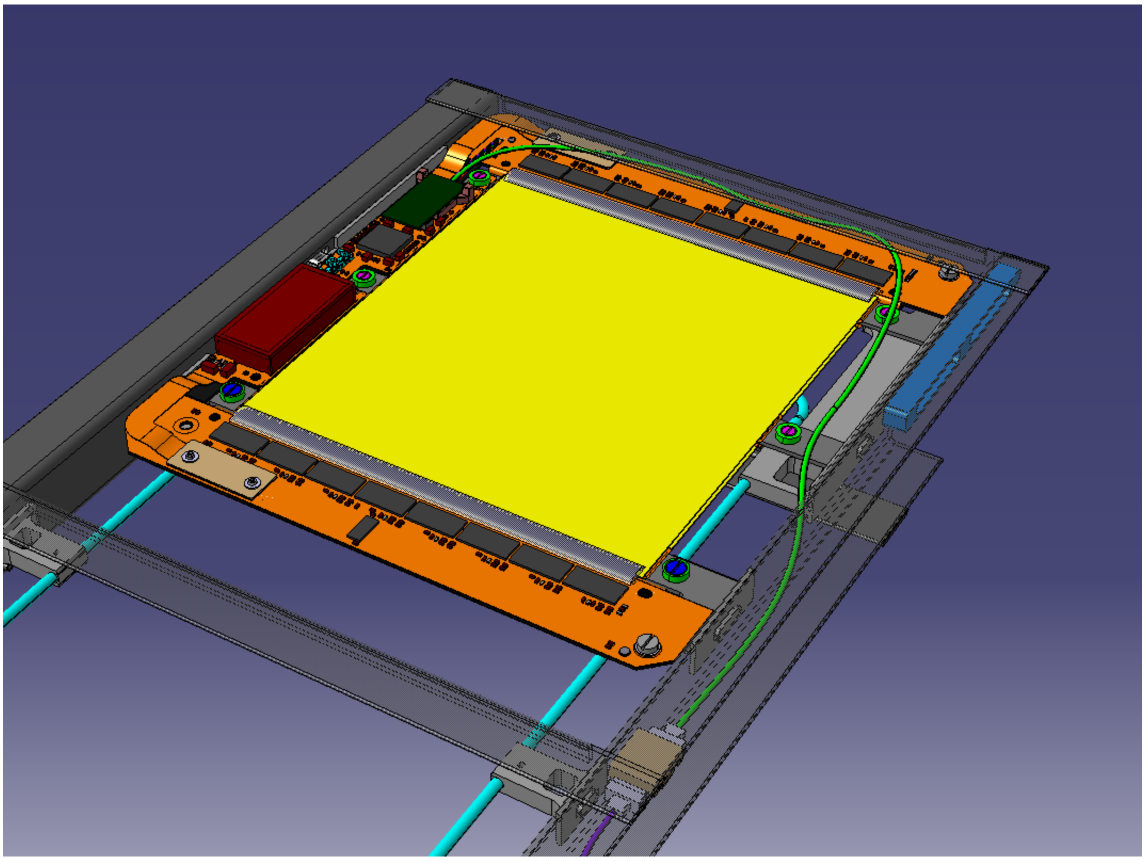

Figure 31: Module #1's optical pigtail routing. The crossbars and the C-profile are transparent for clarity. The special insert geometries were adjusted for better heat transfer towards the further module pads.

As it was discussed in chapter 3.2, using the same standard C-profile used in the rest of the frame as the basis of the front panel had to be abandoned due to the physical constraints set by the MT-MPO -adapter. The front panel has to be taller from the middle to be able to support the adapter, but from the sides it must be equal sized to the C-profiles as they will be glued together from the flanges. Exceeding the frame height envelope like this is allowed for the front panel, since it will remain fully outside the wheel when installed (Figure 23). Making the front panel out of carbon fibre was still desirable, as a mismatch on the coefficient of thermal expansion (CTE) between different components in a precise structure like the ladder could lead to severe issues. Also, the requirement for angled fixation of the adapter is further complicating the geometry, so it was essential to first consider the feasible manufacturing methods available that would be suitable for these constraints.

SMC/BMC (Sheet/Bulk moulding compound) is an advanced manufacturing method broadly used in the composite industry. It offers a good combination of available material compositions, mechanical precision, and production efficiency. In the SMC/BMC -process, the piece is moulded from a compound of polyester resin reinforced with chopped glass- or carbon fibre. The raw material charge is placed inside a metal mould, which is pressed shut and heated coincidentally. The pressure and heat together soften the raw material, and it starts to flow and fill the cavities of the mould forming the shape of the product. The pressure is then released, the mould split, and the piece is demoulded using pins or temporary features in the product specially designed for demoulding. The cycle time for the whole process can be just couple of minutes, but often the piece needs some finishing steps like removing flash or temporary features after the moulding. (European Alliance for SMC/BMC 2018.)

SMC raw material is produced as rolled sheet, whereas BMC is resembling more of a paste-form. Hence SMC is used in applications where the product is more sheet-like, like in car bodywork. BMC on the other hand is used when the shape is more complex like in electric appliance casings, as the fibres in it are shorter and more dispersed. (European Alliance for SMC/BMC 2018.) SMC/BMC was considered to be an ideal manufacturing method for the front panel, because of enabling both low CTE of carbon fibre, and allowing the complex geometry driven by the functionality. Also, the relatively large series of the pieces needed to be manufactured advocates for the SMC/BMC, compared for example to manual pre-impregnated lamination work which is very much more laborious.

Functionally the front panel needs to support the MT-MPO -adapter, the electrical octopus, the cooling pipe connection sleeves, and the pre-heater connectors. All the elements fixed to the front panel, and the routings initiating from it need to fit inside the Z-direction envelope behind the PP0s (Figure 23). Also, the front panel geometry needs to be such, that it will not collide with the other front panels of the adjacent ladders in the wheel. Hence the maximum envelope for the height is ~29mm, but some millimetres of installation clearance to the adjacent ladder is needed to be deducted from that. The module #12 is constraining the geometry in Y-direction from below, as it reaches all the way to until the front face of the panel.

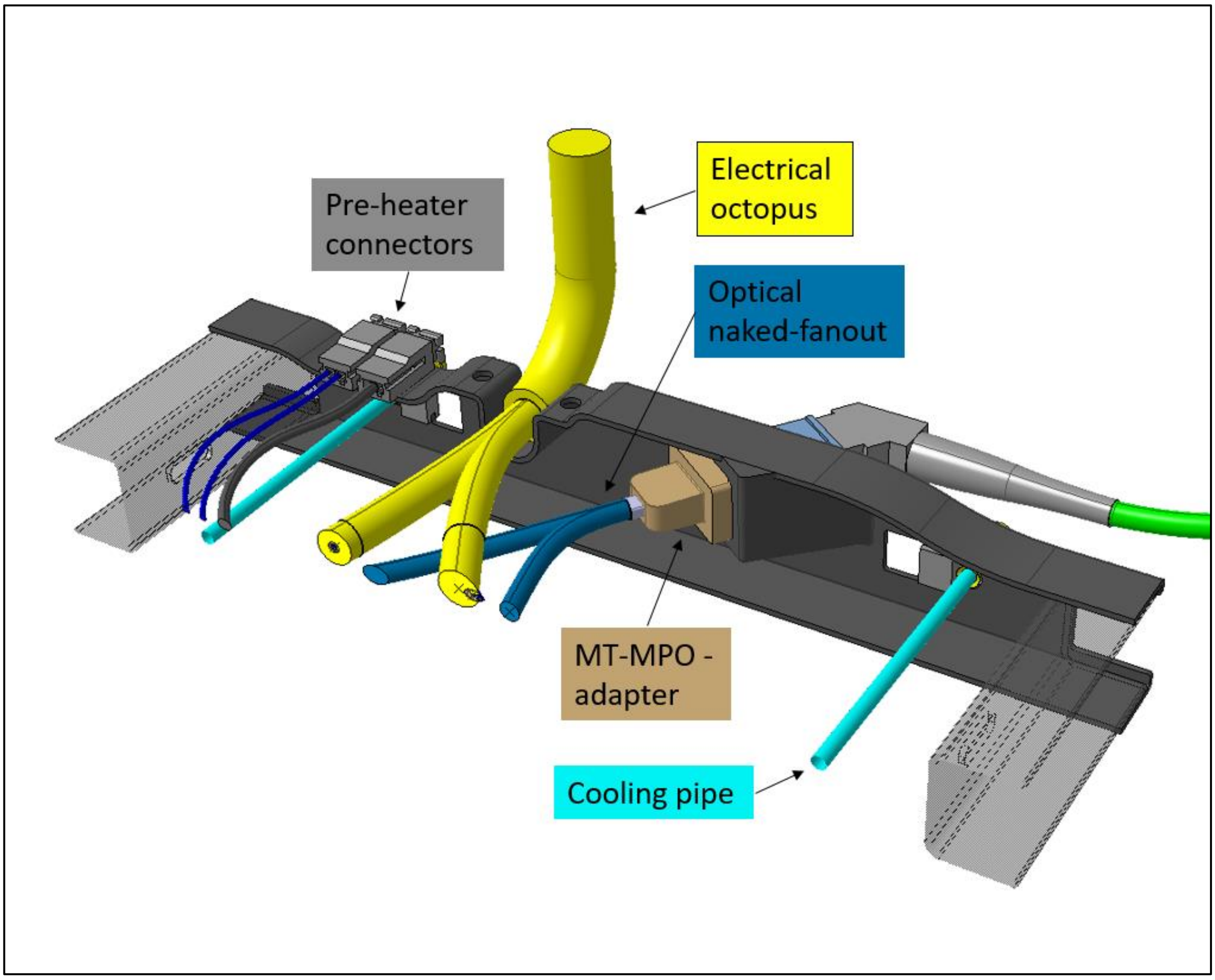

Figure 32: The front panel with the service elements attached. Module #12, its inserts, and the service support plate are hidden for clarity.

The angled MPO-connector has an angle of 125° for the cord initiation compared to its plugging axis, so an additional 35° fixing angle is needed for the MT-MPO -adapter for the cord to initiate perpendicularly to the front panel face towards negative X. The adapter-connector position was defined to the X- -side of the front panel, such that it would be as low as possible in the height envelope, but high enough that the MPO-connector boot passes above the inlet pipe of the ladder cooling circuit. To support the adapter, a triangular tab was merged to the front face and the upper flange, and a rectangular gate was placed in the middle of the tab to position the adapter to the correct location and alignment.

The electrical octopus needs to be supported from the middle of its length, as it does not terminate to the front panel but continues towards the PP0. If the support feature in the front panel would be a closed cross-sectioned gate, it would have to be large enough to thread whether the module- or the PP0-connectors through. As especially threading the PP0-connectors through the front panel would take a substantial footprint of the limited space, instead of making a gate it was made as a U-shaped open cross-sectioned slot towards positive Y. Hence the electrical octopus can be easily brought to the ladder from above of the service support plate and routed into the C-profiles, and just in the very end the main trunk would be inserted to the slot and secured in with a cable tie. The upper flange was kept continuous

such that it goes below the slot and above the closed MT-MPO -adapter fixing, to keep the mechanical strength of the C-shaped cross-section.
The gates for the cooling pipe sleeves were made such that they would not constrain the pipe in Z-direction. This is because the cooling pipe contracts substantially in length during the operational temperature cycle, and it would be enough to distort or damage the front panel. The cooling pipe is installed after the ladder frame gluing with the connection sleeves soldered into their place. Hence the gate has a larger portion on the inner side, where the sleeve is first passed through. After that it is slipped to the narrow pocket, and a clip is glued to the root of the pocket to secure the sleeve into its place in X and Y.

As the pre-heater is positioned to the inlet pipe just on the front of the ladder, the front panel is the convenient place to neatly handle the electrical services. Initially the pre-heater was specified to have two AWG24-wires for the actual resistors, and four AWG28 wires for its temperature sensors (Figure 19). Since the available space in the front panel was getting crowded, it was requested that the number of temperature sensor wires would be decreased from four to two downwards from the PP0. This would enable to use two two-pinned Hirose DF3 -connectors which take a reasonably small footprint. A lowered section was made to the upper flange on the X+ -side of the panel, where the connectors would be fixed in. The pre-heater wires are routed along the octopus from PP0 all the way into the ladder, where they are looped back to the connectors on top of the service support plate.

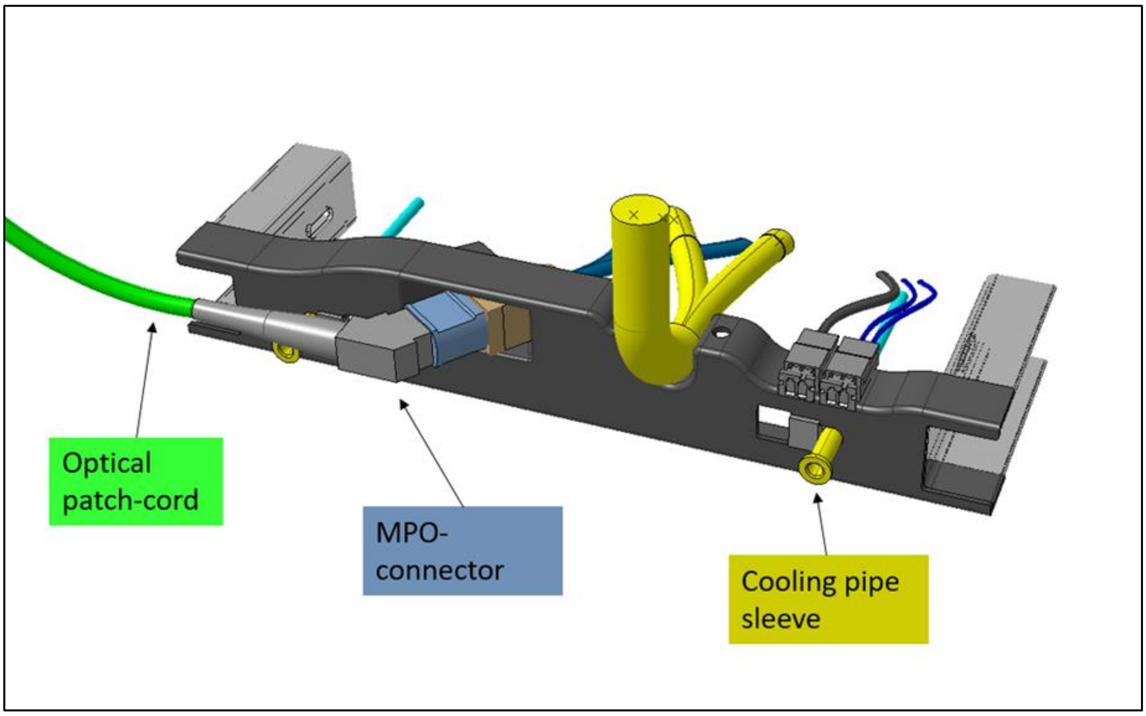

Figure 33: The front panel with the service elements attached. Module #12, its inserts, and service support plate hidden for clarity.

The SMC/BMC -manufacturing method requires some specific attention on the design phase already. Most importantly there has to be an angular draft through-out the piece in the direction of the mould insertion, so that separating the piece from the mould is possible. For example, the main flanges are 1° more open from perpendicular relative to the front face, and the same goes to all other pocket faces and features. The end openings were closed, and a 5 mm brim was added around the whole piece, to give it more rigidity when it is demoulded. These are temporary features, that will have to be removed after the moulding process by sawing and grinding.

The mould design was divided into four partitions, such that when they are assembled together, they form a cavity in the middle which has the volumetric geometry of the final piece. The three pieces making the bottom mould make the external shapes of the front panel, and the top mould correspondingly makes the internal shapes. An exploded view of the mould assembly is illustrated on Figure 34, where the red, blue, and white blocks make the bottom mould, the green block is the top mould, and the purple object in the middle is the resulting front panel component. The brown platforms on the bottom and the top are the heated beds of the machine, that are hydraulically pressed together during the moulding process. There are alignment pins going from the bottom bed through the bottom baseplate (white) all the way to the top mould, to ensure that the opposite features align properly. The moulds are pre-aligned on the machine, the screws are then tightened to the beds fixing the alignment, and the pins can be removed to avoid over-constraining the machine. The side halves of the bottom mould (red and blue) are aligned to each other with pins and fixed together with screws. They align to the baseplate directly from the moulding features on the middle of the baseplate and are fixed to it by the two screws. When the moulding action is done, the side halves of the bottom mould are forced clear from each other, and the resulting peace is demoulded carefully from the baseplate.

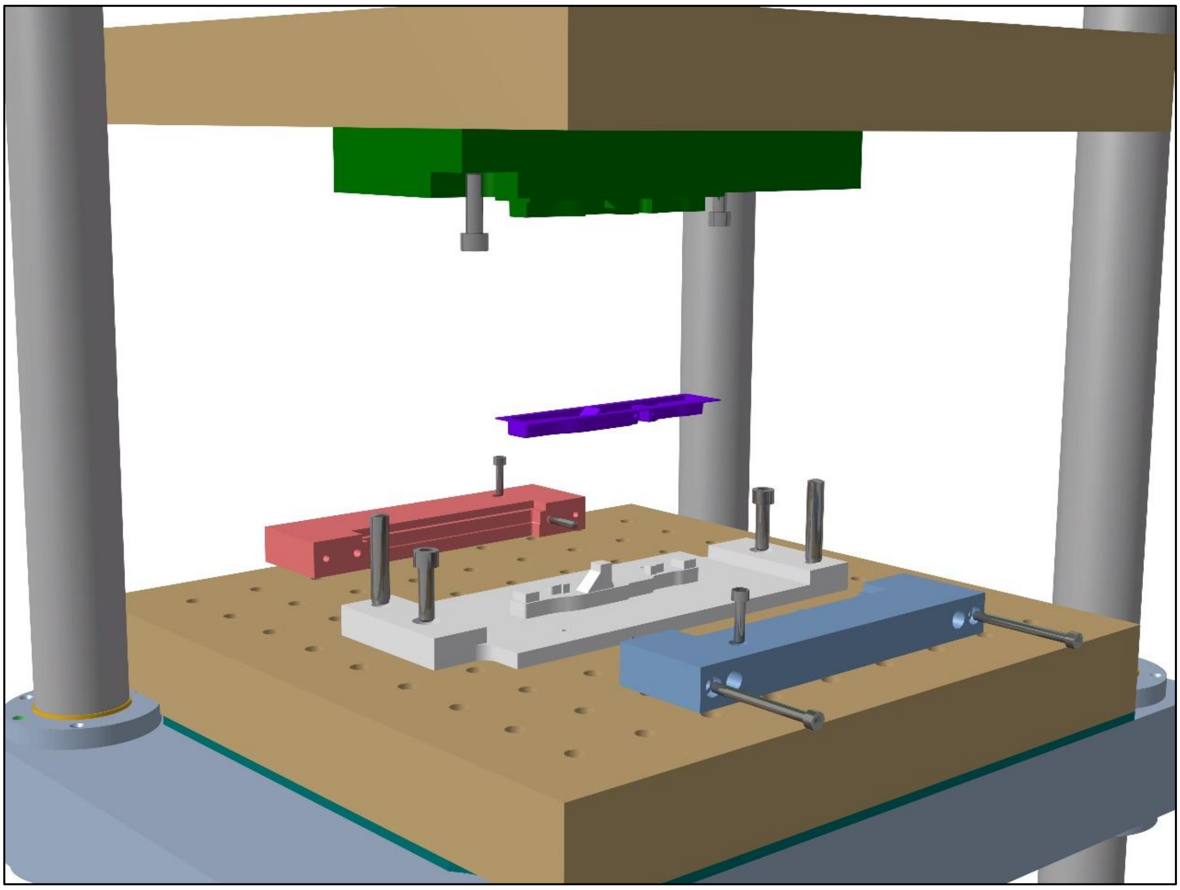

Figure 34: An exploded view of the mould and the front panel with the temporary features.

The service support plate is cut from 1 mm thick carbon fibre sheet to a simple rectangular shape. There are small cut-outs in front of the main entry gates to allow the bend towards the C-profile, and one larger in front of the MT-MPO -adapter which is needed for a special tool to remove the MT-ferrule from the adapter if needed. The plate is glued to the module #12's inserts, and there are holes on the plate on top of the insert threaded holes to prevent the capillary glue from flowing to the holes. Only 6.4 mm of height is available from the plate surface to the top frame envelope, which is the crossbar top surface. To make sure that the electrical octopus halves do not exceed the envelope while they are routed on top of the plate, their spiral wrapping is dismantled in between the C-profile main entry gates and the front panel exit slot. This way the octopus trunks can be "spread" a bit to be more of oval cross-sectioned when they need to pass over the naked-fanout trunks, because summing the nominal diameters together would exceed the envelope. Starting from the front panel, both the electrical octopus and the naked-fanout divide in to two main trunks which enter to the C-profiles and branches break-out from the wrapping ~50 mm before the nominal connector position. Custom snap-fit housings were designed to secure the connectors in place.

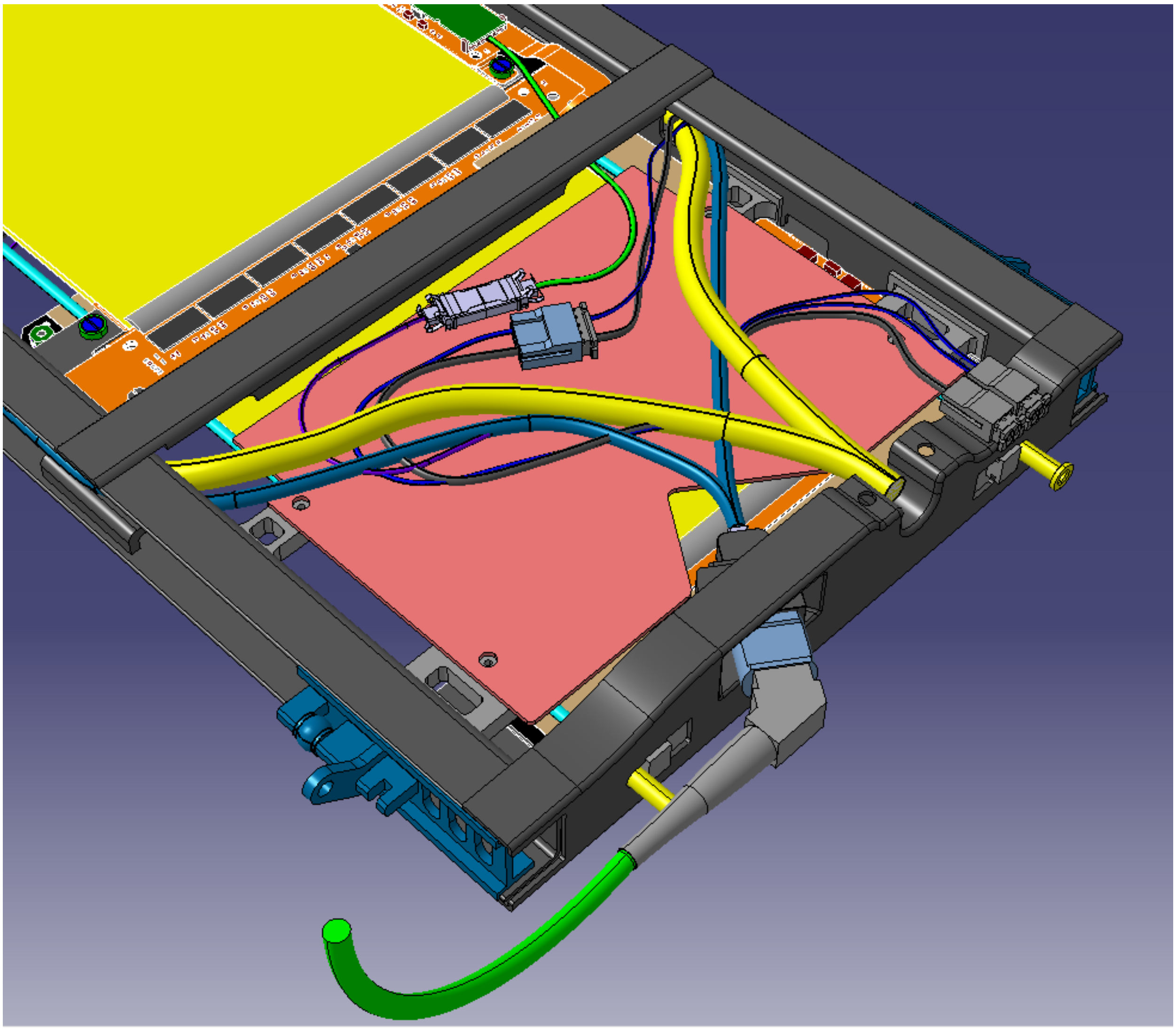

Figure 35: The routing arrangement on top of the service support plate.

When the modules have been installed to the ladder and they have been equipped with the services, the ladders will be assembled to the TB2S wheel from the gates that are on circular patterns on both ends of the wheel. A special tool is needed to support the ladder precisely on the desired alignment when it is slid in and the spheres are mated with the corresponding slot inserts in any ladder position along the pattern. In the TOB a construction of a slider mechanism supported radially from the middle of the barrel was used. The rod (corresponding structure to the current ladder) was inserted through the barrel gate with the slider, which was supported from an arm that took alignment from a disk with patterned holes in the middle. The arm was extended to reach further radial layers, and the disk fixing holes were changed to move angularly on the pattern. A mock-up that was made to test the system before TOB construction is illustrated on Figure 36. The rod supported to the slider with a "fork", which extending arms went into the rod C-profiles and took support from the sphere support brackets and from two further inserts.

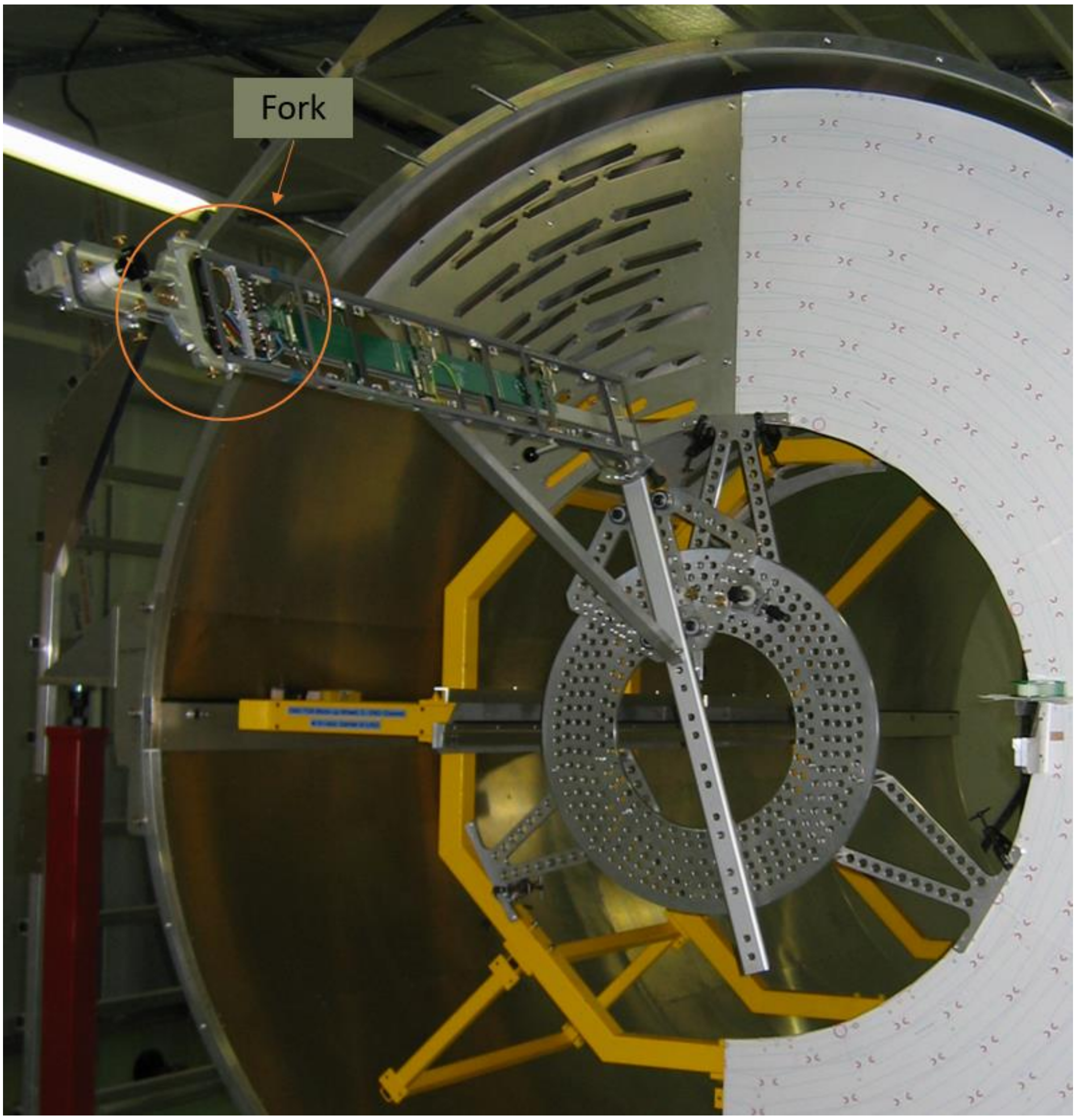

Figure 36: An old mock-up made to test the rod installation tooling for the TOB. The rod gates are visible in the metallic sector on the top side of the barrel. The rod in the foreground of the image is attached to the slider with the fork piece.

To a large extent a similar concept of the installation tooling could be utilized for the TB2S as well, just adjusted for the new main dimensions. Only the fork-piece needed some heavier re-engineering because it is the interface towards the ladder, and the space inside the C-profiles is much more constrained due to the different service concept of the TB2S ladder compared to the TOB rod. The fork arms in the rod's case were extended rather deep to the C-profiles first through the outer sphere inserts and taking the second support from similar inserts attached ~150 mm further inwards on the C-profiles. Following this same strategy in the ladder the inner contact inserts for the fork could be attached only ~50 mm further from the sphere support brackets, due to the module #12 pigtail and the octopus and naked-fan-out trunks routing through the main entry gate. As the ladder will be hanging in the fork like a cantilever beam supported from these two points, the force induced by the momentum directed to the inserts therefore to the C-profiles would be substantially larger with the reduced lever arm length. This could lead to cracking of the C-profile, as it is locally weaker due to the large gates just on the area where the momentum is on its highest.

Hence for the ladder, the fork-piece had to be designed such that there is a small cross-sectioned arm extending below the module #12 pigtail- and the main entry gates to maximize the lever arm length to decrease the momentum. The second gates are made from 10x10x2 standard carbon fibre box-profile, which are cut in half and chamfered from the other cut edge. They are glued to the C-profile flanges below the main entry gates, leaving some space forwards for the octopus and naked-fanout to route in between the gate and the module #11 electrical pigtail snap-fit housing on the X+ -side, which is the more constrained one. The sphere support brackets were extended outwards as much as possible, and the internal flange was removed to enable to introduce and retract the fork by pivoting the tool to avoid collision with the module #12 pigtail.

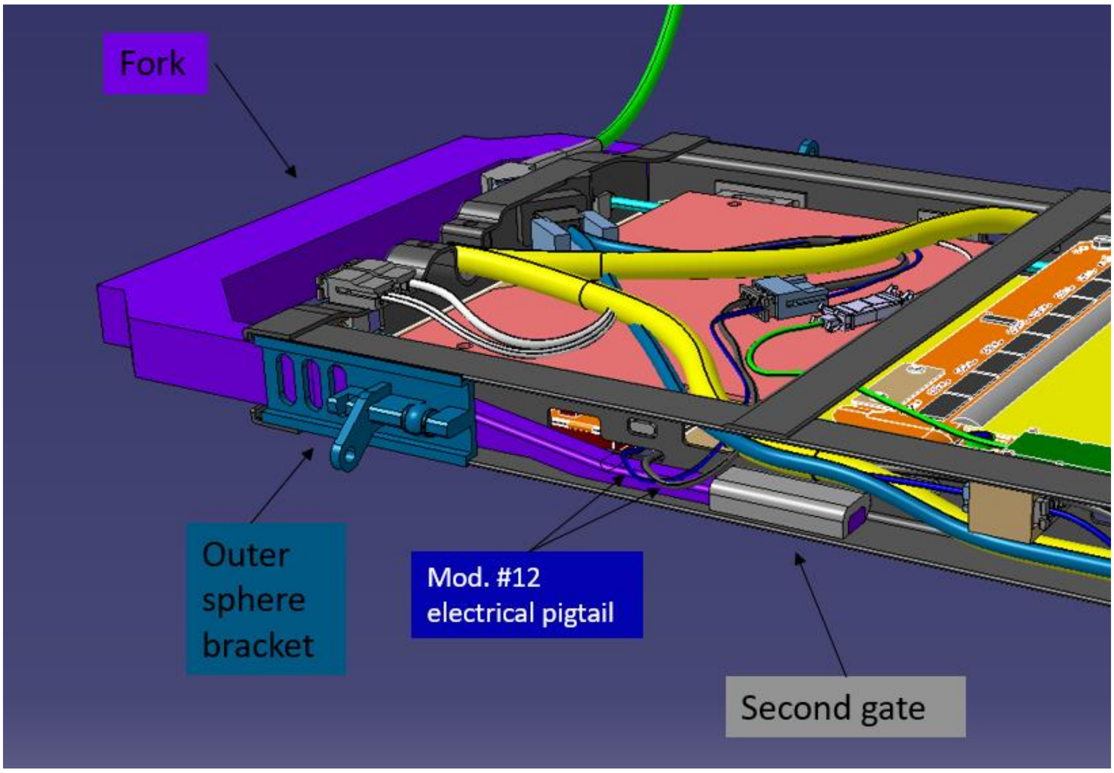

Figure 37: The re-designed fork for the TB2S ladder.

Thermal FEM-simulations that were done in the OT-collaboration showed, that the 2S-module cooling performance was insufficient on some high radiation exposure sections of TB2S and TEDD. To solve this issue, a 2S-module design variant with a second stump bridge and thus a sixth contact point to the cooling circuit was created by the module design team (Figure 18). On TB2S, this module variant was taken into use for module #1's on all three layers, as they have partially impaired cooling because of the special inserts (Figure 21). On layer 1, also modules #2-#12 were changed to this variant because of high radiation exposure close the IP. On the ladder design second small inserts were added to all module positions, and the special insert design was optimized to have better heat flow towards the further contact pads (Figure 31) based on the feedback obtained from the FEM-simulations.

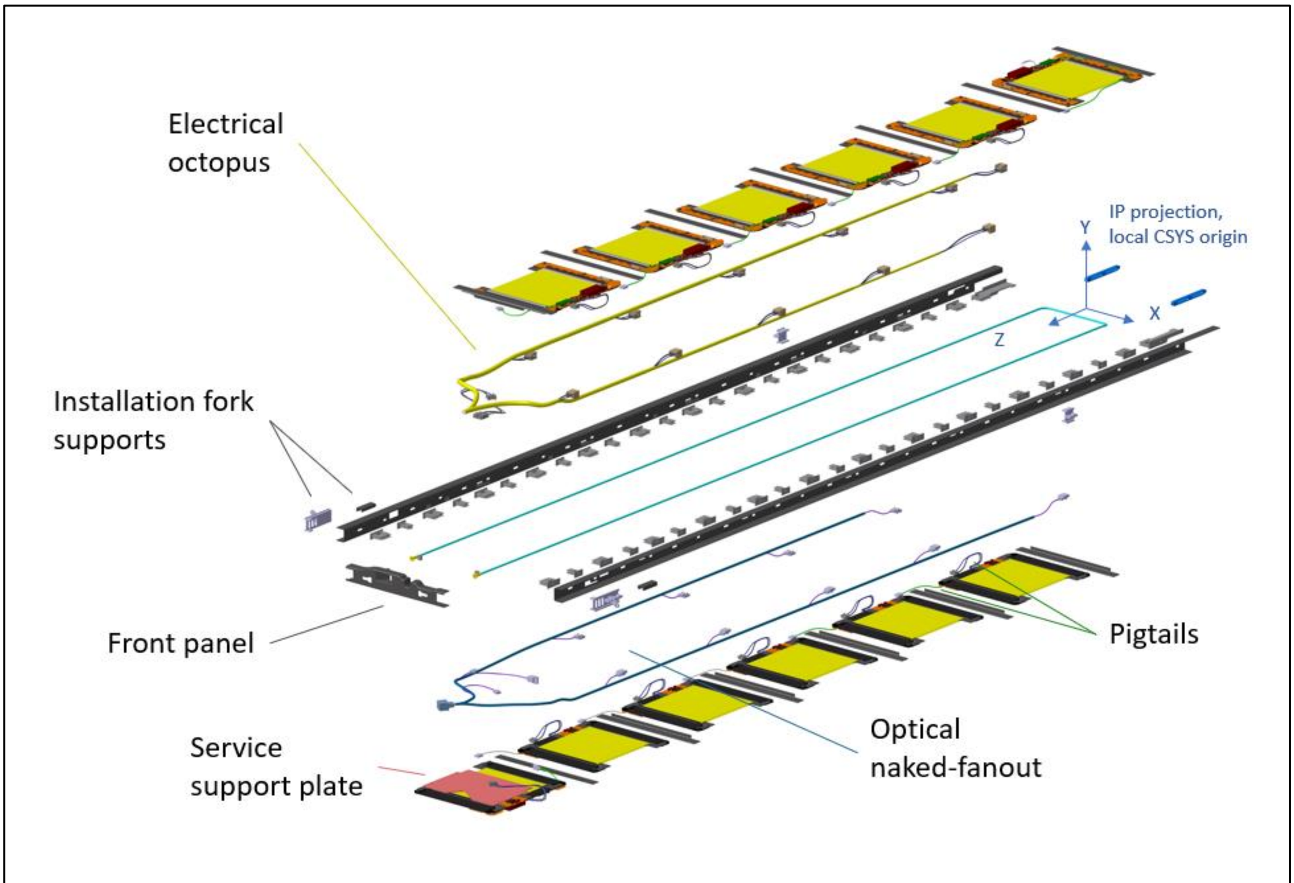

Figure 38: An Exploded view of the service features integrated to the ladder baseline design.

The designed service features were added to the baseline ladder design (Figure 38). The parts and sub-assemblies were documented in mechanical drawings, and the installation sequence and responsibilities were discussed between NCP and IPHC. The installation fork supports, the snap-fit connector housings, the service support plate and the MT-MPO -adapter would be ideally fixed to their places on the same stage as the rest of the frame is glued in NCP. Then in the module assembly stage in IPHC the electrical octopus and optical naked-fanout could be simply connected to their designated interfaces, and no additional gluing or other assembly work would be required. The electrical octopus should be installed and fixed first, so that the more fragile naked-fanout can be installed as the latter one.

3.4 Advanced modelling methods

As discussed in chapter 2.3, modelling cables in CAD is not so straightforward compared to solid mechanical parts due to their flexible and slender nature. Using a representation of extruding a circular cross-section along a defined polyline or spline has been the most common modelling strategy in CERN as well, and even though it is modelling-wise simple and neat, it can lead to problems of not corresponding to the real-world behaviour of cables and fibres very well. Dassault offers an add-on package called Electrical harness discipline integrated to their CATIA CAD-system, and the tools in this package were utilized in the routing design described in chapter 3.3.

The topological product-part data structure is fundamentally similar that it is when working with the normal CATIA mechanical workbenches. Now however when building the electrical harness in the Electrical harness -discipline, the product is referred as “geometrical bundle”, and the parts inside can be either normal “part”-documents, “multi-branchable” -documents or “bundle segment” -documents. The normal part-documents can be for example connectors or other solid components, but the actual bundle geometries are created as bundle segment- or multi-branchable -documents. A multi-branchable -document allows one to create the whole harness with multiple bundle segments inside a single CATPart-file, whereas the bundle segment -document can only contain one bundle geometry. The multi-branchable -document thus allows substantially simplifying the data structure, if desired. (Dassault Systèmes 2017.)

The major benefit in the Electrical harness discipline compared to the traditional modelling environments is that it uses a designated FLEX-algorithm when computing the routing for the bundle in question. Instead of purely mathematical approximation, the FLEX-algorithm is based on finite element method and takes into account the bundle properties such as the cross-section shape and size, elasticity, and the composition of the harness if it is defined through the electrical library. It also allows local longitudinal deformation, axial torsion and bending of the object. (Dassault Systèmes 2017.)

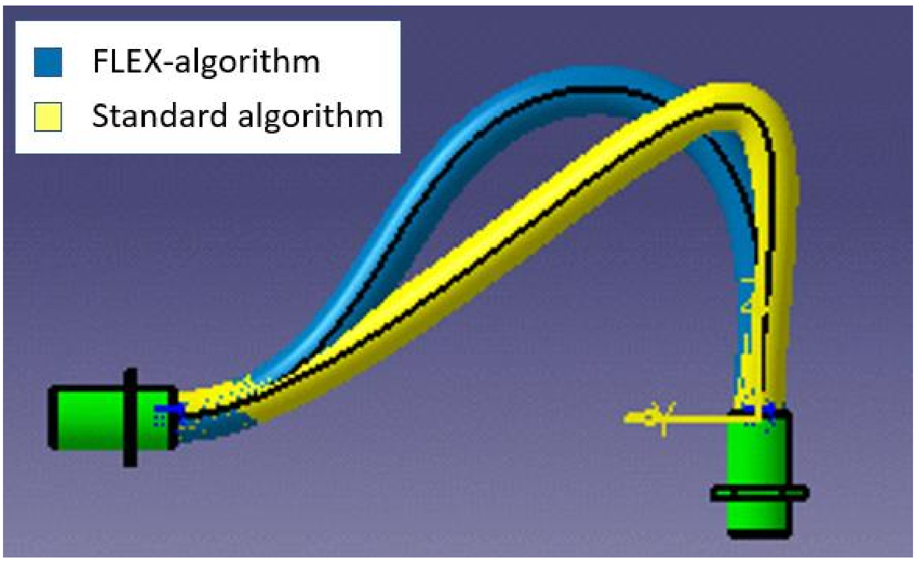

Figure 39: Comparison of a simple tube bend using FLEX- and standard algorithms. (Dassault Systèmes 2017.)

In the ladder service routing design both the electrical octopus and the optical naked-fanout were created as multi-branchable -documents to simplify the data structure. The actual bundle geometry definition is done through an interface specific for the Electrical harness -discipline, where first the bundle parameters are set. The user can define the bundle size through diameter or cross-section and designate the minimum bending radius which has a different effect to the routing depending on the build mode used. The bundle routing is usually defined between start and end points, and constraining features and points can be added along if applicable. One should remember when creating the route, that instead of arbitrarily creating points along the route to have a neat looking bundle, there should be real-world objects like clips or tape to constrain the bundle on every location it is correspondingly constrained in the model.

On a multi-branchable -document, there are four different build modes to create the bundle: slack, length, bend, and straight bend. In the slack-mode, a defined percentage of length is added to the minimum length initially created by the set parameters and constraints. This is convenient, because usually some slack is desired in any routing to ease the plugging of connectors and other assembly work. The length-mode works similarly, but here the user defines the length of the bundle, and the slack then sets evenly to the routing. Bend-mode again finds the minimum distance based on the constrain set for the routing. Straight bend forms the routing from straight line segments and constant arcs with minimum bends using the defined minimum bending radius. This is more theoretical and purely mathematical approach and should not be used other than for finding the theoretical minimum length of the bundle. (Dassault Systèmes 2017.)

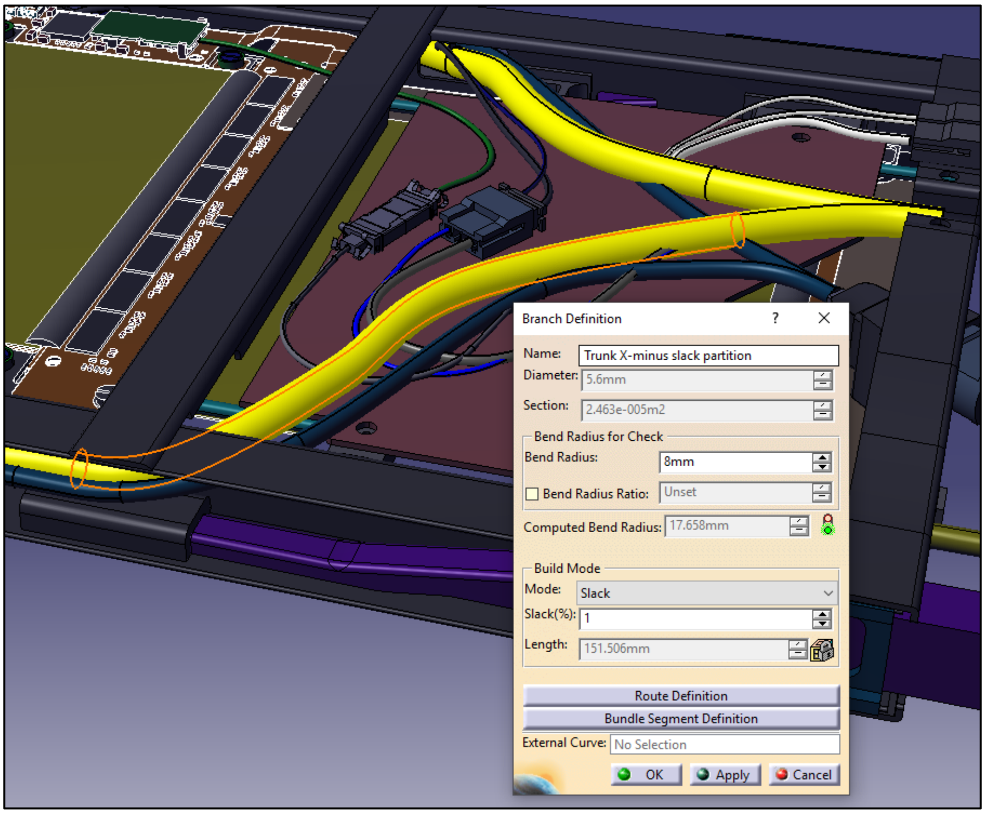

Figure 40: The octopus trunks were divided into two main segments, the one on top of the service support plate containing the slack, and the one sitting tightly inside the C-profile.

The octopus and the naked fanout trunks were modelled as two segments, divided shortly after they enter the C-profiles from the main entry gates. This was done because on top of the service support plate it is desired to have some slack on the routing, but inside the C-profiles the trunks need to be as tightly packed as possible. The C-profile partition was further segmented by using “branch point” -feature which enabled neatly to create the breakout points for the module branches, and after that set the trunk diameter separately for each segment as the diameter decreases after every breakout point. The branch points were set on a constant distance from the connector position. The module branches were modelled as separate bundles inside the same multi-branchable -documents.

The pigtails were modelled as their own multi-branchable -documents using the length-mode, as the exact length options are given in the specification. The end point of the pigtail was linked to the connector pin, and the connector could be then moved to its ideal location while the pigtail representation updated in real time. The corresponding octopus/naked-fanout branch connector position was linked to the pigtail connector, such that the branch geometry updated along the pigtail adjustment.

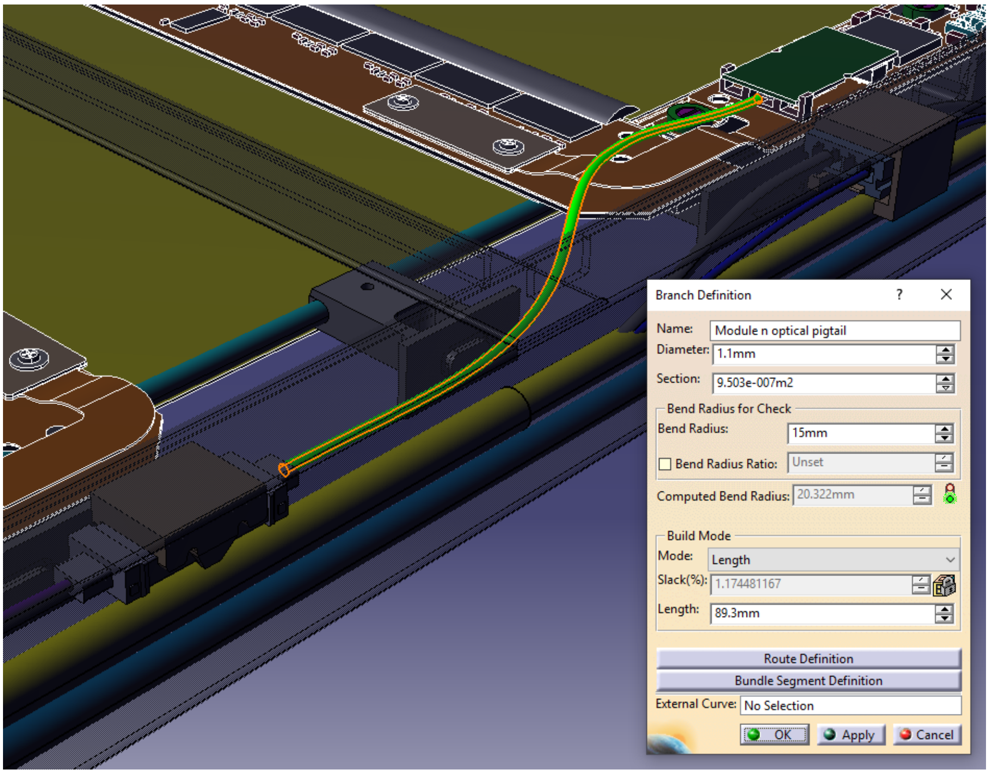

Figure 41: The pigtail routings were defined in length-mode.

The Electrical harness discipline proved out to be an efficient tool for the modelling tasks needed on the ladder service design. The improved representation quality provided by the FLEX-algorithm, and the efficiency through dynamic user interfaces of the workbenches gave both good design quality and productivity. The tools would suite even better into an environment where there is more space, and the routing does not have be so exactly defined through narrow gates and tight channels. The harness internal splicing and the electrical pin-pin wiring was not utilized in this case, but this would even more improve the representation quality through added inputs for the FLEX-algorithm.

3.5 Mock-up studies

Mock-up -prototypes are simplified and low-cost models of the product under the design process, which are used in validating the functionality of the design. A physical tangible object is a fine support element on discussions between different design collaborators, and it reduces misconceptions efficiently. A mock-up enables to demonstrate the product usage in real environment already in early development stage when the design changes are still possible to do without great expenses. (Lyly-Yrjänäinen 2019.)

In the beginning of the project, it was considered that even though modern and advanced digital CAD-tools are primarily utilized in the design, it is still essential to prove the feasibility of the service design with a traditional mock-up -prototype. This is because the cables and fibres are slender and flexible objects, and their realistic behaviour is hard to model exactly in CAD.

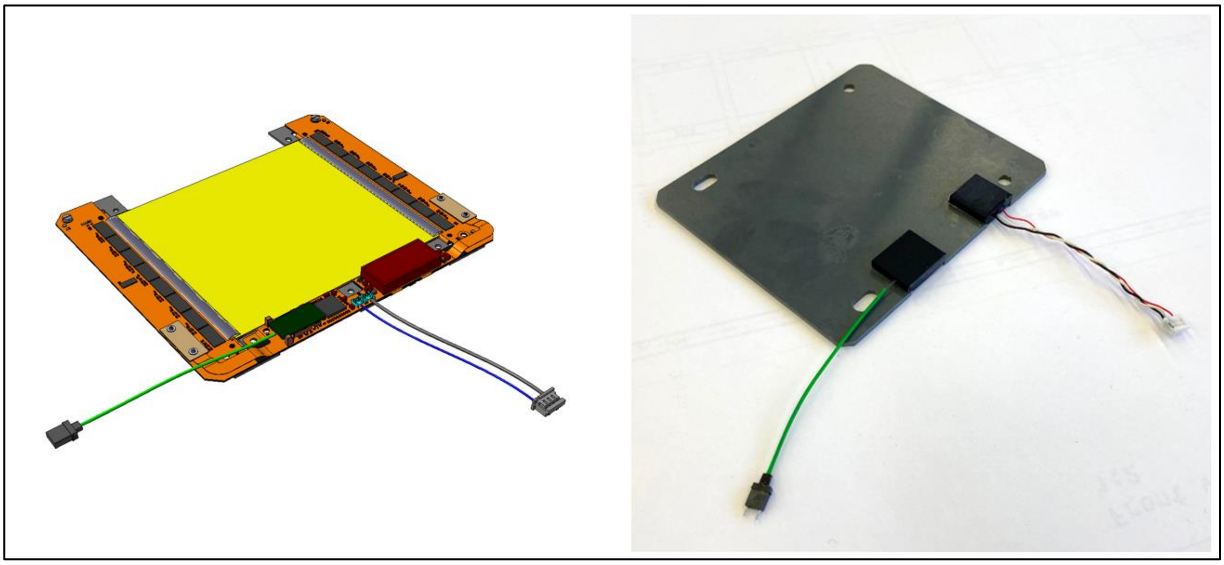

Figure 42: A mock-up 2S-module (right) in comparison to the 3D-design.

The mock-up 2S-modules were waterjet cut according to the real module outer dimensions from a plastic sheet. Cut-outs were done to the SEH's side, and 3D-printed blocks with slots for the wire/fibre initiation were glued to them. The real-spec CCA-wires used in the final detector were not available easily as bulk yet, but wire material with similar outer dimensions was procured both in twisted-pair configuration for the LV's, and as single wire for the HV's. The actual DF3-connectors were also procured, as they are common commercial products. On the optical domain some samples from the VTRx+ -units with pigtails were received from the DAQ-system design team, but as these were not yet done according to the exact dimensions of the ladder service design, they were used as a reference and separate units were prepared for the mock-up use from bulk fibre, ferrule and wrapping materials.

The ladder frame mock-up was modified from an existing aluminium model which had been made earlier for general demonstration purposes. The model was 1:1 scale with some minor simplifications on the X and Y dimensions, and longitudinally it was shortened such, that there were positions for holding four modules. This was enough for the purposes of the service design demonstration, because as described in chapter 3.3 there are exactly four different routing variants in the design for the modules. These are namely the normal routing used for modules #2-#10, and the special routings used for module #1, #11 and #12. The pigtail and the main entry gates were machined to the aluminium C-profiles, and some crossbar flanges and positions were modified. The electrical pigtail gates were slightly shifted to the side from their real position on the design, because the insert flange in the frame mock-up was higher and thus blocking the space for the narrow extension of the gate. This was compensated to the mock-up modules and octopus branch lengths, and it does not affect the demonstration. The MT-MPO -adapter, and the 3D-printed service support plate, the front panel and the snap-fit housings of the connectors were attached to the frame.

Figure 43: The frame mock-up with the gates machined, and the 3D-printed service support plate, front panel and connector housings attached to it.

The naked-fanout and the octopus were prepared with the designated branch dimensions and connector positions for the four modules existing in the mock-up. In addition, loose wires and fibres were added inside to the octopus and naked-fanout wrappings, to match the full-sized configurations as they are for twelve modules to realistically demonstrate the space management inside the C-profiles and on top of the service support plate. The fibres and wires were glued to their connectors instead of real termination techniques, as this mock-up's scope was purely mechanical and functional optical and electrical connections were not needed. The electrical octopus was left short and unterminated on the PP0's side, as this connection would be demonstrated on another mock-up made by the wheel design team. The naked-fanout and the octopus were installed to the frame, and the connectors were attached to their designated positions to be ready for the module installation. The wires and fibres on top of the service support plate were not yet secured down, as this is done only after module installation to manage the slack properly.

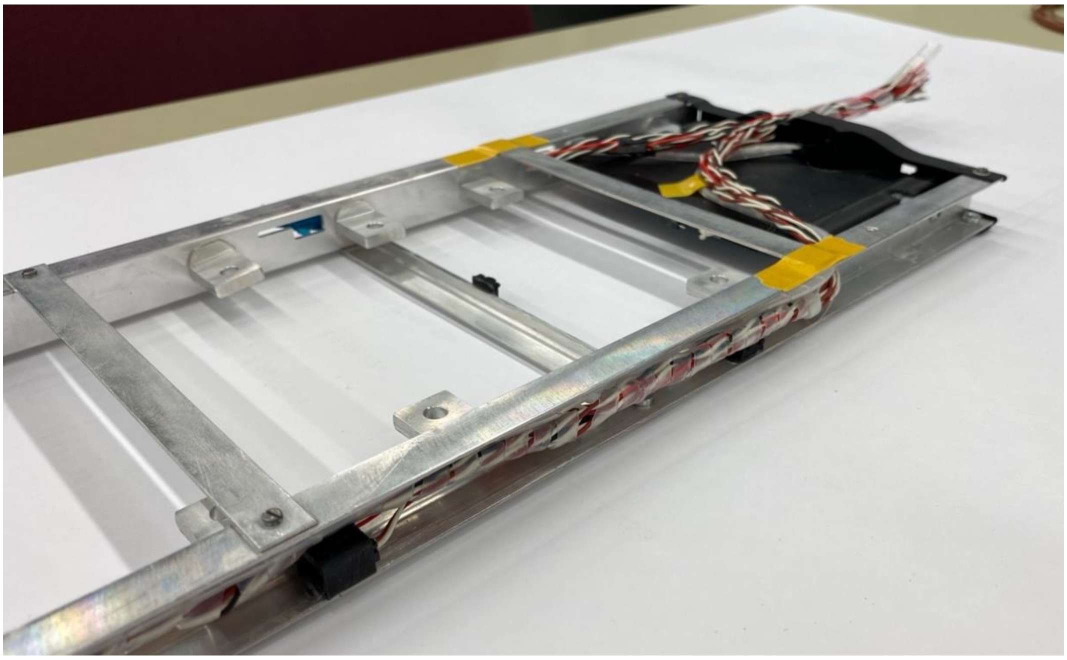

Figure 44: The electrical octopus and optical naked-fanout attached to the frame.

Finally, the modules were attached to the frame and the pigtails were connected and secured. The sequence of bringing the module close, threading the connectors through, and lowering the module was rehearsed multiple times and some notes were taken. The excess slack on the naked-fanout and octopus trunks was tightened and stored to the S-curves in between the main entry gates and the front panel, so that the trunks would stay neatly inside the C-profile envelope and would not sag out (Figure 44).

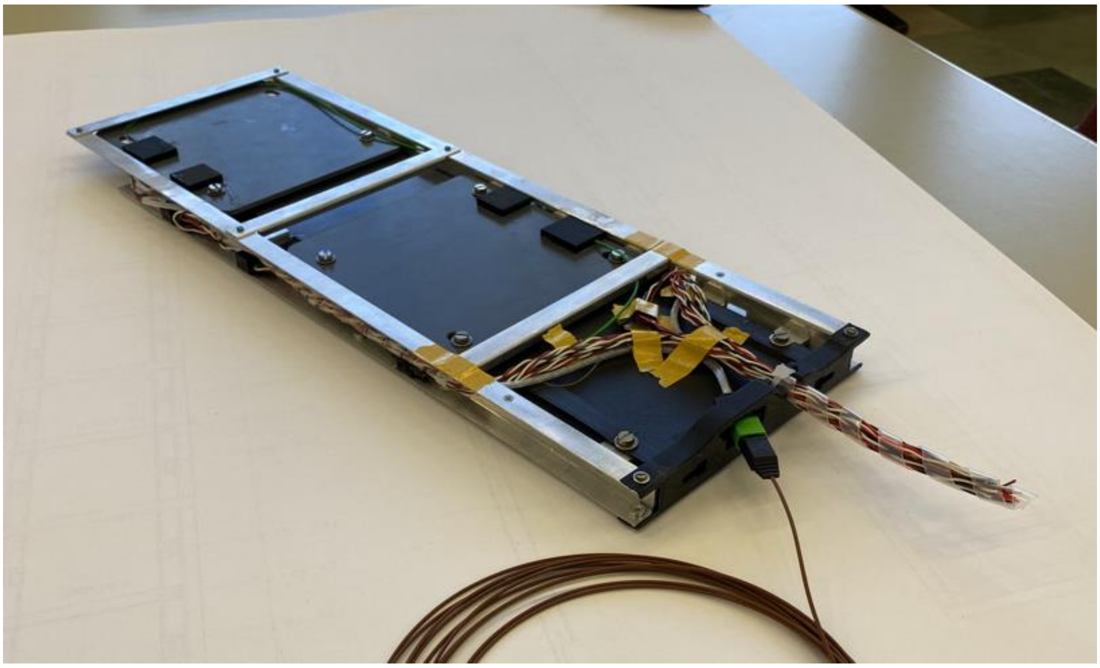

Figure 45: The service mock-up fully assembled. The MPO-connector plugged to the front panel is a straight boot variant, as the angled boot -variant was not available at the time.

Figure 46: Wires and fibres routing inside the C-profile of the service mock-up. The “normal” -case is module on top side of the image. Module #12 optical pigtail is fastened to the crossbar on the left side of the image.

Building the mock-up and doing the assembly exercises with it proved out to be really valuable, and multiple adjustments were made to the design raised from the observations made with the mock-up. For example, the size of the main entry gates was initially a bit too tight, and the electrical connector housings were too bulky and prevented neatly arranging the wires and fibres inside the C-profiles. It was also noted that in the module installation sequence it is the best to bring the module from the side, rather than directly above its position in the ladder. This way one can remain clear vision and access when manipulating the connectors through the gates and supporting the module at the same time. This has to be taken into account when the assembly fixture for the module installing phase is designed, so that there is some clearance directly next to the C-profiles.

It was important to successfully validate the service concept in terms of fitting the routing inside the important envelopes. The production of the final ladder frames is supposed to start earlier than the final production modules start to become available from the module assembly centres. This means that final configuration of the real ladders and modules cannot be assembled than rather late in the project. If any fundamental design flaws would be realized only at this stage, it could become a major issue and lead to modifying or even scrapping produced ladder frames.

4 Discussion

The objectives for the thesis project described on chapter 1.6 were pervasively achieved with successful outcomes. The validated service design was ultimately integrated to the mechanical ladder baseline design, and the final mechanical prototype of the ladder produced in NCP will have the novel features in it. The project was completed inside the pre-defined timeline, and the originally defined scope remained valid and sufficient throughout the project.

The most relevant and recent development from the pertinent research fields was gone through in the literature review of the thesis. The addressed best design philosophies and especially DFMA-thinking related to cable harness design can substantially help designers working on similar assignments and the composed knowledge in the review allows them to approach the problem correctly and to identify the appropriate solutions. Also, the presented knowledge of the novel tools aiming to improve the virtual representations of the designs was identified to be an attractive direction for additional research especially for CERN, because their product development processes rely still heavily on physical mock-ups in the design validation.

The design process of the case-study was carried out according to the proposed sequence of Park et al. (1994) discussed in chapter 2.1, starting from gathering the up-to-date specifications from the service configurations and materials. The initial ladder design was evaluated, and the concept for the service routing was derived. Some architectural change needs on the mechanical design were identified, like flipping some of the module orientations and adjusting the service configurations. The space envelopes for the service routing and exits were defined, and the configuration and the developed routing concept were confirmed to be preliminarily feasible. The need for a fully custom-shaped front panel was recognised, and its driving functionalities were set down.

The adequate module pigtail lengths were selected from the available variants on the specification, so that they would be compact but feasible for the module installation. The pigtail routings, the needed gates on the frame and their connections to the octopus/naked-fanout were designed to be uniform for the majority of the modules, and the special cases for modules #1, #11, and #12 were defined individually. The gathering and the exit interfaces of the services were designed, and necessary accessories like the snap-fit housings, the service support plate and the front panel were designed. The manufacturing of the front panel was considered, and the process and the mould design were established.

The service design was performed on a rather convenient time regarding the state of the overall project, as the life cycle of the mechanical design of the ladder was mature, but still open and capable of absorbing the needed changes. The architectural design changes were luckily fairly minor, and for example the module layout, the size of the C-profile and the frame main dimensions were kept similar as in the initial design. The rather large space requirement for the optical MPO-connector could have been recognized earlier, but luckily the solution of using the angled variant of the connector coupled with the custom front panel was successfully established, and thus the PP0-configuration in front of TB2S remained unaffected.

CATIA electrical harness discipline was utilized as the main tool when designing the detail service routings to improve the virtual representation. There were not a lot of prior experience of the tool usage at CERN, so the experience gained during the thesis project was considered valuable in the context of recognizing possibilities for broader use. The tool turned out to be efficient, the geometry representation done with FLEX-algorithm realistic, and there were no major surprises or design flaws emerging during the validation. Especially the different build-modes in the geometry definition proved to be beneficial, and the multi-branchable -document type allowed to keep the model topology neat and simple. The unusual document types and structures did not cause any incompatibility issues with the SmarTeam -PLM data manager used in CERN, which is a good thing for possible wider utilization of the electrical harness discipline. The tool would be probably even more efficient and practical in use-cases, where the routing environment is less-constrained, and for example dynamic point creation inside the bundle definition sequence could be fully utilized when the environment allows more flexibility. Also, the proper splicing and configuring of the cable harness structure should be investigated in the future, as this will improve the representation even further due to additional inputs for the physics model. Most of the inaccuracies observed during validation related to compatibility of the service elements and the ladder frame were related to the service installation. The installation sequence proved out to be challenging to simulate comprehensively with the CAD-tool, due to the indefinite geometries and shapes of the slender wires and fibres during the assembly stages. Several other CAD-software such as Siemens NX, Autodesk Inventor and PTC Creo include similar cable harness design packages in their platforms as well. A benchmarking study in this context would be worthwhile to do to provide inputs in the future when eventually the successor for CATIA V5 is selected at CERN.

The design was validated with a physical mock-up prototype demonstrating the cases for all the different module routing strategies, and the general octopus/naked-fanout -routing and exit in full-scale. The mock-up included some justified simplifications related to the ladder frame mechanics and service materials. The main goal of the mock-up was to validate that the services fit inside the required space envelopes, and it was successful on proving that. In addition, there were some detail changes emerging from the perceptions done with the mock-up, that were implemented to the mechanical baseline design. Physical mock-ups were noted to have a strong causation in the design especially for demonstrating the service installation. Utilizing the virtual tools side by side with the physical mock-up validation should be continued, but a shift towards an error-free virtual representation alone should be strived towards.

Further work remains on finalizing some details. The front panel mould needs to be manufactured and tested. The moulding process is new and being commissioned in the local workshop at CERN, and it is possible that some adjustments are needed to be made in the design to increase the production efficiency in the perspective of the serial production. The manufacturing method for the snap-fit housings used to fix the pigtail connector pairs inside the C-profiles was left undefined. If the SMC/BMC proves out to be well suited for the front panel production, it could make a good match also with these components. If the manufacturing proves out to be too cumbersome, the housings can also be replaced simply with pieces of tape and glue during the module installation. This would be a bit more untidy solution and would require more labour during the installation, but the solution is simple and light-mass. When the final 2S-modules start to become available from the module assembly centres, the assembly process and service installation needs to be rehearsed with the real

modules on the ladder frame mock-up or even better on a full mechanical prototype. The mock-up modules have validated the concept, but the real modules are complex and fragile, and the handling aspects can be fully validated only with the real modules.
Some uncertainties remain with the services length tolerance specifications, especially on the optical fibres. Joining the individual fibres to the MT-ferrules is a difficult process, and therefore in the production some excess length is typically left for possible re-work of the connection. To handle the additional length some margin for fibre slack absorption was implemented in the design by an S-bend on top of the module FEH's. On the most extreme tolerance case the bending radius of the pigtail fibres starts to be close to the allowed minimum, and the loop would need to be secured to the surface of the FEH to not sag out from the frame envelope while the ladders are installed to the wheel. The whole slack-absorption strategy needs to be confirmed when the fibre length specifications are final, and the S-bend shape needs to be validated with real modules, genuine VTRx+ -pigtails and signal attenuation measurements.

References

Aguirre, E., & Raucent, B. (1994). Performances of wire harness assembly systems. In Proceedings of 1994 IEEE International Symposium on Industrial Electronics (ISIE'94) (pp. 292-297). IEEE. https://doi.org/10.1109/ISIE.1994.333102

Bacchetta, N. (2018). OT Wires and Cables schematics. [Internal presentation].

Boothroyd, G. (1996). Design for manufacture and assembly: The Boothroyd-Dewhurst experience. In *Design for X* (pp. 19-40). Springer, Dordrecht. https://doi.org/10.1007/978-94-011-3985-4_2

Boothroyd, G., Knight W. A. Dewhurst, P. (2010). Product Design for Manufacture and Assembly. Third edition. Boca Raton, Florida; London, England; New York: CRC Press. https://doi.org/10.1201/9781420089288

CERN. (2017). LHC FAQ – the guide. [Brochure]. Available online: https://home.cern/sites/home.web.cern.ch/files/2018-07/CERN-Brochure-2017-002-Eng.pdf

CERN. (2019). CERN Annual report 2019. [Report]. Available online: https://cds.cern.ch/record/2723123/files/AnnualReport2019EN.pdf

CERN. (2020). Facts and figures about the LHC. [Webpage]. Available online: https://home.cern/resources/faqs/facts-and-figures-about-lhc - Cited 27.11.2020.

CMS Collaboration. (1994). CMS, The Compact Muon Solenoid, Technical Proposal. Report / European Laboratory for Particle Physics CERN, no. CERN-LHCC-94-38; LHCC-P-1, Geneva. [Report]. Available online: https://cds.cern.ch/record/290969

CMS Collaboration. (1997a). The CMS muon project: Technical Design Report. Report / European Laboratory for Particle Physics CERN, no. CERN-LHCC-97-032; CMS-TDR-3, Geneva. [Report]. Available online: https://cds.cern.ch/record/343814

CMS Collaboration. (1997b). The CMS hadron calorimeter project: Technical Design Report. Report / European Laboratory for Particle Physics CERN, no. CERN-LHCC-97-033; CMS-TDR-4, Geneva. [Report]. Available online: https://cds.cern.ch/record/357153

CMS Collaboration. (1997c). The CMS electromagnetic calorimeter project: Technical Design Report. Report / European Laboratory for Particle Physics CERN, no. CERN-LHCC-97-031, CMS-TDR-2, Geneva. [Report]. Available online: https://cds.cern.ch/record/349375

CMS Collaboration. (1998). The CMS tracker system project: Technical Design Report. Report / European Laboratory for Particle Physics CERN, no. CERN-LHCC-98-006; CMS-TDR-5, Geneva. [Report]. Available online: https://cds.cern.ch/record/368412

CMS Collaboration. (2006). CMS Physics Technical Design Report Volume I: Detector Performance and Software. Report / European Laboratory for Particle Physics CERN, no. CERN-LHCC-2006-001. Geneva. [Report]. Available online: https://cds.cern.ch/record/922757/

COSTAR. (2004). [Image]. Available online: http://www.costar.hw.ac.uk/images/Figure1_HMD.jpg

Dassault Systèmes. (2017). CATIA V5 Documentation. [Product documentation].

De Sa, A. G., & Zachmann, G. (1999). Virtual reality as a tool for verification of assembly and maintenance processes. Computers & Graphics, 23(3), 389-403. https://doi.org/10.1016/S0097-8493(99)00047-3

European Alliance for SMC/BMC. (2018). A design & technology manual for SMC BMC. [Brochure]. Available online: https://smcbmc-europe.org/design-for-success.php

FCC Collaboration. (2019). FCC Physics Opportunities. Eur. Phys. J. C 79, 474. https://doi.org/10.1140/epjc/s10052-019-6904-3

Hellemans, A. (2007). Manufacturing Mayday. IEEE Spectrum, 44(1), pp. 10-13. https://doi.org/10.1109/MSPEC.2007.273027

Hermansson, T., Bohlin, R., Carlson, J. S., & Söderberg, R. (2016). Automatic routing of flexible 1D components with functional and manufacturing constraints. Computer-Aided Design, 79, 27-35. https://doi.org/10.1016/j.cad.2016.05.018

Hoch, M. CMS-PHO-TRACKER-2008-006-2. [Image]. Available online: https://cds.cern.ch/record/1431473

Kobayashi, M., Hirano, Y., & Higashi, M. (2014). Optimization of assembly processes of an automobile wire harness. Computer-Aided Design and Applications, 11(3), 305-311. https://doi.org/10.1080/16864360.2014.863500

La Rocca, G. (2012). Knowledge based engineering: Between AI and CAD. Review of a language based technology to support engineering design. Advanced engineering informatics, 26(2), 159-179. https://doi.org/10.1016/j.aei.2012.02.002

Lenoir, P. (2021.) CMS Phase-2 -Upgrade Tracker Envelopes. [Drawing]; CERN CDD-number CMS2TGEP0001.

Lv, N., Liu, J., Ding, X., Liu, J., Lin, H., & Ma, J. (2017). Physically based real-time interactive assembly simulation of cable harness. Journal of Manufacturing Systems, 43, 385-399. https://doi.org/10.1016/j.jmsy.2017.02.001

Lv, N., Liu, J., Xia, H., Ma, J., & Yang, X. (2020). A review of techniques for modeling flexible cables. Computer-Aided Design, 122, 102826. https://doi.org/10.1016/j.cad.2020.102826

Lyly-Yrjänäinen, J., Aarikka-Stenroos, L., & Laine, T. (2019). Mock-ups as a tool for assessing customer value early in the development process. Measuring Business Excellence, 23(1), 15–23. https://doi.org/10.1108/MBE-11-2018-0096

Mobs, E. (2016). The CERN accelerator complex. [Schematic]. Available online: https://cds.cern.ch/record/2197559/

Nee, A. Y., Ong, S. K., Chryssolouris, G., & Mourtzis, D. (2012). Augmented reality applications in design and manufacturing. CIRP annals, 61(2), 657-679. https://doi.org/10.1016/j.cirp.2012.05.010

Ng, F. M., Ritchie, J. M. & Simmons, J. E. L. 2000. The design and planning of cable harness assemblies. Proceedings of the Institution of Mechanical Engineers, Part B: Journal of Engineering Manufacture, 214(10), pp. 881-890. https://doi.org/10.1243/0954405001517964

O'B Holt, P., Ritchie, J. M., Day, P. N., Simmons, J. E. L., Robinson, G., Russell, G. T., & Ng, F. M. (2004). Immersive virtual reality in cable and pipe routing: design metaphors and cognitive ergonomics. J. Comput. Inf. Sci. Eng., 4(3), 161-170. https://doi.org/10.1115/1.1759696

Ong, N. S., & Boothroyd, G. (1991). Assembly times for electrical connections and wire harnesses. The International Journal of Advanced Manufacturing Technology, 6(2), 155-179. https://doi.org/10.1007/BF02601438

Park, H., Cutkosky, M. R., Conru, A. B., & Lee, S. H. (1994). An agent-based approach to concurrent cable harness design. AI EDAM, 8(1), 45-61. https://doi.org/10.1017/S0890060400000457

Randall L. (2018). What Is Dark Matter?. Nature, 557(7704), S6–S7. https://doi.org/10.1038/d41586-018-05096-y

Ritchie, J. M., Robinson, G., Day, P. N., Dewar, R. G., Sung, R. C., & Simmons, J. E. (2007). Cable harness design, assembly and installation planning using immersive virtual reality. Virtual Reality, 11(4), 261-273. https://doi.org/10.1007/s10055-007-0073-7

Scully, R. B. (2020). Cable Harness Design For Aerospace Platforms. In 2020 IEEE International Symposium on Electromagnetic Compatibility & Signal/Power Integrity (EMCSI) (pp. 324-327). IEEE. https://doi.org/10.1109/EMCSI38923.2020.9191452

Stjernlöf, P. (2013). The Nobel Prize in Physics 2013. Press release. Available online: https://www.nobelprize.org/uploads/2018/06/press-21.pdf

Troska, J., Kraxner, A., Brandon-Bravo, A., Detraz, S., Scarcella, C., Sigaud, C., ... & Olanterä, L. (2017). The VTRx+, an optical link module for data transmission at HL-LHC. PoS, 048. http://doi.org/10.22323/1.313.0048

Valentini, P. P. (2011). Interactive cable harnessing in augmented reality. International Journal on Interactive Design and Manufacturing (IJIDeM), 5(1), 45-53. https://doi.org/10.1007/s12008-010-0114-4

Vasey, F. (2020). OT Opto fibre schematic. [Schematic]; CERN EDMS Document: 2385554 v.1.

Yang, X., Liu, J., Lv, N., & Xia, H. (2019). A review of cable layout design and assembly simulation in virtual environments. Virtual Reality & Intelligent Hardware, 1(6), 543-557. https://doi.org/10.1016/j.vrih.2019.11.001

Zhu, Z., van Tooren, M., & der Elst, S. (2011). On the development of a heuristic routing application for the automatic wire harness design in the aircraft. In 52nd AIAA/ASME/ASCE/AHS/ASC Structures, Structural Dynamics and Materials Conference 19th AIAA/ASME/AHS Adaptive Structures Conference 13t (p. 2148). https://doi.org/10.2514/6.2011-2148